

The VAST Survey – III. The multiplicity of A-type stars within 75 pc

R. J. De Rosa^{1,2*}†, J. Patience^{1,2}, P. A. Wilson², A. Schneider³, S. J. Wiktorowicz^{4,5},
 A. Vigan^{6,2}, C. Marois⁷, I. Song³, B. Macintosh⁸, J. R. Graham^{4,9}, R. Doyon¹⁰,
 M. S. Bessell¹¹, S. Thomas^{12,13}, & O. Lai¹⁴

¹ School of Earth and Space Exploration, Arizona State University, PO Box 871404, Tempe, AZ 85287-1404, USA

² School of Physics, College of Engineering, Mathematics and Physical Sciences, University of Exeter, Stocker Road, Exeter, EX4 4QL, UK

³ Physics and Astronomy, University of Georgia, 240 Physics, Athens, GA 30602, USA

⁴ Department of Astronomy, University of California at Berkeley, Berkeley, CA 94720, USA

⁵ Department of Astronomy, University of California at Santa Cruz, 1156 High Street, Santa Cruz, CA 95064, USA

⁶ Aix Marseille Université, CNRS, LAM (Laboratoire d’Astrophysique de Marseille) UMR 7326, 13388, Marseille, France

⁷ NRC Herzberg Institute of Astrophysics, 5071 West Saanich Road, Victoria, BC, V9E 2E7, Canada

⁸ Institute of Geophysics and Planetary Physics, Lawrence Livermore National Laboratory, 7000 East Ave, Livermore, CA 94550, USA

⁹ Dunlap Institute for Astronomy and Astrophysics, University of Toronto, 50 St. George Street, Toronto, ON, M5S 3H8, Canada

¹⁰ Département de Physique, Université de Montréal, C.P. 6128, Succ. Centre-Ville, Montréal, QC, H3C 3J7, Canada

¹¹ Research School of Astronomy and Astrophysics, Mount Stromlo Observatory, The Australian National University, ACT 2611, Australia

¹² Gemini Observatory, Southern Operations Center, Casilla 603, La Serena, Chile

¹³ Laboratory for Adaptive Optics, University of California/Lick Observatory, University of California at Santa Cruz, 1156 High Street, Santa Cruz, CA 95064, USA

¹⁴ Canada-France-Hawaii Telescope, 65-1238 Mamalahoa Highway, Kamuela, HI 96745, USA

ABSTRACT

With a combination of adaptive optics imaging and a multi-epoch common proper motion search, we have conducted a large volume-limited ($D \leq 75$ pc) multiplicity survey of A-type stars, sensitive to companions beyond 30 au. The sample for the Volume-limited A-STar (VAST) survey consists of 435 A-type stars: 363 stars were observed with adaptive optics, 228 stars were searched for wide common proper motion companions and 156 stars were measured with both techniques. The projected separation coverage of the VAST survey extends from 30 to 45,000 au. A total of 137 stellar companions were resolved, including 64 new detections from the VAST survey, and the companion star fraction, projected separation distribution and mass ratio distribution were measured. The separation distribution forms a log-normal distribution similar to the solar-type binary distribution, but with a peak shifted to a significantly wider value of 387^{+132}_{-98} au. Integrating the fit to the distribution over the 30 to 10,000 au observed range, the companion star fraction for A-type stars is estimated as 33.8 ± 2.6 per cent. The mass ratio distribution of closer (< 125 au) binaries is distinct from that of wider systems, with a flat distribution for close systems and a distribution that tends towards smaller mass ratios for wider binaries. Combining this result with previous spectroscopic surveys of A-type stars gives an estimate of the total companion star fraction of 68.9 ± 7.0 per cent. The most complete assessment of higher order multiples was estimated from the 156-star subset of the VAST sample with both adaptive optics and common proper motion measurements, combined with a thorough literature search for companions, yielding a lower limit on the frequency of single, binary, triple, quadruple and quintuple A-type star systems of $56.4^{+3.8}_{-4.0}$, $32.1^{+3.9}_{-3.5}$, $9.0^{+2.8}_{-1.8}$, $1.9^{+1.8}_{-0.6}$ and $0.6^{+1.4}_{-0.2}$ per cent, respectively.

Key words: techniques: high angular resolution - binaries: close - binaries: general - binaries: visual - stars: early-type

* E-mail: rjderosa@asu.edu

† Based on observations obtained at the Canada-France-Hawaii Telescope (CFHT) under programme IDs 2008AC22, 2009BC06, 2010AC14 and 2011AC11. Based on observations obtained at the Gemini Observatory under programme IDs GN2008A-Q-74, GN-2008B-Q-119, GN-2010A-Q-75.

See Table 4 for details of data obtained from the CFHT and European Southern Observatory (ESO) archives.

1 INTRODUCTION

Binary stars represent the most common product of the star formation process and a key environmental factor for planet formation. Investigating the properties of binary systems, and dependencies on age (e.g. Ghez et al. 1997; Duchêne 1999; Patience et al. 2002), environment (e.g. Köhler et al. 2006; King et al. 2012; Sana et al. 2013) and primary mass (e.g. Abt 1983; Lada 2006; Lafrenière et al. 2008; Kraus et al. 2011; Sana & Evans 2011) is therefore crucial to our understanding of star formation. Theoretical binary formation models (e.g. Boss & Bodenheimer 1979; Adams et al. 1989; Bonnell et al. 1991; Bonnell 1994; Clarke 1996; Bate & Bonnell 1997; Kratter et al. 2010; Stamatellos et al. 2011) and the results of large numerical simulations of star formation within stellar clusters (e.g. Sterzik & Durisen 2003; Moeckel & Bate 2010; Bate 2012; Krumholz et al. 2012) require large-scale surveys for empirical comparison.

Previous volume-limited surveys utilizing a range of companion detection techniques, collectively sensitive to all possible binary orbits, have provided observational constraints on the frequency and properties of the binary companions to nearby field FGKM stars and field L and T brown dwarfs (e.g. Duquennoy & Mayor 1991; Fischer & Marcy 1992; Burgasser et al. 2006; Reid et al. 2008; Raghavan et al. 2010). For stars more massive than F-type stars, there are no comparable comprehensive surveys covering the full range of binary orbits. A large number of O and B-type stars have been observed with speckle interferometry (e.g. Mason et al. 1997; Hartkopf et al. 1999; Mason et al. 2009); however, the samples typically consist of stars at large distances and the technique is limited in magnitude difference sensitivity and separation range coverage. Greater sensitivity to fainter companion has been achieved using adaptive optics (AO) surveys (e.g. Roberts et al. 2007); however, the sample was magnitude-limited, introducing a potential selection bias. For field A-type stars, spectroscopic work has identified systems with short orbital periods (e.g. Abt 1965; Abt & Levy 1985; Carrier et al. 2002; Carquillat et al. 2003). More recently, A-type stars have been the subject of deep AO imaging searches for extreme mass ratio planetary companions (e.g. Vigan et al. 2012; Nielsen et al. 2013), with several planetary systems discovered (Kalas et al. 2008; Marois et al. 2008; Lagrange et al. 2009; Marois et al. 2010; Carson et al. 2013; Rameau et al. 2013). As the planetary population around A-type stars is revealed, the properties of A-type star binaries will serve as an essential comparison.

This paper is the third in a series on the properties of the Volume-limited A-STar (VAST) survey of A-type stars within 75 pc. The survey was designed to have companion mass ratio sensitivity limits ($M_2/M_1 \gtrsim 0.1$) comparable to previous volume-limited multiplicity surveys and to cover projected separations extending from the peak of the solar-type distribution (~ 40 au). In previous papers, subsets of the VAST survey were investigated to study the unexpected X-ray emission of A-type stars (De Rosa et al. 2011) and orbital motion of known binaries (De Rosa et al. 2012). In this paper, the comprehensive binary statistics are presented. The full sample is defined in Section 2, followed by the data acquisition of both new AO and literature wide field imaging in Section 3. Data analysis techniques applied to identify and characterize the candidate companions and detection limits in both types of images are detailed in Section 4, and the overall survey completeness is quantified in Section 5. The survey results, including the A-type star binary separation distribution, mass ratio distribution and companion star fraction (CSF), are reported in Section 6. Comparisons of the

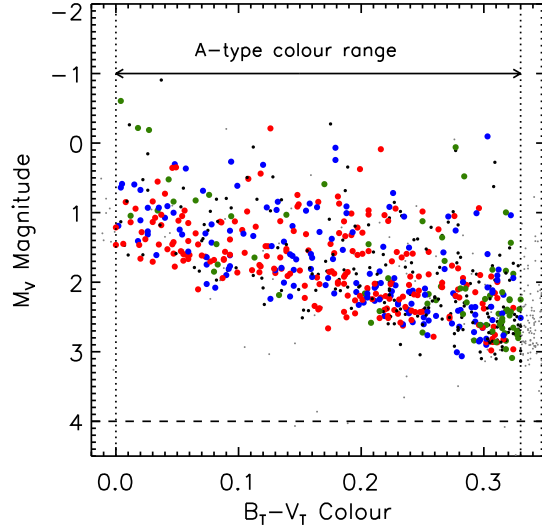


Figure 1. A colour–magnitude diagram demonstrating the selection criteria used to define the volume-limited sample of A-type stars. Of the *Hipparcos* stars within 75 pc (small grey filled points), those with a parallax uncertainty of $\sigma_\pi/\pi \leqslant 0.05$ and with a $B_T - V_T$ colour consistent with A-type stars were selected (dotted vertical lines), with a magnitude cut-off to remove contamination from faint white dwarfs (dashed horizontal line). Of the 636 stars satisfying these criteria, 156 were observed with adaptive optics and are included within the photographic plate search for common proper motion companions (blue points), 207 targets were only observed with adaptive optics (red points), and 72 were only included within the photographic plate sample (green points). The remaining 201 targets without observations, which otherwise satisfied the selection criteria, are plotted for reference (small black points).

VAST results with previous survey and theoretical models are made in the discussion, Section 7, along with a combination of the VAST results and previously known binary companions to investigate the higher order multiple systems. Finally, Appendix 1 describes the procedures employed to estimate the mass and age of the VAST sample members.

2 SAMPLE

To measure the frequency of stellar binary companions, and the distribution of their separations and mass ratios, we have obtained observations of a sample of 435 nearby A-type stars. The sample is composed of two overlapping sets of A-type stars within 75 pc: a 363 star sample observed with AO instrumentation and a 228 star sample investigated with astrometry obtained from all-sky photographic surveys, with an overlap of 156 stars. The 435 observed targets, listed in Tables 1 and 2, were drawn from a volume-limited sample of A-type stars selected from the *Hipparcos* catalogue (ESA 1997; van Leeuwen 2007). The sample was limited to targets within 75 parsecs, corresponding to an *Hipparcos* parallax of $\pi \geqslant 13.3$ mas. High quality parallax uncertainties ($\sigma_\pi/\pi \leqslant 0.05$) are required to place the targets on the colour–magnitude diagram, determine accurate distances to the targets and, consequently, determine the absolute magnitude of any resolved companion candidate. Using the optical magnitudes of each target from the Tycho2 catalogue (Høg et al. 2000), the sample was limited to targets within the A-type star colour range ($0.0 \leqslant B_T - V_T \leqslant 0.33$; Gray 1992).

Table 1. The VAST sample - available in its entirety in the electronic edition of the journal.

HIP	Spectral Type	Distance (pc)	B_T (mag)	V_T (mag)	J (mag)	H (mag)	K_S (mag)	Age ^a (Myr)	Age Ref.	Mass (M_\odot)	Separation Adaptive Optics	Coverage (log a [au]) CPM Search
128	Am...	70.8 ± 1.7	6.73 ± 0.01	6.52 ± 0.01	6.10 ± 0.02	6.06 ± 0.04	6.02 ± 0.02	180	1	1.84	$1.50 \rightarrow 2.90$	$3.60 \rightarrow 4.65$
159	A3	62.5 ± 2.1	7.26 ± 0.01	6.96 ± 0.01	6.33 ± 0.02	6.27 ± 0.02	6.21 ± 0.02	60	1	1.59	$1.50 \rightarrow 2.90$	–
1473	A2V	41.3 ± 0.4	4.59 ± 0.01	4.51 ± 0.01	4.34 ± 0.27	4.42 ± 0.18	4.46 ± 0.29	200	1	2.26	$1.50 \rightarrow 2.55$	$3.60 \rightarrow 4.65$
2355	A7III	62.8 ± 1.7	5.52 ± 0.01	5.25 ± 0.01	4.86 ± 0.25	4.69 ± 0.19	4.46 ± 0.03	710	1	2.20	$1.50 \rightarrow 2.90$	$3.60 \rightarrow 4.65$
2381	A3V	53.1 ± 0.8	5.32 ± 0.01	5.18 ± 0.01	5.28 ± 0.24	4.88 ± 0.08	4.83 ± 0.02	450	1	2.09	$1.50 \rightarrow 2.90$	–

^a - Age rounded to nearest isochrone value. Age estimates from: 1 - this work (CMD), 2 - Zuckerman et al. (2011), 3 - Tetzlaff et al. (2010), 4 - Rhee et al. (2007), 5 - Su et al. (2006), 6 - Rieke et al. (2005), 7 - Perryman et al. (1998), 8 - Barrado y Navascués (1998), 9 - Song et al. (2001), 10 - Westin (1985), 11 - Gerbaldi et al. (1999), 12 - Zuckerman & Song (2004), 13 - Laureijs et al. (2002), 14 - Stauffer et al. (1995), 15 - Paunzen (1997), 16 - Janson et al. (2011), 17 - Torres et al. (2008).

Table 2. Alternative catalogue identifiers - available in its entirety in the electronic edition of the journal.

HIP	Name	Bayer	Flamsteed	HR	HD	ADS	WDS
128					224890		
159					224945		
1473	σ And	25 And	68		1404		
2355		28 And	114	2628	409 AB	J00301+2945	
2381			118	2696			

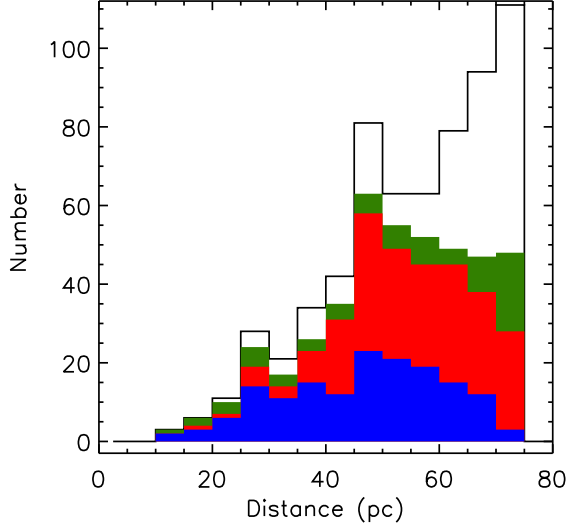


Figure 2. The distribution of distance estimates for the 636 A-type stars within the volume-limited sample. The shading of the histogram indicates whether the target was within both the adaptive optics and photographic plates sample (blue histogram), only the adaptive optics sample (red histogram), only the photographic plates sample (green histogram), or was not within either sample (open histogram). The distance distribution of the observed stars is complete up to approximately 50 pc, beyond which a significant proportion of the volume-limited sample remains unobserved. Targets at close distances were preferentially observed in order to increase the sensitivity to binary companions at small physical separations.

Finally, an absolute magnitude cut-off of $M_V < 4$ was imposed to remove two faint white dwarfs that have colours consistent with A-type stars. Due to their brightness exceeding the magnitude limit of

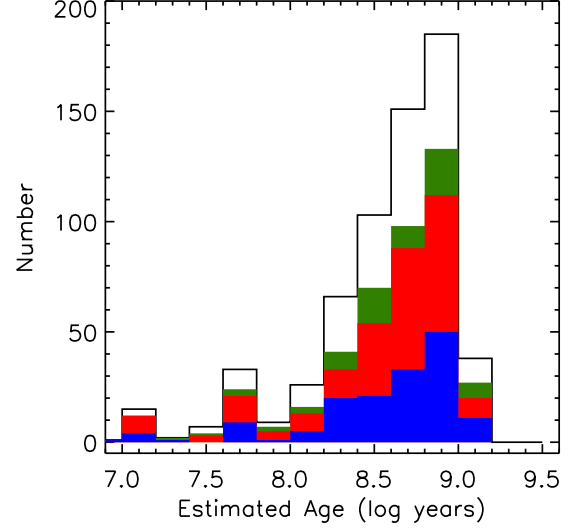


Figure 3. The distribution of the age estimates for each target estimated from solar-metallicity isochrones (Siess et al. 2000). The shading of this histogram is as in Fig. 2.

the Tycho2 catalogue ($V_T \lesssim 2.1$; Høg et al. 2000), seven nearby A-type stars were not listed within the catalogue - α CMa (Sirius), α Gem, β Leo, α Oph, α Lyr (Vega), α Aql (Altair) and α PsA (Fomalhaut) - and were therefore excluded by the sample selection process.

Drawn from the 636 stars which satisfy these selection criteria, the VAST sample consists of 435 A-type stars within 75 pc. The positions of the VAST targets on the colour-magnitude diagram are shown in Fig. 1, and span the full range of A-type stars. A histogram of the distances to the observed targets is shown in Fig.

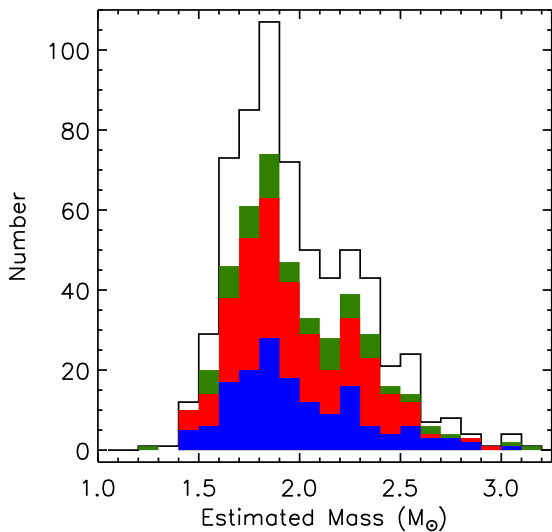


Figure 4. The distribution of the mass estimates for each target estimated from solar-metallicity isochrones (Siess et al. 2000). The shading of this histogram is as in Fig. 2.

Table 4. Sources of archive observations

CFHT archive		ESO archive	
Programme ID	PI	Programme ID	PI
97IIH06	Simon	070.C-0565(A)	Mouillet
98IF12	Corcoran	272.D-5068(A)	Ivanov
98IH02	Simon	073.C-0469(A)	Chauvin
99IF59	Perrier	074.D-0180(A)	Ivanov
00BF1	Gerbaldi	076.C-0270(A)	Galland
01AF11	Gerbaldi	076.D-0108(A)	Ivanov
01AH11A	Jewitt	077.D-0147(A)	Ivanov
01BF21	Catala	079.C-0908(A)	Zuckerman
02AF03	Catala	080.D-0348(A)	Ivanov
03BH59A	Ftaclas	081.C-0653(A)	Lagrange
06BF07	Galland	382.D-0065(A)	Kervella
07BF04	Lagrange	383.C-0847(A)	Schmidt
08AF02/F07	Beuzit		
08AF07	Lagrange		

2, with the VAST sample nearly complete within a distance of 50 pc. In order to convert the measured magnitude difference between an A-type star primary and a resolved companion into a mass ratio for the system, an estimate of the age is required. This is due to the age dependence of the mass-magnitude relation used within this study for A-type stars, and for low-mass M-dwarfs at ages $\lesssim 100$ Myr. The procedure used for estimating the age and mass of each target is given in Appendix 1, with the resulting distribution of ages and masses of the sample given in Figs 3 and 4.

3 DATA ACQUISITION

3.1 Adaptive optics observations

High-resolution AO images of a sample of 363 A-type stars were obtained through a combination of new observations of 257 stars obtained between 2008 and 2011 and archive images of an addi-

Table 5. Sources of photographic plates

Survey	Filter	Declination range	Date range
ESO	R	$-90.0 < \delta < -17.5$	1979–1990
POSS-I	R	$-20.5 < \delta < +2.5$	1949–1957
POSS-I	R	$+2.5 < \delta < +90.0$	1949–1957
POSS-II	B	$+2.5 < \delta < +90.0$	1986–2002
POSS-II	R	$+2.5 < \delta < +90.0$	1986–1999
POSS-II	I	$+2.5 < \delta < +90.0$	1989–2000
UKST	B	$-90.0 < \delta < +2.5$	1974–1993
UKST	R	$-90.0 < \delta < +2.5$	1984–1999
UKST	I	$-90.0 < \delta < +2.5$	1978–2002

tional 106 targets. The details of the new AO observations are reported in Table 3, and the archive AO data included in the sample are summarized in Table 4. For the new observations, images were obtained using a near-infrared filter, decreasing the contrast between the bright A-type star primary and any faint companion candidate relative to optical wavelengths. The observational strategy was designed such that the images would be sensitive to companions at the bottom of the main sequence ($\Delta K \approx 7 - 10$, depending on the primary), at angular separations of $\rho \geq 1$ arcsec. Unsaturated exposures of each target were taken to detect high mass ratio companions at close separations and calibrate the photometry. Longer saturated exposures were also obtained and provided sensitivity to low-mass companions beyond the saturated point spread function of the bright target. A typical unsaturated sequence included exposures obtained with a low transmission narrow-band filter at a number of dither positions, removing the effect of bad pixels and cosmic ray events. For the observations involving CFHT/KIR, Lick/IRCAL and Gemini/NIRI, saturated exposures were then taken using a wide-band filter at a number of dither positions, significantly increasing the sensitivity of the observations to faint companions at the bottom of the main sequence. Saturated exposures were not obtained using Palomar/PHARO; instead, a large number of short exposures were combined to achieve sensitivity to faint companions.

In addition to the new observations presented within this study, VLT/NaCo (Lenzen et al. 2003; Rousset et al. 2003) and CFHT/KIR data taken in similar AO snapshot modes were obtained from the ESO and CFHT science archives. Archived observations which were obtained using complex imaging techniques such as angular differential imaging, primarily used to search for extremely faint planetary-mass companions (Marois et al. 2006), are not included in this study. AO images of 184 of the sample members were obtained from the two science archives, providing measurements of an additional 106 targets not observed as a part of our dedicated observing programme.

3.2 Digitized photographic plates

The high angular resolution AO component of the survey was augmented with a search of astrometric catalogues for wide common proper motion (CPM) companions, confirmed with a visual inspection of digitized photographic plates. Astrometric data were obtained from a number of sources: bright CPM companions were identified from a previous analysis of the *Hipparcos* catalogue (Shaya & Olling 2010), while fainter CPM companions were selected from a union of the SuperCosmos Sky Survey (SSS) Science Archive (Hambly et al. 2001), the PPMXL catalogue (Roeser et al. 2010) and the Fourth US Naval Observatory CCD Astrograph Cat-

Table 3. Observing run details

Telescope	Instrument	Programme ID	Narrow filter	Wide filter	Observed stars ^a
CFHT	KIR	2008AC22	FeII	H	31
		2008AC22	$H_2(v = 1 - 0)$	K'	8
		2009BC06	$H_2(v = 1 - 0)$	K'	46
		2010AC14	$H_2(v = 1 - 0)$	K'	42
		2011AC11	$H_2(v = 1 - 0)$	K'	5
Gemini North	NIRI	GN-2008A-Q-74	$B\gamma$	K'	36
		GN-2008B-Q-119	$B\gamma$	K'	78
		GN-2009B-Q-120	$B\gamma$	K'	3
		GN-2010A-Q-75	$B\gamma$	K'	39
Lick	IRCAL	–	$B\gamma$	K_S	81
		2012 SO16	$H_2(v = 1 - 0)$	K_S	13
Palomar	PHARO	–	$CH4_S$	(H) ^b	34
		–	$B\gamma$	(K) ^b	31
		–	K_S	(K) ^b	8

^a - These totals include targets with multiple epochs of observations

^b - The wide band filter was not used for data obtained with PHARO

KIR – Doyon et al. (1998)

NIRI (Near InfraRed Imager and Spectrometer) – Hodapp et al. (2003)

IRCAL (IR Camera for Adaptive Optics at Lick) – Lloyd et al. (2000)

PHARO (Palomar High Angular Resolution Observer) – Hayward et al. (2001)

alog (UCAC4; Zacharias et al. 2012). In order to estimate the innermost separation at which these catalogues were sensitive to all stellar companions, and to select a subsample of stars with a high apparent motion, digitized scans of photographic plates from the UK Schmidt (UKST), ESO Schmidt and Palomar Oschin Schmidt (POSS) sky surveys (Table 5) were obtained from the SSS Science Archive (Hambly et al. 2001) for each of the 636 stars within the sample.

4 DATA REDUCTION AND CANDIDATE IDENTIFICATION AND CHARACTERIZATION

4.1 Adaptive optics observations

Each science image was processed through the standard near-infrared data reduction process, beginning with a dark frame subtraction, and division by a flat-field. The sky background for each target was estimated from a median combination of the science images obtained at different dither positions, unless dedicated sky frames were taken, and was scaled to and subtracted from each science image. Bad pixels and cosmic ray events were flagged and interpolated over, using both a bad pixel map, generated from the flat-field analysis, and a search for pixel outliers within each image. To increase sensitivity to faint companions and increase the signal-to-noise ratio of any detection, the individual science images obtained for each target were aligned to a common centre and combined through a median combination.

The registration of the unsaturated images was achieved by determining the Gaussian centroid of the target within each image; close companions were masked before centroiding. The images of each target were then shifted using cubic interpolation. Prior to performing a median combination of the images, a radial profile was calculated and subtracted. The median of these aligned images was then calculated to create the final science image. For the saturated images, an estimate of the centroid of the target was determined through an analysis of the diffraction spikes from the secondary

mirror supports on each telescope. By cross-correlating the position of the diffraction spikes within each individual saturated exposure of a given target, the offsets required to register each image to a common centre were calculated (Lafrenière et al. 2007). As with the unsaturated exposures, a radial profile was calculated and subtracted from each aligned image, and a final science image was created through a median combination.

Companion candidates were identified through a visual inspection of the final science images. The centroid of each companion candidate was compared with the centroid of the target in order to measure the separation and position angle of the companion. These measurements were converted into an on-sky separation and position angle (ρ, θ) using the pixel scale and angle of North of the detector, estimated from observing an astrometric field (the Trapezium; McCaughrean & Stauffer 1994) or a calibration binary. The magnitude difference measured between each companion candidate and the central target was estimated using aperture photometry, with the flux of the central target scaled as a function of the filter transmission and exposure time for companions resolved within the saturated exposures. The aperture was twice the full width at half-maximum (FWHM) measured within the final science frame, with a sky annulus between six and eight times the FWHM. The uncertainties of the separation, position angle and magnitude difference were estimated from the standard deviation of the astrometric and photometric measurements obtained from each individual exposure prior to combination.

The angular separation of each companion was converted to a projected separation (a_{proj}) using the distance to the primary obtained from the *Hipparcos* catalogue (van Leeuwen 2007). The magnitude difference between each primary and companion was converted to both a secondary mass (M_2) and mass ratio ($q = M_2/M_1$), using the absolute magnitude of the primary obtained from 2MASS and theoretical solar-metallicity isochrones (Siess et al. 2000; Baraffe et al. 1998). For candidates at close separations ($\lesssim 5$ arcsec), the absolute magnitude of the primary obtained from the 2MASS catalogue is based on the sum of the flux

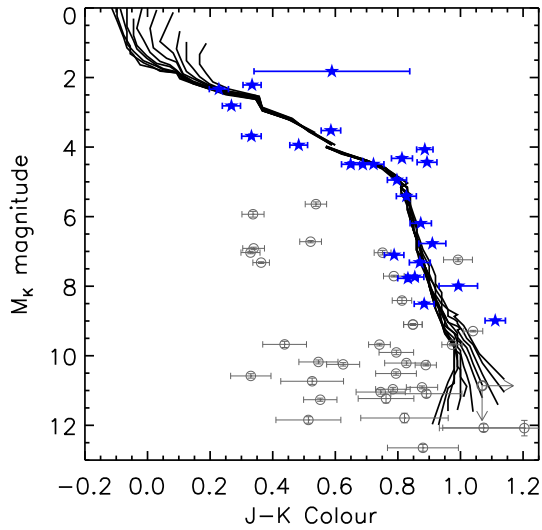


Figure 6. The position of each common proper motion candidate on the colour–magnitude diagram was compared with theoretical isochrones (black lines, Baraffe et al. 1998; Siess et al. 2000) in order to reject background objects with the same apparent motion. Those candidates thought to be physically associated based on their proper motion and position on the colour–magnitude diagram are highlighted (blue stars). Candidates with mass ratios of $q < 0.05$, but otherwise consistent with being physically associated, were excluded.

from both primary and companion. The contamination of the magnitude of the primary caused by the presence of a bright companion was removed using the magnitude difference measured within this study, prior to the estimation of the mass of the companion and the mass ratio of the system.

With only one epoch for most targets, the assessment of physical association was based on a statistical cut-off estimated using 2MASS source counts. The spatial distribution of the targets, superimposed on the surface density of 2MASS point sources, is shown in Fig. 5. Using the 2MASS catalogue, a power law was fit to the cumulative number of 2MASS J , H and K_S point sources per square arcsecond as a function of magnitude (De Rosa et al. 2011). For each companion candidate resolved within this study, the corresponding probability of finding a 2MASS point source of the same magnitude or brighter within the same radius was calculated. Only companion candidates with less than 5 per cent chance of being a chance superposition were included in the final results and discussion.

4.2 Digitised photographic plates

In order to ensure that the CPM companion detections were reliable, a subsample was designed to remove those targets with very small proper motions. As the astrometric data obtained from the SSS Science Archive represent the data set with the shortest time baseline over which to measure proper motions, a lower limit on the total expected proper motion of a bound CPM of 4 pixels (> 2.7 arcsec) was applied to the complete sample. Using the longest time baseline between the photographic plates obtained from the SSS Science Archive, and the annual proper motions reported within the *Hipparcos* catalogue, a sample of 228 stars was selected. As the level of sensitivity to faint stellar companions varies as a func-

tion of separation, and the brightness of target itself, the innermost separation to which the astrometric catalogues were sensitive to all stellar companions was estimated from the photographic plates. For each of the 228 targets, the innermost separation was estimated as the separation at which the flux of the primary reduced to 75 per cent of its peak value, a conservative estimate based on an analysis of the magnitudes of the background objects within each field.

Bright ($V \lesssim 8$) CPM companions were drawn from an analysis of the *Hipparcos* catalogue, taking into account both the proper motions and parallax measurements (Shaya & Olling 2010). Companions below the limiting magnitude of the *Hipparcos* catalogue were identified based on their proper motion from the three astrometric catalogues described previously; the SSS Science Archive (Hambly et al. 2001), the PPMXL catalogue (Roeser et al. 2010) and the UCAC4 catalogue (Zacharias et al. 2012). Only those objects with a proper motion within 1.5σ of the motion of the primary stated within the *Hipparcos* catalogue were selected. In order to ensure a CPM companion was not missed during this automated procedure, the position of each source within the astrometric catalogues were marked within the mosaic of each target, revealing the presence of any source not included within the astrometric catalogues.

The relative position and brightness of each identified CPM companion was determined from the astrometry and photometry within the 2MASS catalogue, from which the projected separation and position angle were calculated. The magnitude difference between the target and the comoving companion was converted into a secondary mass and a mass ratio using theoretical solar-metallicity isochrones (Baraffe et al. 1998; Siess et al. 2000), in the same manner as the AO companions. Finally, the CPM companions were plotted on a colour–magnitude diagram (Figure 6), to reject background objects with similar proper motions but an unphysical location on the colour–magnitude diagram, assuming the primary and companion are at the same distance.

5 SURVEY COMPLETENESS

The completeness of the observations was estimated in order to minimize any bias within the distribution of companion properties measured within the survey. For the AO data, a one-dimensional sensitivity curve was created for each image, with the sensitivity limit at radius r calculated as the standard deviation of the image pixel values within a circular annulus of width $2\lambda/D$. The faintest companion to which the data were sensitive was estimated as a signal five times this standard deviation. The largest separation considered for each target was the radius at which at least 90 per cent of the position angles were sampled by the images. For targets with multiple observations, the best contrast achieved at a given separation was used as the formal detection limit at that separation. The average detection limits for observations obtained using each instrument are shown in Fig. 7, while the overall completeness of the survey is given in terms of both observable (ρ , Δm) and physical quantities (a_{proj} , q) in Fig. 8.

6 RESULTS

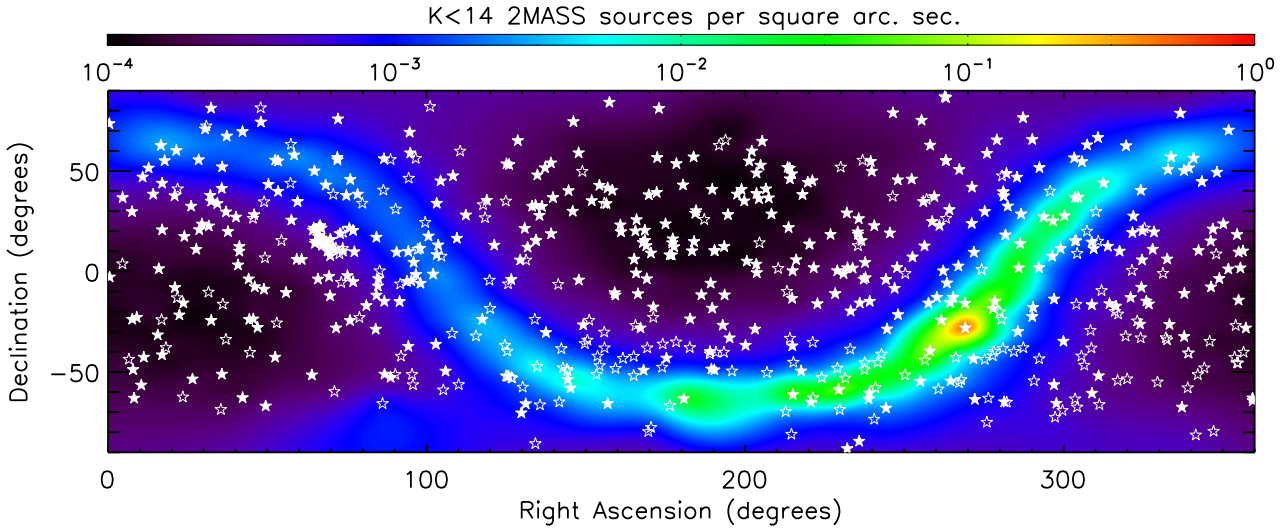


Figure 5. The sample target members are distributed evenly throughout the celestial sphere (open and filled star symbols), with the exception of the Hyades open cluster. The observed and unobserved VAST sample members are shown as filled and open stars, respectively. The surface density of 2MASS point sources with a magnitude of $K_S < 14$, within an area of 1 square arc second surrounding each member of the VAST sample, is depicted by the coloured surface. The path of the Galaxy through the sky is apparent, with the Galactic Centre showing a significant increase in the surface density of 2MASS point sources $N(K_S < 14) > 10^{-1}$.

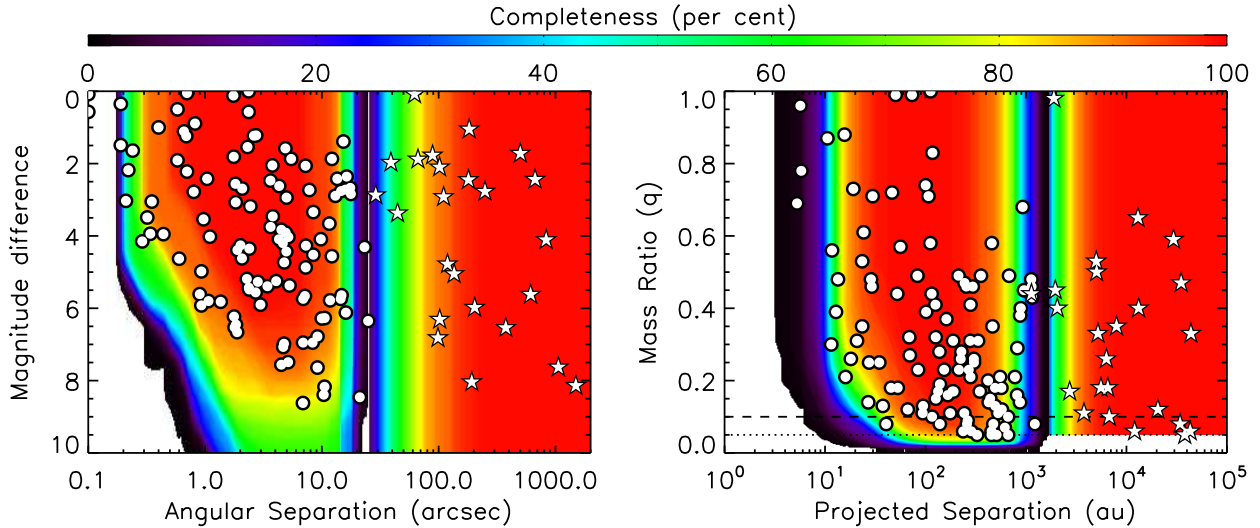


Figure 8. The completeness of the adaptive optics observations ($N = 363$, $\rho \lesssim 15$ arcsec, $a_{\text{proj}} \lesssim 2,000$ au) and the analysis of the photographic plates ($N = 228$, $\rho \gtrsim 15$ arcsec, $a_{\text{proj}} \gtrsim 2,000$ au), expressed in terms of (left-hand panel) angular separation and magnitude difference, and (right-hand panel) projected separation and mass ratio. The companion candidates identified within the adaptive optics data set (white filled points) and CPM companions identified within the photographic plates (white filled stars) are plotted. The regions of phase space not sampled by the observations are shown in white for clarity.

Table 6: Binary companions identified within the adaptive optics observations

HIP	WDS Desig.	ρ (arcsec)	a_{proj} (au)	θ (deg.)	Band	Δm (mag)	M_1 (M_\odot)	M_2 (M_\odot)	q	Date
HIP 128	AC	0.98	68.9	80.6	K	3.52	1.84	0.58	0.32	20/09/2008
HIP 1473	*	6.91	285.5	146.3	K	6.95	2.26	0.14	0.06	31/08/2009
HIP 2355	AB	2.01	126.3	15.9	K	4.26	2.20	0.71	0.32	16/10/2008
HIP 2381	–	1.77	93.9	279.1	K	6.23	2.09	0.23	0.11	26/09/2007
HIP 2852	–	0.93	45.4	260.6	K	5.00	1.66	0.30	0.18	17/10/2008
HIP 3277	–	13.06	875.4	252.5	K	2.89	2.14	0.81	0.38	29/09/2007
HIP 4979	* ^a	14.50	872.0	250.0	K	5.74	1.80	0.25	0.14	16/10/2008

Table 6: Binary companions identified within the adaptive optics observations

HIP	WDS Desig.	ρ (arcsec)	a_{proj} (au)	θ (deg.)	Band	Δm (mag)	M_1 (M_\odot)	M_2 (M_\odot)	q	Date
HIP 4979	\star^a	15.89	955.6	254.4	K	2.72	1.80	0.81	0.45	16/10/2008
HIP 5300	–	0.11	5.8	126.7	K	0.57	2.10	1.64	0.78	20/09/2007
HIP 5310	–	0.36	16.0	175.0	K	3.72	1.83	0.39	0.21	16/10/2008
HIP 8847	\star	11.58	820.4	262.7	K	3.66	1.87	0.54	0.29	31/08/2009
HIP 9480	AB	0.67	24.2	297.4	K	1.20	1.93	1.17	0.61	01/09/2009
HIP 9480	AC	23.16	816.5	52.5	K	4.31	1.93	0.31	0.16	01/09/2009
HIP 11102	–	2.28	138.8	153.8	K	5.19	1.77	0.34	0.19	07/11/2005
HIP 11569	AaAb	0.58	23.4	43.5	K	1.91	2.19	1.15	0.53	16/10/2008
HIP 11569	AB	2.74	111.8	230.6	K	1.22	2.19	1.27	0.58	16/10/2008
HIP 11569	AC	7.25	295.2	115.3	K	2.06	2.19	1.01	0.46	16/10/2008
HIP 12706	AB	2.31	56.3	298.5	K	1.54	2.09	1.20	0.57	17/10/2008
HIP 13133	AC	7.30	473.1	71.6	K	4.27	2.59	0.20	0.08	16/10/2008
HIP 15353	–	4.91	269.7	17.4	K	3.91	1.71	0.40	0.23	07/11/2005
HIP 16292	AB	14.59	888.6	159.6	K	2.76	2.32	0.93	0.40	16/10/2008
HIP 17954	–	0.20	10.5	194.8	K	0.23	1.94	1.69	0.87	14/11/2008
HIP 18217	–	1.03	52.3	65.0	K	2.41	1.75	0.77	0.44	12/11/2008
HIP 18907	\star	16.05	575.5	182.5	K	6.12	2.35	0.28	0.12	05/02/2010
HIP 20542	\star	9.98	493.9	85.4	K	6.28	2.09	0.26	0.13	17/11/2007
HIP 20648	AB	1.82	83.1	341.4	K	2.56	2.11	1.03	0.49	04/02/2010
HIP 20713	\star	10.38	509.8	146.9	K	8.39	2.24	0.12	0.05	31/08/2009
HIP 21036	\star	4.76	215.2	313.6	K	4.73	1.87	0.43	0.23	05/02/2010
HIP 21036	\star	4.96	224.3	311.3	K	4.43	1.87	0.48	0.26	05/02/2010
HIP 23179	AB	4.87	254.8	3.5	K	1.58	2.39	1.10	0.46	17/10/2008
HIP 23296	AD	9.17	454.7	328.2	K	7.64	1.59	0.09	0.06	05/11/2008
HIP 28614	AB	0.40	19.1	22.0	K	1.00	2.19	1.68	0.77	19/12/2009
HIP 29711	–	4.31	280.4	239.6	K	2.62	1.80	0.73	0.41	04/11/2007
HIP 29852	–	0.22	13.4	210.8	K	2.00	1.95	0.94	0.48	10/11/2005
HIP 30419	AB	12.19	456.9	28.8	K	1.87	2.05	1.19	0.58	01/09/2009
HIP 31167	–	4.50	188.2	89.8	K	3.83	1.68	0.52	0.31	24/01/2002
HIP 33018	\star	2.37	137.6	295.3	K	5.43	2.50	0.70	0.28	05/02/2010
HIP 33018	\star	21.13	1224.8	297.8	K	8.46	2.50	0.19	0.08	05/02/2010
HIP 35350	–	9.80	303.1	33.8	K	4.09	2.39	0.61	0.26	12/04/2008
HIP 41375	\star	10.58	529.1	95.7	K	6.27	1.83	0.20	0.11	08/12/2011
HIP 42313	AB	2.71	133.3	262.7	K	5.56	2.59	0.44	0.17	27/01/2007
HIP 43584	AB	5.17	333.2	275.5	K	4.03	2.03	0.62	0.31	09/12/2011
HIP 44127	AB	2.39	34.7	78.4	K	4.35	1.69	0.43	0.25	05/02/2010
HIP 44127	AC	1.89	27.5	86.7	K	4.39	1.69	0.43	0.25	05/02/2010
HIP 45001	AB	17.72	1151.1	146.8	K	2.84	2.07	0.90	0.43	12/01/2005
HIP 45001	AC	17.51	1137.9	147.6	K	2.67	2.07	0.95	0.46	12/01/2005
HIP 45688	AB ^b	2.62	100.4	224.5	K	1.23	2.19	1.61	0.74	12/04/2008
HIP 47204	–	0.70	50.4	9.1	K	0.05	1.91	1.89	0.99	18/01/2006
HIP 47479	–	0.10	5.7	300.2	K	0.08	2.18	2.10	0.96	15/02/2008
HIP 48319	–	11.78	419.8	295.4	K	5.78	2.20	0.44	0.20	12/04/2008
HIP 48763	–	3.63	244.8	153.0	K	2.47	1.82	0.86	0.47	08/06/2010
HIP 51200	–	2.44	161.3	304.4	K	3.18	1.96	0.72	0.37	04/02/2010
HIP 51384	–	2.08	84.3	212.4	K	4.54	1.69	0.38	0.23	12/04/2008
HIP 51907	\star	6.92	425.9	95.8	H	5.74	1.64	0.23	0.14	14/06/2008
HIP 51907	\star	7.16	440.6	95.1	H	5.66	1.64	0.25	0.15	14/06/2008
HIP 55266	– ^c	0.90	52.9	145.0	K	5.61	2.33	0.43	0.18	23/07/2010
HIP 55705	–	4.98	125.6	93.1	K	2.94	1.81	0.75	0.41	05/02/2010
HIP 56034	AB	5.46	356.1	354.2	K	1.87	2.32	1.14	0.49	23/07/2010
HIP 56083	\star	9.17	616.4	232.4	H	6.78	1.88	0.13	0.07	14/06/2008
HIP 57013	\star	8.44	552.4	182.4	K	4.52	2.35	0.49	0.21	07/02/2005
HIP 57562	AD ^c	2.98	176.2	293.4	K	5.90	2.24	0.25	0.11	04/01/2006
HIP 59923	–	8.45	464.1	281.8	H	3.34	1.94	0.68	0.35	14/06/2008
HIP 61498	AB	7.82	569.3	225.3	K	2.73	2.53	0.45	0.18	07/03/2005
HIP 64979	\star	10.54	663.8	167.4	K	8.17	1.86	0.10	0.05	05/02/2010
HIP 65241	–	0.33	20.8	197.0	K	3.06	2.05	0.64	0.31	08/02/2005

Table 6: Binary companions identified within the adaptive optics observations

HIP	WDS Desig.	ρ (arcsec)	a_{proj} (au)	θ (deg.)	Band	Δm (mag)	M_1 (M_\odot)	M_2 (M_\odot)	q	Date
HIP 65477	CaCb	1.07	26.9	208.9	H	5.80	2.30	0.33	0.14	11/04/2008
HIP 66223	AaAb	1.38	94.7	187.7	K	5.66	1.84	0.23	0.13	13/07/2008
HIP 66249	–	1.79	41.0	154.1	K	6.53	2.14	0.17	0.08	05/02/2010
HIP 66458	AB	1.76	107.0	101.7	H	1.81	2.23	1.58	0.71	05/05/2001
HIP 67782	★	5.28	347.0	122.0	K	5.37	1.97	0.34	0.17	05/02/2010
HIP 69483	–	13.55	678.7	235.5	H	2.42	2.38	1.17	0.49	11/04/2008
HIP 69592	–	4.06	243.2	174.7	H	5.25	1.75	0.20	0.11	12/07/2008
HIP 69995	★	3.80	279.1	226.7	K	3.46	2.16	0.66	0.31	30/06/2004
HIP 70022	★	1.84	116.3	53.4	H	6.45	1.84	0.18	0.10	07/06/2001
HIP 70400	★	3.42	166.6	244.1	K	5.39	2.07	0.34	0.16	08/02/2005
HIP 70931	★	0.60	37.6	169.6	K	4.63	1.77	0.23	0.13	30/06/2004
HIP 76878	AB	2.39	126.8	85.9	K	5.48	1.84	0.27	0.15	13/07/2008
HIP 76952	–	0.68	29.8	112.7	H	1.11	2.50	1.77	0.71	11/04/2008
HIP 77660	–	0.25	11.7	71.9	K	1.49	2.05	1.15	0.56	30/06/2004
HIP 80170	★	8.33	491.8	176.1	K	6.95	2.50	0.46	0.18	05/02/2010
HIP 80628	AaAb	0.67	28.7	22.6	K	2.07	1.92	0.92	0.48	12/04/2008
HIP 80953	–	16.30	1129.8	195.6	K	2.36	2.13	1.02	0.48	24/07/2008
HIP 82321	AB	2.08	115.1	37.8	H	2.69	2.31	1.01	0.44	12/07/2008
HIP 82321	AC	1.83	101.4	33.7	H	3.07	2.31	0.91	0.39	12/07/2008
HIP 84012	AB	0.58	15.6	239.8	K	0.50	2.52	2.21	0.88	12/04/2008
HIP 84379	AB ^c	12.18	280.6	285.5	K	4.56	2.15	0.46	0.21	25/07/2008
HIP 85822	★	4.50	237.4	67.3	K	7.56	2.55	0.16	0.06	01/09/2009
HIP 87813	★	1.88	138.8	60.2	K	6.66	2.11	0.17	0.08	27/06/2004
HIP 88726	–	1.75	73.4	3.6	K	0.12	1.43	1.41	0.99	02/07/2009
HIP 88771	AB	24.88	662.6	297.7	K	6.35	2.08	0.21	0.10	05/02/2010
HIP 90156	AB	3.77	212.9	348.3	H	2.05	2.23	1.10	0.49	12/07/2008
HIP 91919	AB	2.36	117.3	347.6	K	0.57	2.13	1.76	0.83	19/06/2008
HIP 91926	CD ^d	2.36	112.4	259.0	K	0.00	1.99	1.99	1.00	19/06/2008
HIP 93506	AB	0.19	5.3	31.1	H	1.49	2.51	1.74	0.69	14/06/2008
HIP 93747	AB	7.27	185.1	46.6	K	4.87	2.93	0.50	0.17	17/11/2007
HIP 95077	★	4.67	258.7	326.6	K	7.07	1.87	0.15	0.08	27/06/2008
HIP 95077	★	4.74	262.5	321.8	K	6.98	1.87	0.16	0.09	27/06/2008
HIP 96313	★	15.30	927.7	101.5	H	1.39	1.42	0.97	0.68	12/07/2008
HIP 97423	★	4.64	303.7	189.7	K	4.20	1.93	0.49	0.25	18/06/2008
HIP 98103	–	2.83	190.4	184.4	K	5.27	2.39	0.40	0.17	18/06/2008
HIP 103298	AaAb	0.22	13.3	115.7	K	2.96	2.06	0.81	0.39	08/09/2008
HIP 104521	AB	0.80	29.2	257.4	H	2.78	1.89	0.87	0.46	14/06/2008
HIP 106711	–	6.89	453.6	57.0	K	8.62	2.20	0.12	0.05	08/09/2008
HIP 107302	★	4.29	227.4	229.0	K	4.09	1.77	0.49	0.28	24/07/2008
HIP 109667	–	1.10	69.8	284.4	K	4.04	1.86	0.51	0.27	25/06/2010
HIP 109667	★	5.14	326.1	181.4	K	7.49	1.86	0.10	0.05	10/09/2008
HIP 109857	AaAb	0.44	11.5	84.0	H	3.95	1.87	0.57	0.30	14/06/2008
HIP 110787	–	0.29	18.1	211.1	K	3.89	2.00	0.51	0.26	17/09/2008
HIP 111674	★	14.74	776.0	214.8	K	5.64	2.20	0.45	0.21	08/09/2008
HIP 113048	AB	0.82	46.4	234.9	K	0.89	1.83	1.32	0.72	31/08/2009
HIP 116611	AaAb	0.95	66.6	173.1	K	5.93	2.34	0.28	0.12	29/09/2008
HIP 117452	AB ^b	3.64	153.4	237.5	K	3.75	2.47	0.58	0.23	30/08/2009
HIP 118092	★	0.35	23.4	328.8	K	3.05	2.04	0.71	0.35	04/01/2006

★ – A newly resolved binary without a designation assigned within the WDS catalogue.

a – HIP 4979 B is resolved into a binary system itself.

b – The secondary in this pair is a known binary which is unresolved within the AO observations

c – The primary in this pair is a known binary which is unresolved within the AO observations

d – HIP 91926 CD is a wide CPM companion to HIP 91919 AB.

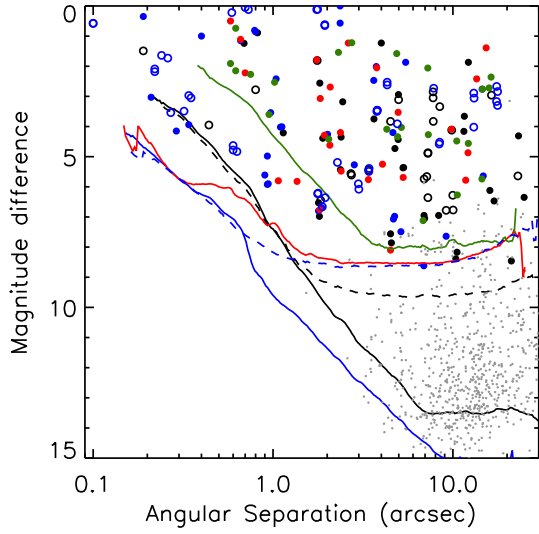


Figure 7. The average sensitivity of the observations obtained using KIR at the CFHT (black solid curve), NIRI at Gemini North (blue solid curve), PHARO at Palomar (red solid curve), IRCAL at the Lick Observatory (green solid curve), and observations obtained from the CFHT/KIR (black dashed curve), and ESO/NaCo (blue dashed curve) science archives. Companion candidates have been coloured corresponding to the instrument with which they were detected, with open circles corresponding to the two archive sources. Those companion candidates which fail the statistical criterion described in this section, or have mass ratios of $q < 0.1$ are denoted by small grey points. Duplicate observations of the same companion have not been removed from this figure.

Table 7: Binary companions identified within the astrometric search

HIP	CPM Companion	WDS Desig.	ρ (arcsec)	a_{proj} (au)	$\log a$	θ (deg.)	ΔK (mag)	M_1 (M_\odot)	M_2 (M_\odot)	q
HIP 2355	2M J00300625+2948173	*	192.1	12,057.2	4.08	355.8	8.04	2.20	0.14	0.06
HIP 12489	BD+26 443B	AB	28.9	2,048.9	3.31	0.8	2.87	2.32	0.93	0.40
HIP 19990	HD 284336	AB	180.0	5,209.7	3.72	118.4	2.45	1.41	0.47	0.33
HIP 21547	GJ 3305	AC	66.5	1,956.8	3.29	162.5	1.88	1.39	0.62	0.45
HIP 22300	TYC 3737-1375-1	*	669.1	35,033.6	4.54	142.4	2.44	1.61	0.75	0.47
HIP 23585	2M J05041356+4547206	AB	44.5	2,724.4	3.44	321.8	3.37	1.42	0.25	0.17
HIP 23875	2M J05074827-0508303	*	203.5	5,575.9	3.75	11.6	5.98	2.44	0.43	0.18
HIP 45688	2M J09185718+3649084	*	98.7	3,778.4	3.56	53.1	6.82	2.19	0.25	0.11
HIP 51200	2M J10273634+4135220	*	102.1	6,750.9	3.83	114.2	6.31	1.96	0.20	0.10
HIP 55266	HIP 55316	*	500.1	29,417.5	4.47	127.5	1.72	2.33	1.37	0.59
HIP 63320	2M J12585275+2809512	*	612.6	43,143.2	4.63	155.9	5.62	1.69	0.10	0.06
HIP 65728	HIP 65756	CA	182.6	13,033.3	4.12	110.2	1.05	2.37	1.55	0.65
HIP 69713	HD 234121	AB	39.0	1,133.7	3.05	32.8	1.97	1.81	0.80	0.44
HIP 74000	2M J15071551+1827568	*	110.3	7,967.2	3.90	321.3	2.92	2.09	0.73	0.35
HIP 76878	2M J15413725+1828082	AC	249.1	13,220.0	4.12	274.1	2.77	1.84	0.74	0.40
HIP 80883	BD+02 3118C	AC	119.0	6,316.1	3.80	169.5	4.78	2.42	0.64	0.26
HIP 85829	HIP 85819	AB	62.2	1,895.9	3.28	311.2	0.08	1.70	1.67	0.98
HIP 85922	2M J17332793-0546538	*	135.6	6,524.5	3.81	192.1	5.05	1.84	0.33	0.18
HIP 86263	2M J17383714-1514293	*	1,059.4	34,197.7	4.53	57.8	7.63	2.20	0.17	0.08
HIP 90156	HD 238865	AC	88.7	5,007.3	3.70	19.5	1.77	2.23	1.18	0.53
HIP 93747	2M J19065609+1340323	*	1,494.5	38,048.5	4.58	116.9	8.14	2.93	0.14	0.05
HIP 97421	CD-56 7835	AB	101.9	5,049.6	3.70	333.3	2.10	1.96	0.97	0.50
HIP 106786	2M J21372826-0755550	*	375.6	20,567.9	4.31	221.8	6.54	2.39	0.28	0.12
HIP 111674	TYC 3632-1527-1	*	832.6	43,822.0	4.64	190.7	4.11	2.20	0.72	0.33

* – A newly resolved binary without a designation assigned within the WDS catalogue.

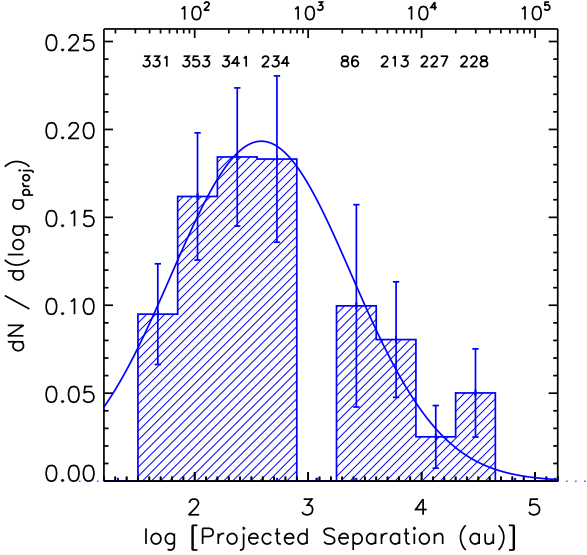


Figure 9. The final separation distribution was created from a synthesis of six subsamples, minimizing the biases introduced by a non-uniform level of completeness to companions within the adaptive optics observations and photographic plates. The separation distribution is constructed from two distinct data sets, the companion candidates resolved within the adaptive optics observations ($30 - 800$ au), and the common proper motion companions detected within the photographic plates ($1,800 - 45,000$ au). The number of stars comprising the subsample used to estimate the frequency of companions within each bin of the distribution are given above the corresponding bin of the histogram. The gap in the distribution is caused by the lack of sensitivity within the adaptive optics observations to wide binary systems ($a_{\text{proj}} \gtrsim 10^3$ au), and the saturation of the bright targets within the digitised photographic plates ($a_{\text{proj}} \lesssim 10^3$ au). Assuming a log-normal distribution, as measured in the separation distribution for companions to solar-type stars (Raghavan et al. 2010), the location of the peak of the distribution was estimated as $\log a_{\text{proj}} = 2.59 \pm 0.13$, corresponding to $a_{\text{proj}} = 387^{+132}_{-98}$ au, with a width of $\sigma_{\log a_{\text{proj}}} = 0.79 \pm 0.12$.

6.1 Identified companion candidates

The companions identified both within the AO observations and from a search for CPM companions, are plotted as a function of projected physical separation and mass ratio in Fig. 8. A total of 108 companion candidates satisfying the 5 per cent statistical criterion with mass ratios of $q \geq 0.05$, corresponding to a companion mass of $0.08 M_{\odot}$ around a $1.5 M_{\odot}$ primary, were identified within the high-resolution AO observations. The observed and derived parameters of each resolved companion is listed in Table 6. The companions span a range of separations between 0.08 and 23.2 arcsec, and secondary masses spanning from A-type companions ($q \approx 1$) to late M-type companions at the bottom of the main sequence ($q \approx 0.05$). Of the 113 identified companions within the AO observations, 51 were newly resolved as a part of the VAST survey (De Rosa et al. 2011, 2012), 33 of which are presented for the first time within this paper. These 113 AO imaging companions were complemented by an additional 24 CPM companions, the observed and derived parameters of which are listed in Table 7.

6.2 Separation distribution

The binary separation distribution was constructed over eight equally wide bins in $\log a_{\text{proj}}$ – four bins spanning $\log a_{\text{proj}} =$

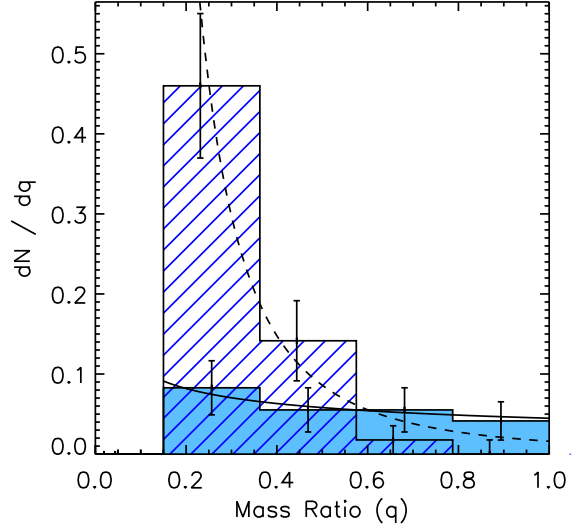


Figure 10. The q -distribution of companions resolved within this study with separations of $30 - 125$ au (filled histogram) and $125 - 800$ au (line-filled histogram). A power law has been fit to the two cumulative distributions, with a power law index of $\Gamma = -0.5^{+1.2}_{-1.0}$ for the inner distribution (solid curve), and $\Gamma = -2.3^{+1.0}_{-0.9}$ for the outer distribution (dashed curve). The distribution shows a greater abundance of lower mass companions within the outer distribution, with the inner distribution relatively flat for companions with $q \geq 0.15$.

$1.5 - 2.9$ (approx. $30 - 800$ au) for the AO companions, and four bins spanning $\log a_{\text{proj}} = 3.25 - 4.65$ (approx. $1,800 - 45,000$ au) for the wide CPM companions. For each bin, the subsample of targets used to determine the frequency of companions within that bin is the set of targets with sensitivity covering 95 per cent of the companion phase space. Within each bin, this companion phase space is defined by the inner and outer edge of the bin, and a mass ratio range of $q \geq 0.1$. The frequency within each bin was thus determined from the number of companions with separations within the inner and outer edges of the bin, resolved around targets within the subsample described previously. As the majority of the orbital parameters for each resolved system are not known, the separations within this study are expressed as projected separations, without applying a correction factor to estimate the true semi-major axis (Kuiper 1935; Couteau 1960).

The A-type star binary separation distribution is shown in Fig. 9, with the number of targets used to determine the frequency within each bin listed. Similar to previous multiplicity surveys (Duquennoy & Mayor 1991; Raghavan et al. 2010), a log-normal function was fitted to the measured separation distribution. The resulting fit has a peak located at $\log a_{\text{proj}} = 2.59 \pm 0.13$, corresponding to $a_{\text{proj}} = 387^{+132}_{-98}$ au, and a width of $\sigma_{\log a_{\text{proj}}} = 0.79 \pm 0.12$. The measured separation distribution is fit well by a log-normal function, with a slight over-abundance of CPM companions at separations of $4.25 \leq \log a_{\text{proj}} < 4.65$.

6.3 Mass ratio distribution

The mass ratio of each companion resolved within this study is shown as a function of projected separation in Fig. 8. The apparent deficiency of $q > 0.7$ companions resolved beyond ~ 100 au suggests that the shape of the mass ratio (q -) distribution may be

dependent on the projected separation range over which it is constructed. In order to test this, two q -distributions were constructed from the AO-resolved companions between 30 – 800 au. An inner and an outer q -distribution were constructed, with the dividing separation marched from 30 to 800 au in steps of $\log a_{\text{proj}} = 0.05$. The statistical similarity of the two distributions at each dividing separation was determined using a two-sided Kolmogorov-Smirnov (KS) test. A minimum value of the KS statistic was found at a separation of $\log a_{\text{proj}} = 2.1$ (125 au), with the inner (30 – 125 au) and outer (125 – 800 au) q -distributions being statistically distinct with a KS statistic of 3.47×10^{-3} . To minimize bias introduced by contamination from background stars falsely identified as companions, which will be most significant at the lowest mass ratios, only those companions with a mass ratio of $q \geq 0.15$ were considered when constructing the q -distributions.

The two resulting q -distributions, an inner distribution consisting of companions with separations of $\log a_{\text{proj}} = 1.5 – 2.1$ (30 – 125 au) and an outer distribution with $\log a_{\text{proj}} = 2.1 – 2.9$ (125 – 800 au), are shown in Figure 10. The inner q -distribution, comprising 18 companions resolved around 341 targets, is consistent with a flat distribution, while the outer q -distribution, comprising 35 companions resolved around 266 targets, shows a significant increase in companion fraction as a function of decreasing mass ratio.

6.4 Companion star and multiplicity fractions

There are two different quantities which can be used to express the fraction of stars within multiple systems; the multiplicity fraction (MF; Reipurth & Zinnecker 1993), defined as

$$\text{MF} = \frac{B + T + Q \dots}{S + B + T + Q \dots} \quad (1)$$

and the CSF (Goodwin et al. 2004), defined as

$$\text{CSF} = \frac{B + 2T + 3Q \dots}{S + B + T + Q \dots} \quad (2)$$

where B , T and Q are the number of binary, triple and quadruple systems, respectively. From our AO observations, the CSF between 30 – 800 au ($\text{CSF}_{30-800\text{au}}$) was calculated by summing the inner four bins of the separation distribution in Fig. 9, leading to a CSF of 21.9 ± 2.6 per cent for companions with $q \geq 0.1$. As a large-subset of the AO observations were sensitive to stellar companions with $q < 0.1$, a lower limit of the $\text{CSF}_{30-800\text{au}}$ value including all stellar companions with $q \geq 0.05$ was estimated to be 26.0 per cent. The CSF over a wider separation range (30 – 10,000 au; $\text{CSF}_{30-10,000\text{au}}$), calculated by integrating the fit to the separation distribution shown in Fig. 9, was estimated to be 33.8 ± 2.6 per cent. These three estimates of the CSF are given in Table 8, alongside the separation range over which they were constructed, and the mass range of companions included.

The total CSF for A-type stars, considering companions at all possible separations, can be estimated by combining the $\text{CSF}_{30-10,000\text{au}}$ measurement from this study with the results of previous spectroscopic surveys. These surveys typically measured the frequency of companions to three categories of A-type stars; normal (30.9 ± 7.5 per cent; Abt 1965), metallic-lined (63.7 ± 8.4 per cent; Carquillat & Prieur 2007) and chemically peculiar (43.0 ± 6.0 per cent; Carrier et al. 2002). When weighted according to the fraction of the VAST sample within each of these categories (normal - 85.3 per cent, Am - 11.5 per cent, Ap - 3.2 per cent), the weighted frequency becomes 35.1 ± 6.5 per cent. The total CSF for A-type stars was then calculated as the sum of the $\text{CSF}_{30-10,000\text{au}}$

measurement from this study, and the weighted frequency from the spectroscopic surveys, a total of 68.9 ± 7.0 per cent (Table 8). Although not significantly higher than the value for solar-type primaries, measured to be 61.0 ± 3.7 per cent (Raghavan et al. 2010), the completeness of the spectroscopic surveys has not been assessed, and binaries with separations of the order of 10 au may have been missed due to their small radial velocity variations over the time period in which they were observed spectroscopically.

Additionally, a lower limit of the MF over all companion separations was estimated for the sample of 156 A-type stars which both have AO observations and were searched for wide CPM companions, providing sensitivity to companions over the widest separation range, and crucial for the best assessment of the frequency of higher order multiples (described in Section 7.6). This lower limit of 43.6 ± 5.3 per cent, listed in Table 8, was calculated using the companions reported within Tables 6 and 7, combined with physically associated binaries recorded within the Washington Double Star Catalog (WDS; Mason et al. 2001), the Ninth Catalogue of Spectroscopic Binary Orbits (SB9; Pourbaix et al. 2004) and eclipsing binaries within the General Catalogue of Variable Stars (GCVS; Samus et al. 2009), which are all listed in Table 9.

7 DISCUSSION

7.1 Comparison samples of different masses and ages

In order to place the results of this volume-limited multiplicity of A-type stars into context, it is necessary to consider samples against which the results will be compared. The results of the VAST survey are compared to volume-limited multiplicity surveys of lower mass solar-type, M-dwarf and brown dwarf primaries (Fischer & Marcy 1992; Reid et al. 2008; Raghavan et al. 2010), allowing for an investigation of the various multiplicity statistics as a function of primary mass. The results cannot be easily compared to more massive stars within the field given the very small number of stars with spectral type earlier than B7 within 75 pc (Abt 2011). The VAST results are also compared with B- and A-type stars within the nearby ScoCen OB association (Kouwenhoven et al. 2005), allowing for a comparison of the multiplicity statistics between cluster and field populations. For each of these comparison samples, the separation and mass ratio of each companion is known, so a fair comparison can be made between the various surveys over a common range of companion separation and mass ratios (Table 8). More recent studies of M-dwarf multiplicity have not been included as comparison samples as these surveys do not have sensitivity to companions with separations $\gtrsim 200$ au (Bergfors et al. 2010; Janson et al. 2012).

7.2 Multiplicity as a function of primary mass

7.2.1 Observed trend

The A-type star CSF was calculated and compared with other samples over two separation ranges – the 30 – 800 au range continuously covered by the AO data, and the 30 – 10,000 au range which was estimated from the fit to the separation distribution shown in Fig. 9. The $\text{CSF}_{30-800\text{au}}$ measured within the VAST survey is plotted alongside the observed $\text{CSF}_{30-800\text{au}}$ for solar-type (Raghavan et al. 2010), M-dwarf (Fischer & Marcy 1992) and B- and A-type Sco OB2 (Kouwenhoven et al. 2005) primaries in Fig. 11. The $\text{CSF}_{30-800\text{au}}$ values for these three literature surveys were restricted to only include companions with a mass ratio of

Table 8. Companion star and multiplicity fractions from various surveys

Spectral Type	Type	Separation range log [au]	Companion mass range	Value per cent
A	CSF	$1.5 \leq \log a_{\text{proj}} < 2.9$	$q \geq 0.10$	21.9 ± 2.6
A	CSF	$1.5 \leq \log a_{\text{proj}} < 2.9$	$q \geq 0.05$	≥ 26.0
A	CSF	$1.5 \leq \log a_{\text{proj}} < 4.0$	$q \geq 0.10$	33.8 ± 2.6
A	CSF	<i>all</i>	$M_2 \geq 0.08 M_\odot$	68.9 ± 7.0
A	MF	<i>all</i>	$M_2 \geq 0.08 M_\odot$	$\geq 43.6 \pm 5.3$
BA (ScoCen)	CSF	$1.5 \leq \log a_{\text{proj}} < 2.9$	$q \geq 0.10$	25.1 ± 3.6
BA (ScoCen)	CSF	$1.5 \leq \log a_{\text{proj}} < 2.9$	$q \geq 0.05$	≥ 28.1
FGK	CSF	$1.5 \leq \log a_{\text{proj}} < 2.9$	$q \geq 0.10$	19.6 ± 2.1
FGK	CSF	$1.5 \leq \log a_{\text{proj}} < 4.0$	$q \geq 0.10$	27.8 ± 2.5
FGK	CSF	<i>all</i>	$M_2 \geq 0.08 M_\odot$	61.0 ± 3.7
FGK	MF	<i>all</i>	$M_2 \geq 0.08 M_\odot$	46.0 ± 2.0
M	CSF	$1.5 \leq \log a_{\text{proj}} < 2.9$	$M_2 \geq 0.08 M_\odot$	17.1 ± 5.4
M	CSF	$1.5 \leq \log a_{\text{proj}} < 4.0$	$M_2 \geq 0.08 M_\odot$	24.6 ± 6.5
M	MF	<i>all</i>	$M_2 \geq 0.08 M_\odot$	42.0 ± 9.0
LT	CSF	$\log a_{\text{proj}} \geq 1.6$	$M_2 \geq 0.03 M_\odot$	≤ 2.3
LT	MF	<i>all</i>	$q \geq 0.20$	12.5 ± 3.0

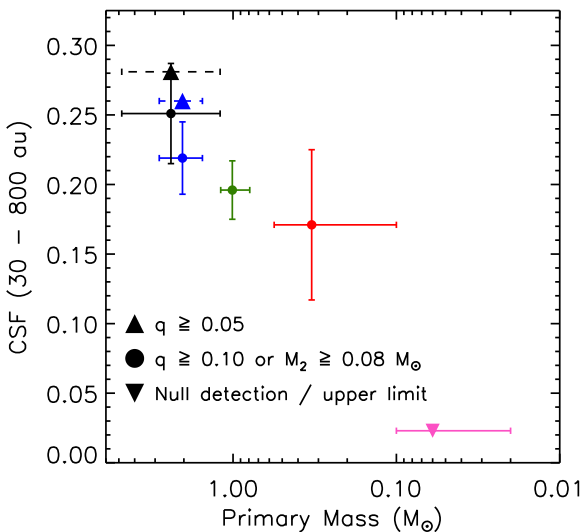


Figure 11. The CSF_{30–800au} measured within the separation range 30–800 au measured for, from left to right, Sco OB2 primaries (black point, Kouwenhoven et al. 2005), field A-type stars (blue point, this study), field solar-type stars (green point, Raghavan et al. 2010), field M-dwarf primaries (red point, Fischer & Marcy 1992). The upper limit for companions to brown dwarfs within this separation range is also shown (pink downward triangle, Allen et al. 2007). A lower limit on the CSF_{30–800au} including all stellar companions to A-type stars ($q \gtrsim 0.05$) was estimated by including companions resolved within this study with mass ratios within the range $0.05 \leq q < 0.1$ (blue upward pointing triangle, dashed error bars). Similarly, for the study of Sco OB2 primaries, the CSF including all stellar companions is plotted (black upward pointing triangle, dashed error bars).

$q \geq 0.1$, and projected separations between 30 and 800 au, ensuring a fair comparison between all surveys with a uniform mass ratio limit. For the surveys of nearby solar-type stars and Sco OB2 primaries, the CSF_{30–800au} value could be calculated directly from the table of companions presented within each study. For the sur-

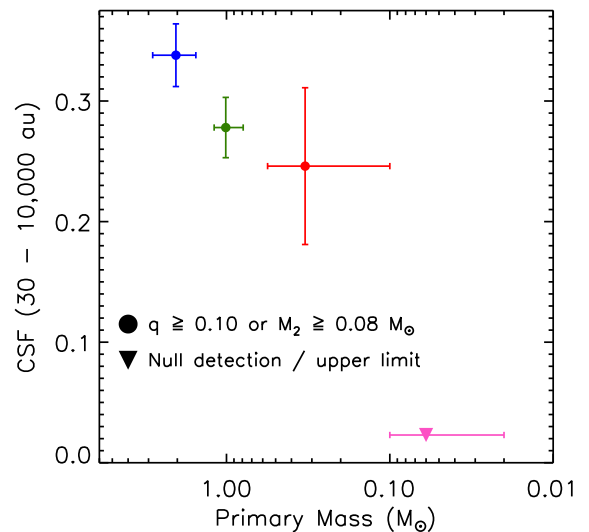


Figure 12. The CSF_{30–10,000au} is estimated from the log-normal fit to the separation distribution within the range 30–10,000 au for, from left to right, field A-type stars (this study, blue point), solar-type stars (green point, Raghavan et al. 2010) and field M-dwarf primaries (red point, Fischer & Marcy 1992). The upper limit for companions to brown dwarfs within this separation range is also shown (pink downward triangle, Allen et al. 2007).

vey of nearby M-dwarfs, the CSF_{30–800au} value was estimated from an integration of the frequency of companions per primary per au given over several discrete separation ranges (Fischer & Marcy 1992). In addition to the stellar results, the upper limit to the L-dwarf CSF beyond 40 au is plotted (Allen et al. 2007). The measured CSF for A-type primaries is similar to that of early-type stars within the young Sco OB2 stellar association (Kouwenhoven et al. 2005), when limited to a common separation and mass ratio range (Fig. 11).

While the uniform $q \geq 0.1$ limit reaches the bottom of the

Table 9. Companions listed within the literature used in the calculation of the lower limit of the multiplicity fraction

HIP	WDS Desig.	$\log P_d$	ρ (arcsec)	Reference	HIP	WDS Desig.	$\log P_d$	ρ (arcsec)	Reference
128	AB	0.98	—	Carquillat et al. (2003)	54746	—	—	3.80	Tokovinin (2012)
2578	AaAb	—	0.10	van den Bos (1927)	55266	—	0.41	—	Lloyd (1981)
3414	—	0.29	—	Mannino & Grubisich (1955)	57562	AaAb	—	0.40	McAlister et al. (1989)
6514	—	1.55	—	Fekel et al. (2011)	57606	—	4.69	—	Brendley & Mason (2006)
6686	—	2.88	—	Samus et al. (2009)	57646	—	0.44	—	Petrie (1926)
8588	AB	—	178.00	Tokovinin & Lépine (2012)	58001	AB	—	20276.12	Shaya & Olling (2010)
8903	—	2.03	—	Pourbaix (2000)	58758	—	1.39	—	Moore (1931)
9153	AB	—	37.10	Halbwachs (1986)	61932	AB	4.49	0.50	Malkov et al. (2012)
9480	AC	—	23.20	Mason et al. (2001)	61932	AD	—	2719.24	Shaya & Olling (2010)
9836	—	1.18	—	Jones (1931)	61937	AC	—	5590.10	Shaya & Olling (2010)
10064	—	1.50	—	Pourbaix (2000)	62983	—	—	< 0.10	Africano et al. (1975)
11486	—	—	0.10	Horch et al. (2008)	64692	—	—	0.60	McAlister et al. (1993)
11569	CaCb	—	0.40	Christou & Drummond (2006)	69483	BaBb	3.25	—	Kiyaeva (2006)
12706	AC	—	843.10	Alden (1924)	69483	AC	—	108.80	Tokovinin & Lépine (2012)
12828	—	3.08	—	Abt (1965)	69974	—	2.32	—	Stickland (1990)
13133	AaAb	0.08	—	Duerbeck & Haenel (1979)	70931	Aa1Aa2	1.07	—	Kaufmann & Klippel (1973)
15197	—	1.25	—	Abt & Levy (1985)	71075	AaAb	—	0.10	Morgan et al. (1978)
15197	—	—	1383.23	Shaya & Olling (2010)	72622	AD	—	8977.46	Shaya & Olling (2010)
16591	—	-0.04	—	Rucinski et al. (2005)	74000	—	3.47	0.10	Eggen (1946)
19893	—	—	—	Samus et al. (2009)	75695	—	3.58	—	Neubauer (1944)
20087	—	3.62	—	Pourbaix (2000)	76852	AB	3.90	0.10	Muterspaugh et al. (2010)
20713	—	3.72	—	Abt (1965)	76996	AB	—	65.90	Mason et al. (2001)
20894	—	2.15	—	Torres et al. (1997)	77233	AD	—	1643.04	Shaya & Olling (2010)
21029	—	—	249.80	Peterson et al. (1981)	80628	—	1.43	—	Gutmann (1965)
21039	—	1.77	—	Debernardi et al. (2000)	80628	AB	—	18227.26	Shaya & Olling (2010)
21273	—	2.69	—	Abt (1965)	80883	AB	4.67	—	Heintz & Strom (1993)
21402	Aa1Aa2	0.55	—	Lane et al. (2007)	84379	AaAb	—	0.10	Bonneau & Foy (1980)
21402	Ab1Ab2	0.90	—	Lane et al. (2007)	84606	—	—	0.92	Horch et al. (2011)
21402	AaAb	3.82	—	Lane et al. (2007)	85829	AaAb	1.58	—	Margoni et al. (1992)
21547	CaCb	—	0.20	Kasper et al. (2007)	86263	AaAb	—	0.30	Isobe et al. (1990)
21644	—	—	0.10	Horch et al. (2004)	86263	Aa1Aa2	0.36	—	Young (1910)
21673	—	1.59	—	Abt & Levy (1985)	87212	AaAb	—	0.10	McAlister et al. (1987)
22287	AaAb	—	0.40	Horch et al. (2011)	87212	AB	—	209.10	Lépine & Bongiorno (2007)
23296	AaAb	0.91	—	Fekel et al. (2006)	89925	—	0.74	—	Fekel et al. (2009)
23983	—	2.19	—	Debernardi et al. (2000)	90156	AaAb	—	—	Frost (1924)
24340	—	—	0.10	Mason et al. (1999)	90156	CaCb	0.43	—	Halbwachs et al. (2012)
26309	AB	—	1211.97	Shaya & Olling (2010)	91919	ABCD	—	208.80	Shaya & Olling (2010)
26563	—	2.65	—	Abt (1965)	91971	AaAb	0.63	—	Abt & Levy (1985)
28614	AaAb	0.65	—	Muterspaugh et al. (2008)	91971	AD	—	41.10	Shaya & Olling (2010)
28614	BaBb	0.68	—	Muterspaugh et al. (2008)	92024	BaBb	—	0.20	Biller et al. (2007)
29850	AaAb	3.53	—	Hartkopf et al. (1996)	92024	AB	—	71.40	Mason et al. (2001)
30060	—	—	—	Samus et al. (2009)	98103	AB	0.52	—	Lucy & Sweeney (1971)
33202	AB	5.85	7.40	Hopmann (1974)	101093	—	2.92	—	Abt (1962)
33202	AD	—	152.50	Tokovinin & Lépine (2012)	101800	—	1.04	—	Harper (1935)
41081	AB	—	1119.82	Shaya & Olling (2010)	106786	—	3.90	—	Abt (1965)
42806	AaAb	—	—	Lee (1910)	107556	—	0.01	—	Batten & Fletcher (1992)
43970	AB	—	975.90	Shaya & Olling (2010)	113048	AaAb	1.38	—	Margoni et al. (1992)
45688	BaBb	—	0.20	McAlister et al. (1993)	113996	AB	3.90	—	Hartkopf et al. (1996)
54214	—	—	0.60	Tokovinin (2012)	116611	Aa1Aa2	-0.30	—	Rucinski et al. (2005)

main sequence for the solar-type and lower mass samples, this limit does not include all stellar companions to A-type stars. To compare the $\text{CSF}_{30-800\text{au}}$ values with a common companion mass limit, the q limit for the A-type stars needs to be extended to include systems with $q \geq 0.05$. For the VAST and Sco Cen OB2 samples, the $\text{CSF}_{30-800\text{au}}$ was calculated with a limit of $q \geq 0.05$, and the values are listed in Table 8 and plotted in Fig. 11. These values represent lower limits to the $\text{CSF}_{30-800\text{au}}$, since the data are not uniformly sensitive to companions at these extreme mass ratios.

Extending the range of companion separations considered, the $\text{CSF}_{30-10,000\text{au}}$ values were estimated from the fit to the ob-

served companions to solar-type (Raghavan et al. 2010) and M-dwarf (Fischer & Marcy 1992) primaries, and are listed in Table 8 and plotted in Fig. 12. A similar value was not calculated for the Sco OB2 primaries, as the observations were only sensitive to companions with separations within 1600 au. The increase in the CSF as a function of increasing primary mass is apparent over both separation ranges, albeit within the large uncertainty of the CSF for M-dwarf primaries (Figs 11 and 12).

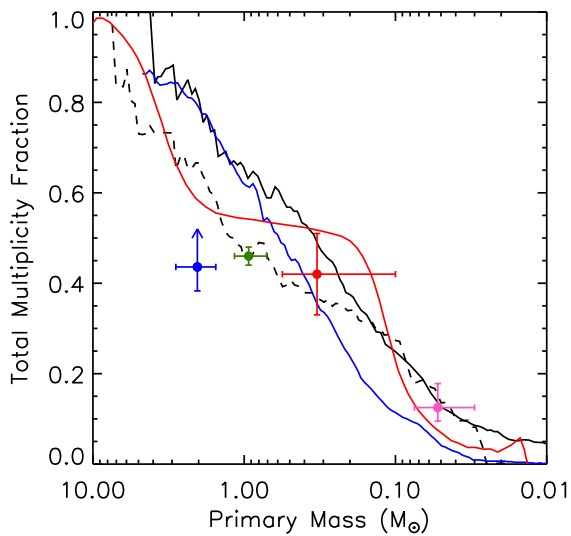


Figure 13. The measured multiplicity fraction of four stellar clusters simulations as a function of primary mass. The results of barotropic and radiation hydrodynamical simulations are plotted as black solid and dashed lines, respectively (Bate 2009, 2012), a numerical Monte Carlo calculation looking at small- N interactions are plotted as a solid blue line (clusters with $N < 10$ stars; Sterzik & Durisen 2003), and an ensemble of small N -body clusters are plotted as a solid red line (a ring of $N = 6$ stars, with mass dispersion of $\sigma_{\log M} = 0.2$; Hubber & Whitworth 2005). Overplotted for reference are, from left to right, the lower limit on the multiplicity fraction of A-type stars measured within this survey, and the observed multiplicity fraction of nearby solar-type (Raghavan et al. 2010), M-dwarf (Fischer & Marcy 1992) and brown dwarf (Reid et al. 2008) primaries.

7.2.2 Theoretical predictions

Hydrodynamical (Bate 2009, 2012) and numerical N -body (Durisen et al. 2001; Sterzik & Durisen 2003; Hubber & Whitworth 2005) simulations of stellar clusters predict that the total multiplicity increases with increasing primary mass with different functional forms, as shown in Fig. 13. Both types of models reproduce the observed trend of multiplicity, however some discrepancies are present when the predictions are examined over a specific mass range. For example, the tight constraint on the measurement of the MF of solar-type primaries is lower than the predictions emerging from the barotropic hydrodynamical simulation (Bate 2009), and numerical N -body interactions (Sterzik & Durisen 2003; Hubber & Whitworth 2005), while being consistent with the radiation hydrodynamical simulation (Bate 2012). As there was not uniform sensitivity to stellar companions to A-type primaries over the full range of companion separations, only a lower limit to the MF was estimated. Combining the results of the VAST survey with known binaries resolved in previous interferometric, spectroscopic and AO imaging surveys, leads to a lower limit on the total MF shown in Fig. 13. The comparison to the various simulations would suggest a significant number of companions interior to ~ 30 au remain unresolved.

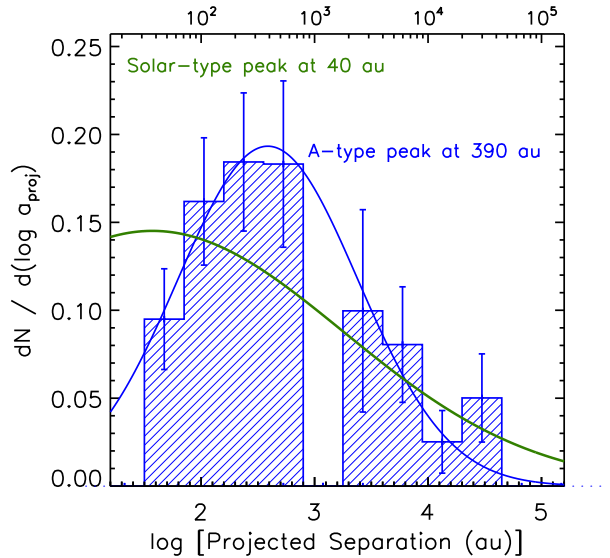


Figure 14. The separation distribution (blue histogram) and corresponding log-normal fit (blue curve), are plotted alongside the log-normal fit to the separation distribution of companions resolved within the Raghavan et al. (2010) survey (green curve).

7.3 Separation distribution

7.3.1 Comparison with previous observations

The trend of a wider separation peak to the distribution as a function of increasing primary mass is consistent with previous multiplicity surveys of brown dwarf (Burgasser et al. 2006) and M-dwarf (Fischer & Marcy 1992) primaries (Figs 14 and 15). The log-normal fit to the measured distribution is also significantly narrower than the solar-type companion separation distribution, with a standard deviation of $\sigma_{\log a} = 0.79 \pm 0.12$ compared to $\sigma_{\log a} \approx 1.68$ for solar-type companions (Fig. 14), although the fit to the solar-type separation distribution included companions at all separations. Extrapolating the fit to the A-type star companion separation distribution to closer separations suggests a complete lack of companions with separations of $\log a_{\text{proj}} < 0$, inconsistent with known spectroscopic companions to normal and metallic-lined A-type stars (Abt 1965; Carquillat et al. 2003). These spectroscopic systems are not included within the separation distribution plotted in Fig. 9, as the companion mass ratio sensitivity limits are not quantified. It is evident that further investigations are required in order to fully constrain the shape of the separation distribution, with wide-field direct imaging filling the gap in the separation distribution between the AO observations and photographic plates presented within this work, and observations with high-order AO systems providing sensitivity to companions of mass ratio $q \geq 0.1$ with projected separations between 10 and 100 au. For companions at separations interior to the angular resolution of AO instruments, radial velocity monitoring provides the only method sensitive enough to detect companion with mass ratios as extreme as $q = 0.1$, with current-generation interferometric techniques restricted by their limited dynamical range.

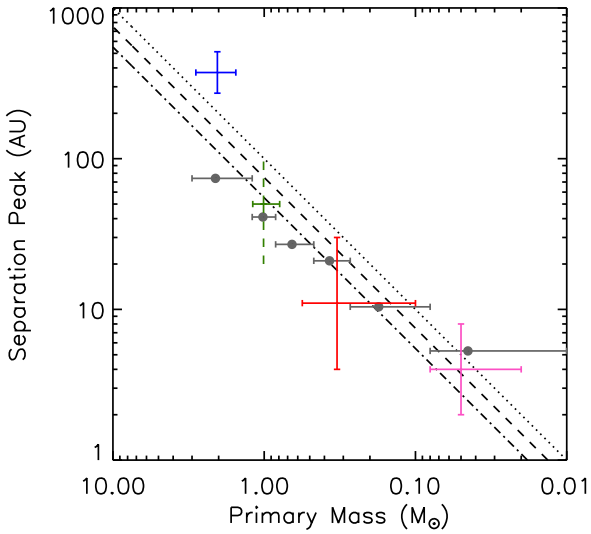


Figure 15. The location of the peak of the separation distribution as a function of primary mass for, black data points from left to right; A-type (this study), solar-type (Raghavan et al. 2010), M-dwarf (Fischer & Marcy 1992) and brown dwarf (Burgasser et al. 2006) primaries. As the uncertainty in the location of the peak of the separation distribution was not provided by Raghavan et al. (2010), the corresponding vertical error bar is dashed. The observations show a clear trend of an increase in the peak of the distribution as a function of primary mass, similar to the theoretical predictions from dynamical simulations (grey points; Sterzik & Durisen 2003), and from models of secondary fragmentation (black lines; Whitworth & Stamatellos 2006).

7.3.2 Comparison with theoretical models

Simulations of dynamical interactions within stellar clusters and numerical calculations of companion formation through disc fragmentation both predict an increase in the location of the peak of the separation distribution as a function of increasing primary mass, and the different predictions are shown in Fig. 15 (Sterzik & Durisen 2003; Whitworth & Stamatellos 2006). These results are consistent with hydrodynamical simulations showing stellar binaries have a wider median separation (~ 26 au) than brown dwarf binaries (~ 10 au), although the latter result may be affected by the resolution limit of the calculation (Bate 2009).

Measurements of the position of the peak of the companion separation distribution for lower mass primaries are consistent with these predictions (Fischer & Marcy 1992; Burgasser et al. 2006; Raghavan et al. 2010), while the A-type star separation peak occurs at a wider separation than expected (Figure 15). Although this peak occurs at a significantly wider separation than that of resolved planetary-mass companions to nearby A-type stars (Kalas et al. 2008; Marois et al. 2008; Lagrange et al. 2009), the dynamical interaction between a disc and a companion at the typical separation of ~ 390 au may lead to a truncation of the disc to a radius as small as ~ 50 au (Artymowicz & Lubow 1994). Interior to the disc truncation radius, the perturbations induced by the companion may significantly affect the planet formation process (Nelson 2000; Kley & Nelson 2008). This would suggest that a majority of A-type star binaries, and as such a significant minority of A-type stars in general, may not be amenable to the formation of planetary-mass companions.

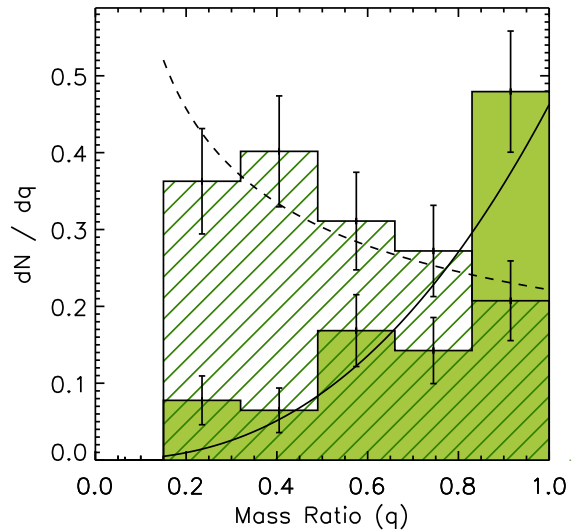


Figure 16. The q -distribution of companions resolved to solar-type stars, with separations ≤ 30 au (filled histogram), and those with separations > 30 au (line-filled histogram). The separation and mass ratio of each component were obtained from fig. 11 of Raghavan et al. (2010). The two populations are statistically distinct, with a KS statistic of 10^{-8} . A power law has been fit to the two cumulative distributions, with a power law index of $\Gamma = 2.5_{-1.3}^{+0.9}$ for the inner distribution (solid curve), and $\Gamma = -0.5_{-0.4}^{+0.5}$ for the outer distribution (dashed curve).

7.4 Mass ratio distribution

7.4.1 Comparison with previous observations

Determining how the q -distribution changes as a function of separation for different primary masses will allow for a greater insight into the various formation processes for binary companions which may dominate over different separation regimes. As the q -distribution for companions to A-type stars has been divided into two statistically distinct subsamples (Fig. 10); a similar technique was applied to the companions resolved around solar-type stars (Raghavan et al. 2010). The inner and outer subsamples were found to be most statistically distinct at a dividing separation of $\log a = 1.5$ (~ 30 au), with a KS statistic of 9.92×10^{-9} . The inner and outer q -distributions are plotted in Fig. 16, showing that lower mass companions to solar-type primaries are preferentially found in wider orbits. The cumulative q -distribution of these two distinct subsamples are plotted in Fig. 17, alongside the two cumulative distributions measured for companions to A-type primaries, and the functional form of the cumulative q -distribution of companions to brown dwarf primaries (Burgasser et al. 2006). By fitting a power law to each of the five distributions, the best-fitting power-law index was estimated and plotted as a function of separation (Fig. 18). This shows a trend of a greater frequency of lower mass companions at wider separations for both A-type and solar-type primaries, although the A-type comparison is made over a significantly narrower separation range. The cumulative q -distribution for companions to M-dwarf primaries is not plotted, although the results of recent surveys are consistent flat distribution between 1 and 200 au (Bergfors et al. 2010; Janson et al. 2012).

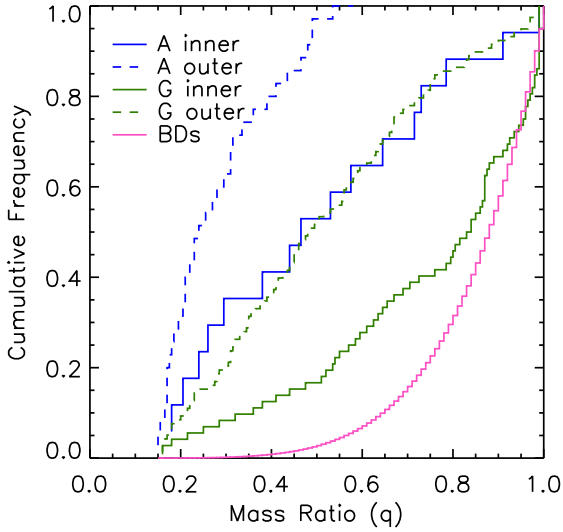


Figure 17. The cumulative q -distribution for companions resolved around A-type primaries, with separations of 30 – 125 au (blue solid histogram – inner distribution) and 125 – 800 (blue dashed histogram – outer distribution). The greater frequency of lower mass companions within the outer distribution is apparent. For solar-type primaries, a similar division into an inner and outer distribution was performed, with those companions with separations of ≤ 30 au (green solid histogram – inner distribution) and > 30 au (green dashed histogram – outer distribution). Each cumulative q -distribution only include those companions with mass ratio of $q \geq 0.15$. The functional form of the observed q -distribution for companions to brown dwarf primaries is also plotted, considering all companions resolved with separations ≥ 2 au (pink solid histogram, Burgasser et al. 2006).

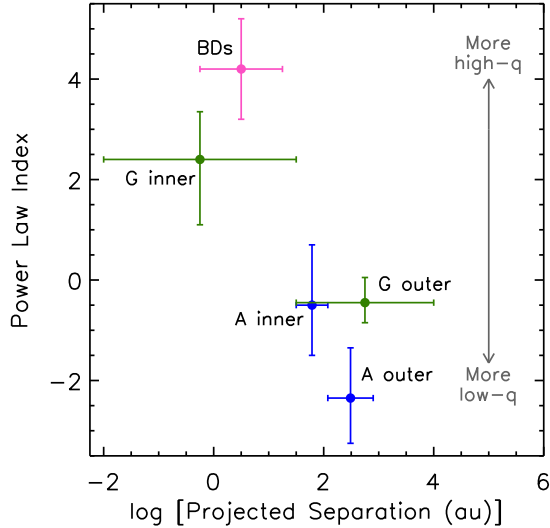


Figure 18. The power law index best fit to the cumulative q -distributions presented in Figure 17, for A-type primaries (blue points), solar-type primaries (green points) and brown dwarf primaries (pink point). The data are indicative of a trend of a greater frequency of equal-mass companions at closer separations, for both A-type and solar-type primaries.

7.4.2 Comparison with theoretical models

Two binary formation scenarios are thought to pre-dominate over the 30 – 10,000 au separation range to which this study is complete, the initial fragmentation of a pre-stellar molecular cloud (e.g. Boss & Bodenheimer 1979; Bonnell et al. 1991) and fragmentation of a large circumstellar disc (e.g. Adams et al. 1989; Bonnell 1994; Woodward et al. 1994). The initial fragmentation of a cloud prior to the formation of protostellar objects can produce binary systems with separations ranging between 10^1 and 10^4 au, with a wide range of companion mass ratios (Boss 1986; Bonnell et al. 1991; Bonnell & Bastien 1992; Bate et al. 1995). A scale-free fragmentation model, in which the companion q -distribution is independent of the initial clump mass (Clarke 1996), can be tested against the observations presented here. The initial fragmentation model predicts an MF which is weakly dependent on primary mass, and a mass ratio distribution which is independent, or weakly dependent on primary mass. These predictions are inconsistent with both the observed trend in multiplicity as a function of primary mass for stellar primaries (Figs 11 and 12), and the observed variation in the companion q -distribution between companions to solar-type and A-type primaries (Fig. 17). Star formation within a more clustered environment may introduce a dependence on primary mass, with more massive primaries having q -distributions skewed towards less massive companions (Bonnell & Bastien 1992; Bate 2001). Simulations of the dynamical decay of small clusters, formed through the fragmentation of an initial cloud (Sterzik & Durisen 1998), have produced companion q -distributions which are consistent with observed companion q -distributions, and its dependence on primary mass.

Subsequent to the fragmentation of an initial cloud the conservation of angular momentum causes the infall of material from the surrounding cloud to form a protostellar disc (Bonnell 1994). These discs can fragment to produce substellar and stellar companions, provided that a mechanism for the disc to become gravitationally unstable, and subsequently cool efficiently, is present (e.g. Kratter et al. 2010). This formation process is thought to be more important for more massive stars (Kratter 2011), due primarily to the large reservoir of material within the massive discs of these stars (e.g. Fukagawa et al. 2010). This process may lead to a significant number of disc-born lower mass companions to more massive stars (Kratter et al. 2010; Stamatellos et al. 2011), with the preferential equalisation of the mass ratios of those binaries formed at close separations (Bate & Bonnell 1997; Bate 2000).

The measured q -distribution presented within this study, with a greater abundance of lower mass companions around more massive stars, is consistent with predictions from both initial and disc fragmentation. The shape of the q -distribution for companions resolved between 30 to 800 au is consistent with a population of disc-born companions (Kratter et al. 2010), and such companions are within a separation range coincident with the extent of known circumstellar discs of pre-main sequence A-type stars (e.g. Dent et al. 2006; Hamidouche et al. 2006; Fukagawa et al. 2010). For the widest companions, formation via disc fragmentation is not possible, and the observed frequency of wide ($\geq 10^3$ au) binary companions is consistent with a population of companions formed through initial fragmentation (Bonnell & Bastien 1992). In reality, the observed population is likely a synthesis of, at least, these two types of fragmentation. Hydrodynamical simulations which incorporate both of these processes are able to produce companions over a wide range of separations (Bate 2009, 2012), consistent with the observed separation distribution for solar-type stars, although these

simulations are not yet large enough to include a statistically significant number of A-type stars.

7.5 Multiplicity of A-type star subsamples

Metallic-line (Am) A-type stars are distinct from normal A-type stars due to an overabundance of heavy elements within their observed spectra, with the notable exception of calcium and scandium (Boffin 2010). These anomalous abundances can be explained by diffusion within the stellar atmosphere (Michaud 1980; Talon et al. 2006), which can only occur for stars with rotational velocities of $v \lesssim 100 \text{ km s}^{-1}$ (Michaud et al. 1983). As they do not possess sufficiently strong magnetic fields to induce magnetic breaking (Conti 1970; Aurière et al. 2010), Am stars must either form with a lower rotational velocity than normal A-type stars, or this initial fast rotational velocity is reduced through the tidal breaking caused by an orbiting companion (Roman et al. 1948). In order to effectively reduce the rotational velocity of the primary necessary for diffusion to occur, the companion must be on a relatively short orbit with $P \lesssim 35 \text{ d}$ (Budaj 1997), consistent with the observed abundance of short-period spectroscopic companions to Am stars (Abt & Levy 1985; Carquillat & Prieur 2007). For the 50 stars within the VAST sample classified as metallic-lined within the SIMBAD data base, an MF of $58.0^{+6.5}_{-7.1}$ per cent was estimated based on a combination of those companions resolved in this study, and those previously reported within the literature. This is significantly higher than the multiplicity fraction for the sample of 371 normal (non-Am non-Ap) A-type stars, at $37.6^{+2.6}_{-2.4}$ per cent, a discrepancy which can be attributed to the relatively large number of known spectroscopic components to the Am stars within the VAST sample (e.g. Abt 1962; Abt & Levy 1985; Carquillat & Prieur 2007).

Like Am stars, chemically peculiar (Ap) A-type stars are also observed to have low rotational velocities (Abt et al. 1972). The low frequency of close binary companions to Ap stars is inconsistent with the tidal breaking mechanism used to explain the low rotational velocities of Am stars (Babcock 1958; Carrier et al. 2002), and instead an alternate mechanism involving magnetic breaking is thought to predominate (Abt & Snowden 1973). The strong magnetic fields measured in non-HgMn Ap stars precludes the presence of a close binary companion (Abt & Snowden 1973), consistent with the observed deficiency of binary companions with periods $\lesssim 3 \text{ days}$ (Carrier et al. 2002). With the full VAST sample, only 14 stars are classified as being chemically peculiar (Ap) within the SIMBAD data base. Combining those companions measured within this study with known literature companions (Table 9), we find an MF of $50.0^{+12.4}_{-12.4}$ per cent for this Ap subsample, somewhat larger than, but still consistent with, the MF of the non-Am non-Ap subsample of 371 stars of $37.6^{+2.6}_{-2.4}$ per cent.

Another subsample of A-type stars of particular note are those known to host extrasolar planets, of which two such examples exist within the VAST sample - β Pic (HIP27321; Lagrange et al. 2009) and HR 8799 (HIP 114189; Marois et al. 2008, 2010). No stellar companions were identified to either of these stars within the AO observations presented within this study, and no wide CPM companions were identified up to a separation of 45,000 au around either HR 8799, consistent with previously published analyses (Close & Males 2009) and β Pic. Although β Pic was not originally included in the wide CPM companion search described in Section 4.2 due to its relatively low proper motion, it is included here for completeness. This subsample was expanded by including all known exoplanet-hosting main sequence A-type stars which were not included within the VAST survey - Fomal-

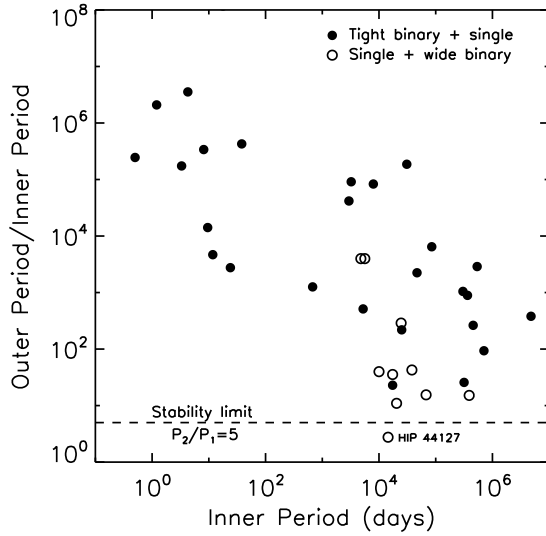


Figure 20. The ratio of the outer and inner period plotted as a function of the inner period for hierarchical triple systems consisting of a tight binary and a wide tertiary component (filled circles), and those consisting of a single star with a distant pair of lower mass components in a tight orbit (open circles). For binary systems without an orbital period, the period has been estimated from the projected separation. The stability limit of $P_2/P_1 = 5$ is also shown (dashed line), with systems below this line being susceptible to dynamical processing (Eggleton 2006). The only hierarchical triple system found to be in a potentially unstable configuration within this study is indicated.

haut (Kalas et al. 2008), κ And (Carson et al. 2013) and HD 95086 (Rameau et al. 2013). Excluding the known comoving companions to Fomalhaut, TW PsA (Luyten 1938; Shaya & Olling 2010) and LP 876-10 (Mamajek et al. 2013), no additional wide CPM companions up to a separation of 45,000 au were identified using the same procedure as described in Section 4.2. Assuming that all of the stellar components within each system have been resolved, the MF of the known exoplanet-hosting A-type stars can be estimated as 20^{+25}_{-8} per cent, a preliminary approximation given the extremely small sample size.

7.6 Higher order multiples

Separations of less than 30 au are not fully covered by the VAST survey, but combining the spatially resolved systems from this study, with spectroscopic, speckle and interferometric binaries (Mason et al. 2001; Pourbaix et al. 2004), allowed for a lower limit estimate of the population of higher order multiples. Among the 156 VAST targets which had both AO observations and were searched for CPM companions - providing sensitivity to the widest range of separations - the number of single, binary, triple, quadruple and quintuple systems were 88, 50, 14, 3 and 1, respectively ($56.4^{+3.8}_{-4.0}$, $32.1^{+3.9}_{-3.5}$, $9.0^{+2.8}_{-1.8}$, $1.9^{+1.8}_{-0.6}$, $0.6^{+1.4}_{-0.2}$ per cent). These relative frequencies are comparable to the ratio of multiple systems measured for solar-type stars (Raghavan et al. 2010), although the A-type star frequencies will change as new components are resolved. Expanding the analysis to include the full VAST sample of 435 stars, the relative frequencies remain statistically consistent, with the number of single, binary, triple, quadruple and quintuple systems found to be 259, 129, 37, 8 and 2, respectively ($59.5^{+2.3}_{-2.4}$,

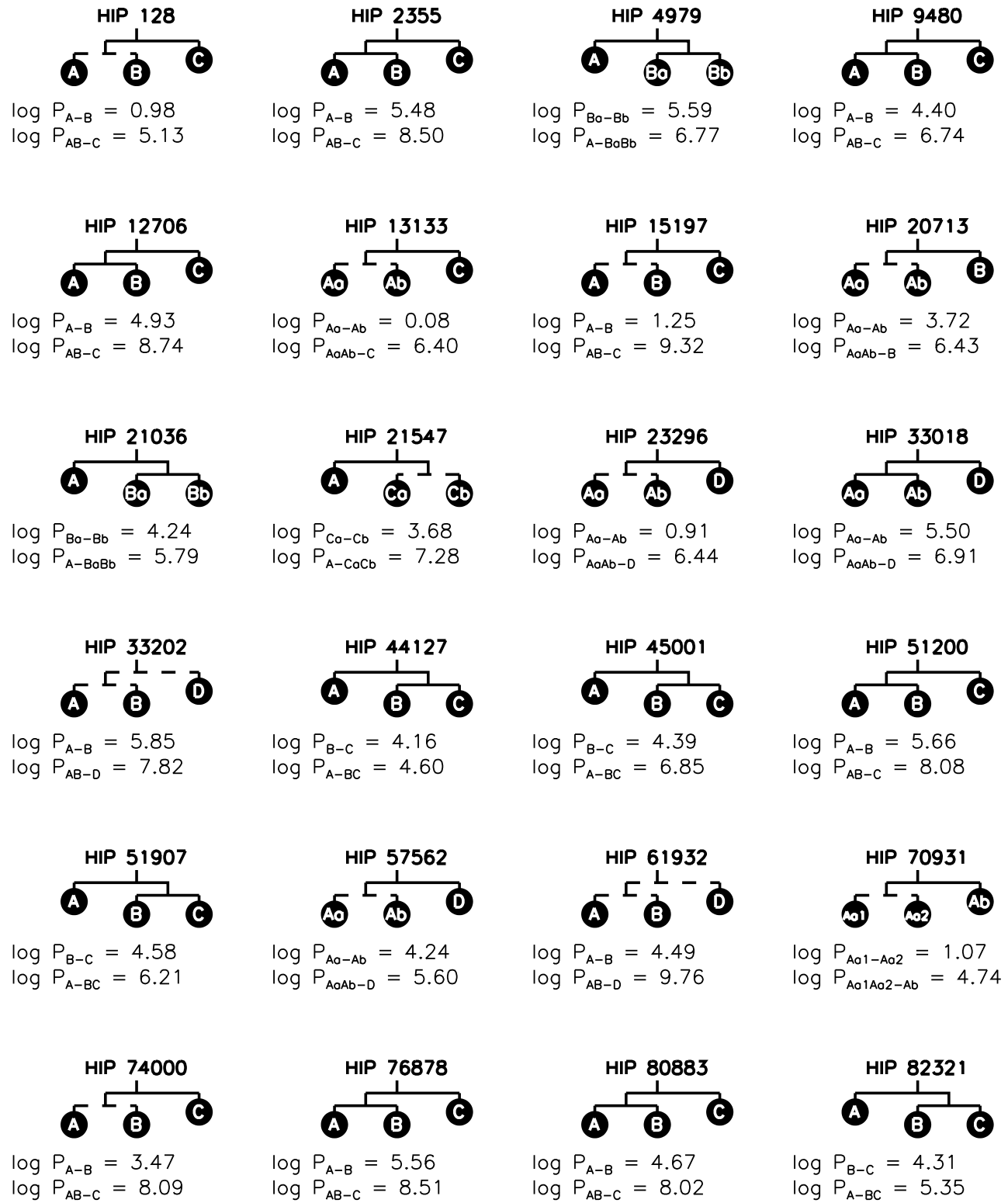


Figure 19. Schematic representations of the higher order multiple systems, combining those systems resolved within this study and previously known systems obtained from the literature. The components which were not resolved within this study are indicated by a dashed connection - for example, the B component of the HIP 128 system was not resolved as it is a spectroscopic binary with a ~ 10 day period. The period is given for each hierarchical system, obtained from either a spectroscopic orbit fit, or an estimate based on the projected physical separation.

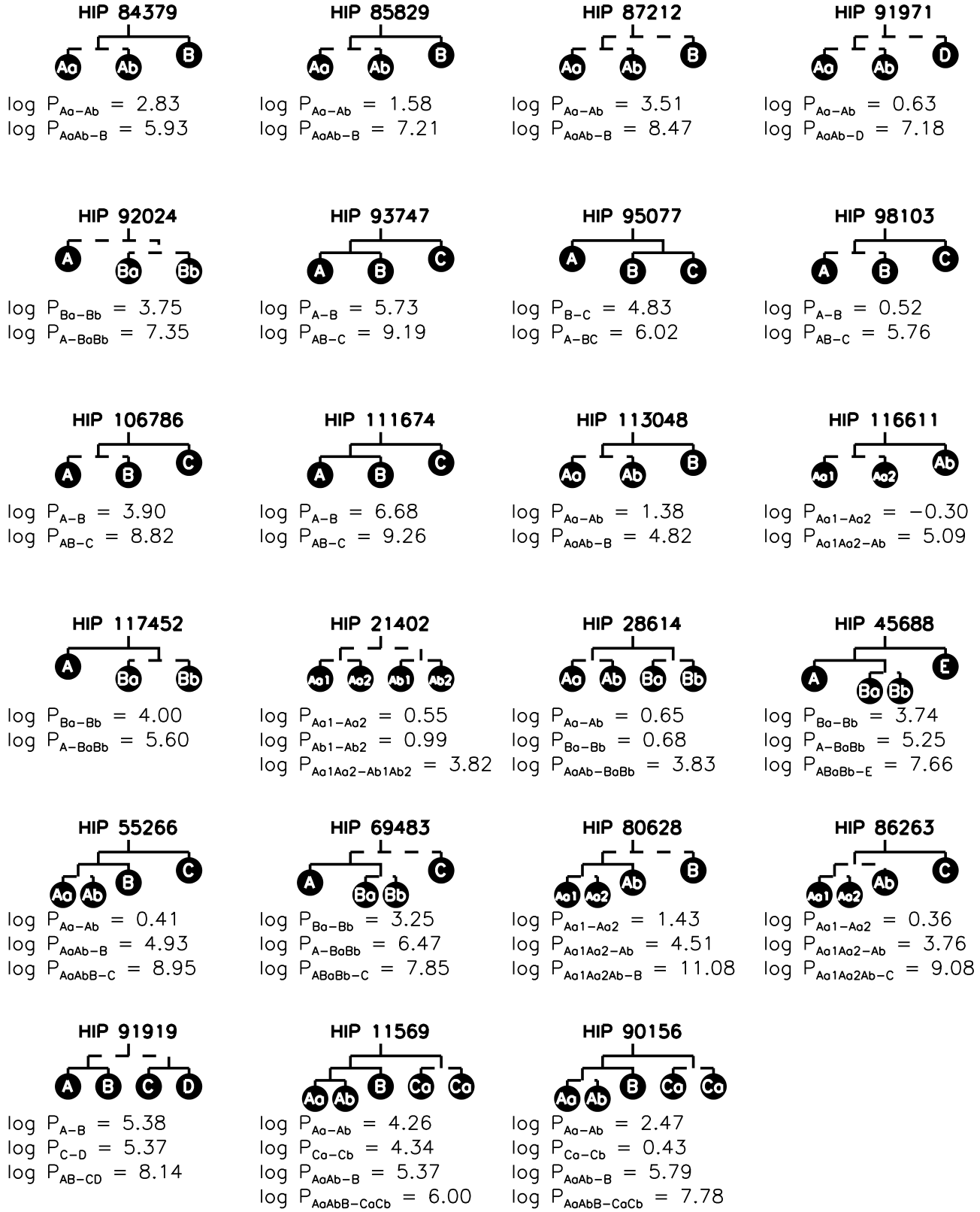


Figure 19. (Continued) Schematic representations of the higher order multiple systems, combining those systems resolved within this study and previously known systems obtained from the literature. The components which were not resolved within this study are indicated by a dashed connection - for example, the B component of the HIP 128 system was not resolved as it is a spectroscopic binary with a ~ 10 day period. The period is given for each hierarchical system, obtained from either a spectroscopic orbit fit, or an estimate based on the projected physical separation.

$29.7^{+2.3}_{-2.1}$, $8.5^{+1.5}_{-1.1}$, $1.8^{+0.9}_{-0.4}$, $0.5^{+0.6}_{-0.1}$ per cent). Schematic representations of the 47 systems with three or more components are given in Fig. 19.

Of the 37 triple systems, 27 consist of a tight binary system orbited by a distant, typically lower mass component. The remaining 10 systems are composed of a single primary, with a distant pair of lower mass components in a tight orbit. A preference of hierarchical triple systems consisting of a tight binary orbited by a more distant tertiary is found for solar-type primaries (Raghavan et al. 2010), and while a similar preference is observed for A-type primaries, significant observational biases still exist. The greater frequency of this type of system would suggest that a more distant pair in a wide orbit around a single primary is either formed less frequently, or more susceptible to dynamical processing. Fig. 20 shows the ratio of the inner and outer period plotted as a function of the inner period for the 37 triple systems. All of the triple systems with a single primary and a distant pair in a tight orbit are found closer to the stability limit; however, this also coincides with the portion of the diagram to which the AO observations are sensitive to companions. To determine if the clustering of these single plus wide binary systems near the stability limit is simply an observational bias, high-resolution measurements of the secondary components of wide binary systems identified within this study are required in an attempt to resolve them into hierarchical triples.

Of the eight known quadruple systems, three are of ϵ Lyr-type, consisting of two pairs of binaries, with similar mass ratios and orbital periods, in a wide orbit (Tokovinin 2008). The remaining five quadruple systems, and the two higher order systems, are all multi-levelled hierarchical systems, potentially products of multiple fragmentation events during the star formation process. All of these hierarchical multiple systems represent ideal candidates for orbital motion monitoring work. With sufficient orbital coverage, model-independent mass estimates can be derived for each component within the system (e.g. Köhler et al. 2012), a useful diagnostic of evolutionary models (e.g. De Rosa et al. 2012).

Two of the hierarchical systems within this study were found to have low period ratios, indicative of a dynamically unstable system (Eggleton 2006); a triple system consisting of a single primary and a wide pair in a tight orbit (HIP 44127 A-BC; ι UMa), and the widest binary component of a higher order system (HIP 11569 AB-CaCb; ι Cas). Both of these systems have indications of youth (Plavchan et al. 2009; De Rosa et al. 2012), which would be consistent with an unstable dynamical configuration (Zhuchkov et al. 2012). As the outer period in both cases are based on the projected separation measured within the AO observations, the systems cannot be conclusively described as unstable – measurements of the true semi-major axes are required.

8 SUMMARY

We have obtained high angular resolution AO observations of 363 nearby ($D \leq 75$ pc) A-type stars in order to characterize the population of binary companions to these intermediate mass ($M = 1.5 - 3.0 M_{\odot}$) stars. Combining these AO data with a search for wide CPM companions of 228 A-type stars using all-sky photographic plates, resulted in sensitivity to separation ranges of 30 – 800 au for the AO data and 1,800 – 45,000 au for the CPM search. A total of 137 companions were identified, consisting of 113 AO companion candidates with ≥ 95 per cent chance of being physically associated and 24 wide CPM companions confirmed by an analysis of their proper motion and position on the CMD. Of the

resolved binary population, 64 were newly identified as companions as a result of this study.

Over a restricted separation range of 30 – 800 au, we measure a CSF of 21.9 ± 2.6 per cent (Fig. 11), compared with 19.6 ± 2.1 per cent for solar-type primaries (Raghavan et al. 2010), and 17.1 ± 5.4 per cent for M-dwarf primaries (Fischer & Marcy 1992). The results are indicative of a trend of increasing multiplicity as a function of increasing primary mass, although the significant error bars prevent this from being a conclusive result (Fig. 11 and 12). This trend is consistent with predictions of the frequency of binary systems determined from numerical simulations (Sterzik & Durisen 2003; Hubber & Whitworth 2005; Bate 2009, 2012), although the functional form of the increase does differ in all but the latter simulation (Fig. 13).

The distribution of companion mass ratios over the 30 – 800 au range was found to consist of two statistically distinct distributions, consisting of AO companions resolved interior to, and exterior to, a separation of ~ 125 au. The inner distribution was measured to be flat for companions with $q \geq 0.15$, while wider systems consisted preferentially of lower mass companions (Fig. 10). By performing a similar analysis on the field solar-type data (Raghavan et al. 2010), we find a similar pattern of a greater frequency of lower mass companions at wider separations (Fig. 16). The relative abundance of equal-mass companions at close separations in both this study, and for solar-type primaries, is consistent with the equalisations of the masses of companions at close separations (Bate & Bonnell 1997; Bate 2000). For wide companions ($a_{\text{proj}} \gtrsim 125$ au), the high frequency of lower mass companions may be indicative of a large population of companions formed through either initial (Bonnell & Bastien 1992) or disc fragmentation (Kratter et al. 2010).

We have presented the first comprehensive multiplicity statistics for A-type stars over a wide separation range, with sensitivity extending to the lowest mass stellar companions. These results are crucial for providing empirical comparisons to theoretical predictions of binary star formation over a range of stellar masses, and companion separations, and comparisons to previous multiplicity surveys of lower mass primaries. An important extension of this survey would be to search for companions interior to the detection limits of the AO data presented within this paper ($a_{\text{proj}} \lesssim 30$ au). Interferometric and spectroscopic monitoring of these targets will provide sensitivity to companions interior to this limit, and future high-contrast AO instruments can be used to tightly constrain the population of low-mass stellar companions to these stars within a more restricted separation range of 10 – 100 au.

NOTE ADDED IN PROOF

While the manuscript was being proofed, an investigation of the companion to HIP 96313 resolved within the AO data set revealed it to be a background giant star, based on its brightness and extremely red colour. At ~ 930 au, it lies outside of the projected separation ranges considered when constructing the separation and mass ratio distributions (30–800 au and 1,800–45,000 au), and as such this misidentification has a minimal effect on the final statistics presented within this study. An investigation performed on the remaining AO-resolved binary companions revealed no additional contaminations of a similar nature.

ACKNOWLEDGEMENTS

The authors wish to express their gratitude for the constructive comments received from the referee, H. A. Abt. The authors wish to thank M. R. Bate, R. J. Parker and K. M. Kratter for their useful comments and suggestions which helped to significantly improve the paper. The authors also wish to thank N. J. McConnell for helping to obtain a subset of the AO observations, and his contributions to various aspects of this study. The authors gratefully acknowledge several sources of funding. RJDR was funded through a studentship from the Science and Technology Facilities Council (STFC) (ST/F007124/1). RJDR gratefully acknowledge financial support received from the Royal Astronomical Society to fund collaborative visits. JP is funded through support from the Leverhulme Trust (F/00144/BJ) and the STFC (ST/F003277/1, ST/H002707/1). AV acknowledges support from the STFC grant ST/H002707/1. Portions of this work were performed under the auspices of the U.S. Department of Energy by Lawrence Livermore National Laboratory in part under Contract W-7405-Eng-48 and in part under Contract DE-AC52-07NA27344, and also supported in part by the NSF Science and Technology CfAO, managed by the UC Santa Cruz under cooperative agreement AST 98-76783. This work was supported, through JRG, in part by University of California Lab Research Programme 09-LR-118057-GRAJ and NSF grant AST-0909188. Based on observations obtained at the Canada-France-Hawaii Telescope (CFHT) which is operated by the National Research Council of Canada, the Institut National des Sciences de l'Univers of the Centre National de la Recherche Scientifique of France, and the University of Hawaii. Based on observations obtained at the Gemini Observatory, which is operated by the Association of Universities for Research in Astronomy, Inc., under a cooperative agreement with the NSF on behalf of the Gemini partnership: the National Science Foundation (United States), the Science and Technology Facilities Council (United Kingdom), the National Research Council (Canada), CONICYT (Chile), the Australian Research Council (Australia), Ministério da Ciência e Tecnologia (Brazil) and Ministerio de Ciencia, Tecnología e Innovación Productiva (Argentina). The authors also wish to extend their gratitude to the staff at the Palomar Observatory and the UCO/Lick Observatory for their support and assistance provided during the course of the observations. This research is partly based on data obtained from the ESO Science Archive Facility. This research has made use of the SIMBAD data base, operated at CDS, Strasbourg, France. This publication makes use of data products from the Two Micron All Sky Survey, which is a joint project of the University of Massachusetts and the Infrared Processing and Analysis Center/California Institute of Technology, funded by the National Aeronautics and Space Administration and the National Science Foundation. This research has made use of the Washington Double Star Catalog maintained at the U.S. Naval Observatory. This research has made use of data obtained from the SuperCOSMOS Science Archive, prepared and hosted by the Wide Field Astronomy Unit, Institute for Astronomy, University of Edinburgh, which is funded by the UK Science and Technology Facilities Council. This research used the facilities of the Canadian Astronomy Data Centre operated by the National Research Council of Canada with the support of the Canadian Space Agency.

APPENDIX 1 - AGE AND MASS ESTIMATES

In order to convert the measured magnitude difference between an A-type primary and any resolved companion into a mass ra-

tio, an estimate of the age of the primary is required due to their rapid evolution away from the zero-age main sequence. Age estimates can be obtained for A-type stars by virtue of membership of a known moving group (e.g. Zuckerman & Song 2004; da Silva et al. 2009), the detection and characterization of debris disc excesses (e.g. Rieke et al. 2005; Su et al. 2006), or the location on a colour-magnitude diagram (e.g. Paunzen 1997; Song et al. 2001). The limited rotational breaking experienced by an A-type star during its short lifespan precludes age estimation through gyrochronology techniques (Barnes 2003), and chromospheric indicators are not reliable due to the breakdown in the correlation between activity and age for stars with a colour index of $B-V \leq 0.5$ (Mamajek & Hillenbrand 2008).

The position of a star on the colour-magnitude diagram is impacted by several factors – the presence of a binary companion, rapid rotation, and metallicity. A binary companion increases the brightness and shifts the colour to redder values by an amount dependent on the spectral type of the companion. If the shift in magnitude and colour induced by the presence of a companion is not removed, the stars age will be overestimated based on its position on the colour-magnitude diagram. By incorporating the results of this imaging binary survey and previous spectroscopic and interferometric results, we have corrected the positions of the sample stars on the colour-magnitude diagram in an attempt to eliminate the effect of the companions and to determine more accurate ages.

Two factors not considered in this study that can influence stellar ages are stellar rotation and metallicity. Regardless of spin axis orientation, a rotating star will have an older age estimate than a non-rotating star (Collins & Smith 1985), as the locus of shifted locations in the colour-magnitude diagram forms a fan-shape extending to brighter magnitudes for pole-on rotators and redder colours for equator-on rotators, with the apex at the non-rotating position (see fig. 1 in Collins & Smith 1985, and fig. 2 in Gray 2007). While not all A-type stars in this sample have $v \sin i$ values, the range of measured values is 10 to 317 km s⁻¹, with an average and standard deviation of 124 ± 67 km s⁻¹ based on the 350 with measurements reported in the Extended Hipparcos Compilation (XHIP; Anderson & Francis 2011). The effect of rotation has been assessed to over-estimate ages of early-type stars by $\sim 30\text{--}50\%$ (Figueras & Blasi 1998), and becomes prominent when $v \sin i > 100$ km s⁻¹ (Song et al. 2001). The fact that rotation can only make an A-type star appear older on the colour-magnitude diagram may be an explanation as to why ages of known moving group members within the VAST sample, when estimated using the technique described in this section, were often found to be significantly older than the canonical moving group age.

The metallicity of a star can bias the age estimate in both directions – if a star has a higher metallicity than assumed for the isochrones, the age will be overestimated, while the age will be underestimated if the metallicity is lower than assumed. Again, not all the stars have measured metallicity, but for the 108 with [Fe/H] values, the average is near solar at -0.06 ± 0.51 (Anderson & Francis 2011), and as such the net effect on the overall age distribution should be small. Since the rotation and metallicity is not measured for all stars, and the theoretical isochrones used to determine the ages are for the non-rotating case, we have not adjusted the age estimates for either of these effects.

Of the 435 stars with either AO observations, or with proper motions sufficient for the search for CPM companions, 55 are known members of coeval moving groups or stellar clusters with literature ages (Table 10), and 64 have age estimates within the literature derived from theoretical evolutionary models (Table 11).

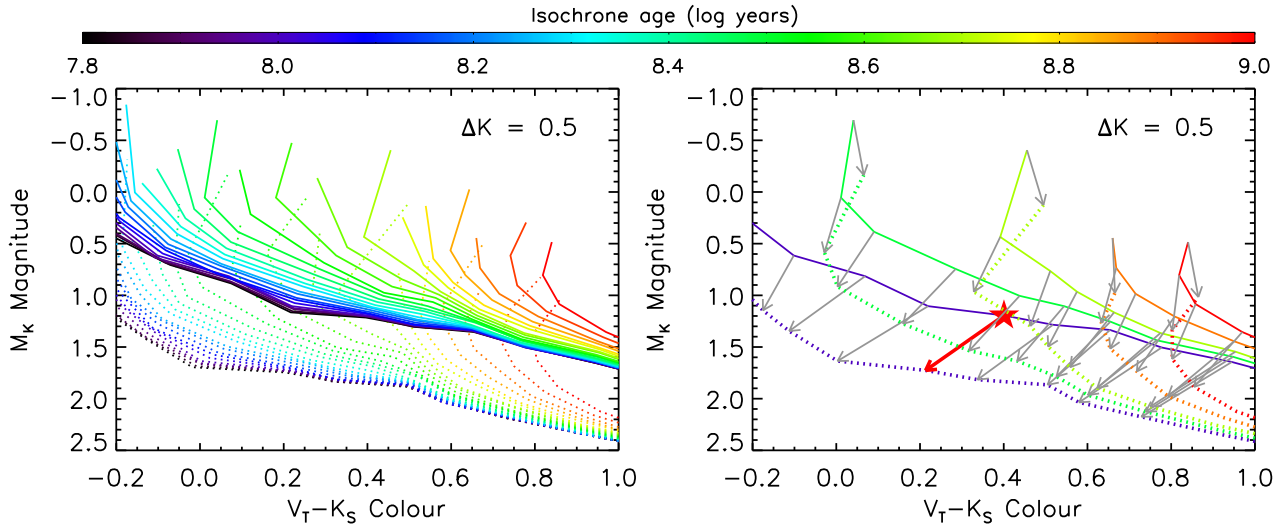


Figure 22. Left-hand panel: A set of binary isochrones was constructed for the full range of isochrone ages available within the models, for each value of the magnitude difference. The example shows the single star isochrone (dotted lines), and the corresponding binary star isochrone for the case of a $\Delta K = 0.5$ companion (solid lines). As the shift in the position of each point on the isochrone is based on an estimate of the companion properties derived from the theoretical models, this process can be carried out for a range of visual magnitude differences (ΔV), for companions resolved with interferometry, or mass ratios (q), for double-lined spectroscopic binaries. Right-hand panel: The magnitude and direction of the shift required to correct the position of the primary on the colour–magnitude diagram due to the presence of a $\Delta K = 0.5$ companion unresolved within the Tycho2 and 2MASS catalogues. For clarity only a subset of the single star (dotted lines) and binary isochrones (solid lines) are shown (10^8 , $10^{8.5}$, $10^{8.7}$, $10^{8.9}$, and 10^9 yrs). At each point on the binary isochrone, a vector is plotted showing the magnitude and direction of the correction required to remove the contamination induced by the companion (grey arrows). As an example, for a binary system with an observed $M_K(AB) = 1.15$ and $(V - K)_{AB} = 0.4$ (red filled star), with a magnitude difference of $\Delta K = 0.5$, the correction estimated for the magnitude and colour is shown (red vector). This correction has reduced the age estimate of this hypothetical primary from 500 to 100 Myr.

Table 10. Literature ages of known moving groups

Moving Group	Number of Stars	Age (Myrs)	Age Reference
TW Hydrae	1	8	Stauffer et al. (1995)
β Pictoris	5	12	Zuckerman et al. (2001)
Tucana-Horologium	8	30	Zuckerman et al. (2011)
Argus	2	40	Torres et al. (2008)
AB Doradus	4	70	Zuckerman et al. (2011)
Castor	2	200	Barrado y Navascués (1998)
Ursa Major	9	300	Zuckerman & Song (2004)
Hyades	24	625	Perryman et al. (1998)

For the remaining 316 stars, the age was estimated based on a comparison of the position of the star on the $V - K$ versus M_K colour–magnitude diagram against theoretical stellar isochrones (Siess et al. 2000). As the presence of a bright binary companion, at an angular separation less than the resolving limit of the Tycho2 and 2MASS catalogues, can introduce a significant shift in the position of a star on the colour–magnitude diagram, the colour and magnitude of the primary was corrected based on the expected $V - K$ colour and M_K magnitude of the companion. The magnitude and direction of these corrections were estimated by constructing a series of isochrones which are shifted due to the presence of a hypothetical binary companion (Fig. 21). Given that the magnitude difference between the primary and companion is known, or the mass ratio of the system in the case of double-lined spectroscopic binaries, the set of binary isochrones corresponding to the configuration of the system can be selected, and used to obtain the predicted shift in the position of the primary on the colour–magnitude

Table 11. Source of literature isochrone ages

Reference	Number of Stars
Gerbaldi et al. (1999)	4
Janson et al. (2011)	1
Laureijs et al. (2002)	1
Paunzen (1997)	3
Rhee et al. (2007)	25
Rieke et al. (2005)	8
Song et al. (2001)	6
Su et al. (2006)	1
Tetzlaff et al. (2010)	12
Westin (1985)	3

diagram (Fig. 22). Combining the companions resolved within this study, with binary companions reported within either the WDS or SB9 catalogues, the positions of 61 stars were corrected (Fig. 23).

With an age estimates obtained for the observed sample (Fig. 3, Table 1), a mass-magnitude relation was constructed for each target in order to estimate the mass of the star and any resolved companions (Fig. 25, left-hand panel). The increasing luminosity of an A-type star, as it evolves away from the zero-age main sequence, leads to a dependence on the mass derived from mass-magnitude relations as a function of age. Similarly, for the youngest M-dwarf companions resolved within this study, a dependence on age of the mass-magnitude relation is caused by the contraction of these low-mass stars on to the main sequence within the first 100 Myr of their lifespan, significantly decreasing their luminosity (e.g. Stauffer 1980; Fig. 25, right-hand panel). For each star within the sample, the mass is estimated using the K -band magni-

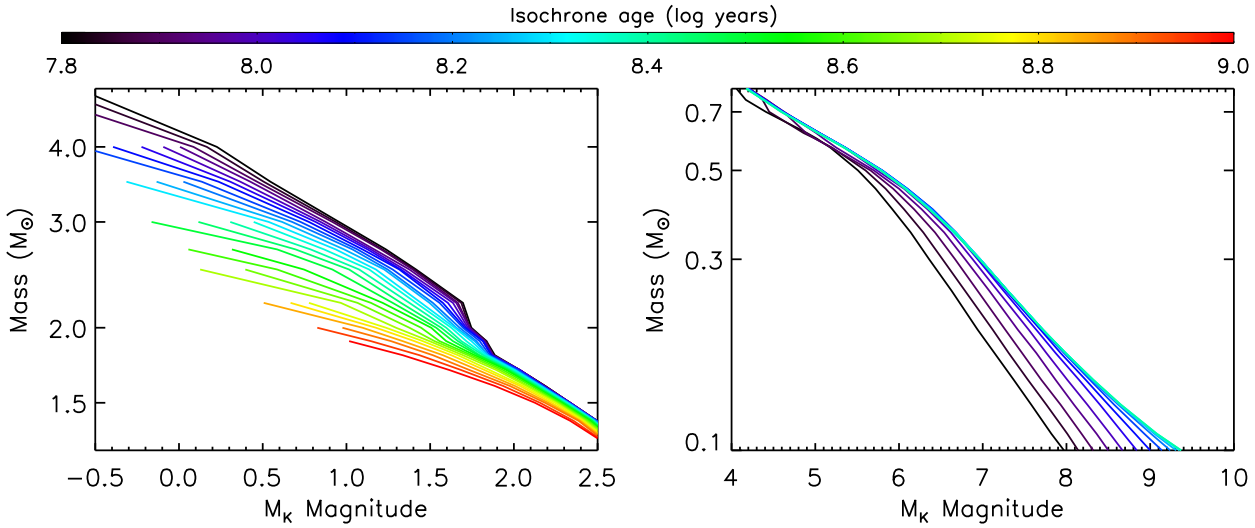


Figure 25. The mass-magnitude relations derived from the theoretical isochrones covering the A-type star mass range (Siess et al. 2000; left-hand panel), and for companions at the bottom of the Main Sequence (Baraffe et al. 1998; right-hand panel). For A-type stars, the mass derived from the mass-magnitude relation is strongly dependent on the age estimate of the system over the full lifespan of a typical A-type star, while for lower mass companions this dependency rapidly becomes negligible at ages older than 10^8 yrs. This demonstrates why an age estimate is necessary prior to estimating the mass of the A-type star, and mass ratio of any resolved binary systems.

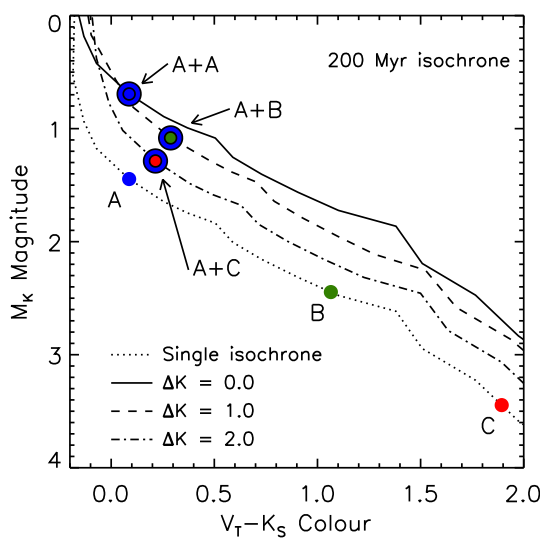


Figure 21. The presence of a companion unresolved within the Tycho2 and 2MASS catalogues can lead to a significant shift in the position of the primary on the colour-magnitude diagram. An example is shown demonstrating the expected shift in the position of a star with an absolute magnitude of $M_K = 1.4$ (A), due to the presence of; an equal mass companion (A+A), a companion with a magnitude difference of $\Delta K = 1$ (A+B) and $\Delta K = 2$ (A+C). For the case of a binary system with two identical components, the primary is only shifted in the magnitude direction, with no change in the colour of the system. The presence of a lower mass companion (B, C) can lead to a significant reddening of the system. This procedure is repeated for each position within the single star isochrone (dotted line) to produce a binary isochrone including the effect of a binary companion at range of magnitude differences ($\Delta K = 0$, solid line; $\Delta K = 1$, dashed line; $\Delta K = 2$, dot-dashed line).

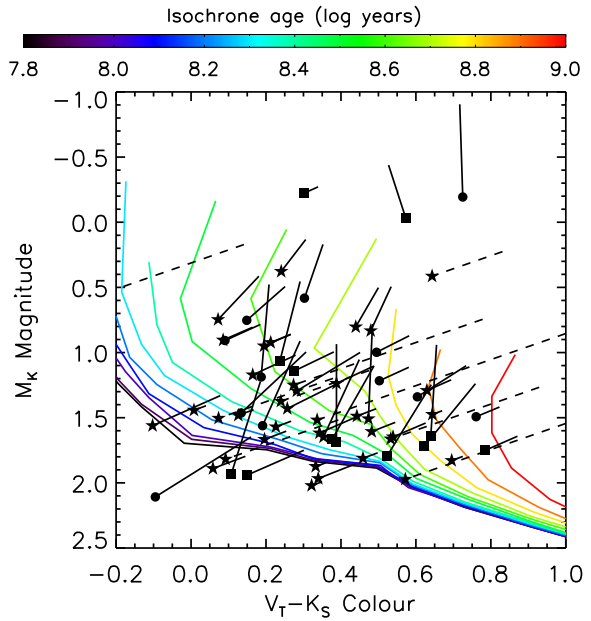


Figure 23. The position of 61 stars is changed due to a presence of a bright binary companion unresolved in either one of, or both, the Tycho2 and 2MASS catalogues. The magnitude and direction of the shift necessary to correct the star (solid line - unresolved in both catalogues, dashed line - unresolved only in 2MASS), is estimated based on the predicted colour and magnitude of the companion derived from the theoretical isochrones. The corrected position of each star is given by a filled symbol, depending on the method through which the companion was resolved. The companion properties are estimated using either the magnitude difference measured within this study (ΔK , filled stars), the magnitude difference reported for companions resolved with interferometric techniques (ΔV , filled circles), or the mass ratio calculated for a double-lined spectroscopic binary (q , filled squares). Theoretical isochrones from Siess et al. (2000) are plotted within the range $7.8 \leq \log t \leq 9.0$, in steps of $\Delta \log t = 0.1$.

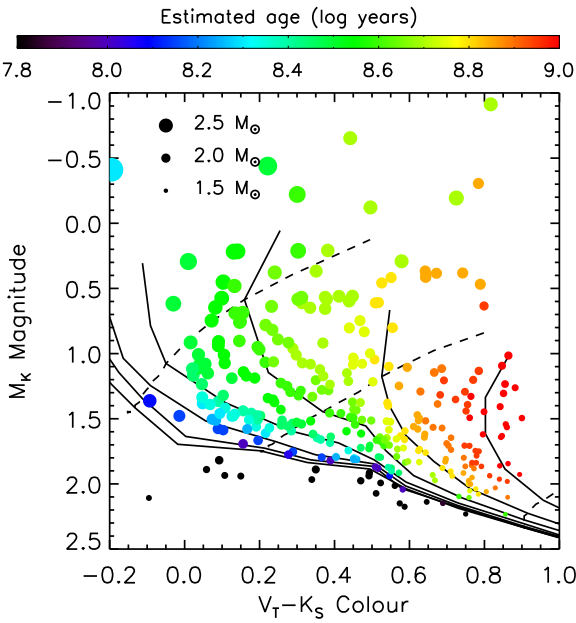


Figure 24. A colour-magnitude diagram of the 316 stars without age estimates presented within the literature. The colour of each symbol denotes the age estimated for each star based on a comparison to theoretical solar-metallicity isochrones (Siess et al. 2000), with the size being proportional to the mass estimated from the theoretical mass-magnitude relations. The theoretical isochrones are plotted within the range $7.8 \leq \log t \leq 9.0$, in steps of $\Delta \log t = 0.2$ (solid lines), alongside the theoretical evolutionary tracks for a 2.5, 2.0 and 1.5 M_{\odot} star (dashed lines, left to right).

tude obtained from the 2MASS catalogue, after correction due to the presence of any known companions within the resolution limit of the 2MASS observations (Fig. 23). The distribution of estimated masses is given in Fig. 4, with the estimate for each star presented in Table 1.

REFERENCES

- Abt H. A., 1962, ApJS, 6, 37
 Abt H. A., 1965, ApJS, 11, 429
 Abt H. A., 1983, ARA&A, 21, 343
 Abt H. A., 2011, AJ, 141, 165
 Abt H. A., Chaffee F. H., Suffolk G., 1972, ApJ, 175, 779
 Abt H. A., Levy S. G., 1985, ApJS, 59, 229
 Abt H. A., Snowden M. S., 1973, ApJS, 25, 137
 Adams F. C., Ruden S. P., Shu F. H., 1989, ApJ, 347, 959
 Africano J. L., Cobb C. L., Dunham D. W., Evans D. S., Fekel F. C., Vogt S. S., 1975, AJ, 80, 689
 Alden H. L., 1924, AJ, 35, 167
 Allen P. R., Koerner D. W., McElwain M. W., Cruz K. L., Reid I. N., 2007, AJ, 133, 971
 Anderson E., Francis C., 2011, VizieR Online Data Catalog, 5137, 0
 Artymowicz P., Lubow S. H., 1994, ApJ, 421, 651
 Aurière M. et al., 2010, A&A, 523, A40
 Babcock H. W., 1958, ApJ, 128, 228
 Baraffe I., Chabrier G., Allard F., Hauschildt P. H., 1998, A&A, 337, 403
 Barnes S. A., 2003, ApJ, 586, 464
 Barrado y Navascués D., 1998, A&A, 339, 831
 Bate M. R., 2000, MNRAS, 314, 33
 Bate M. R., 2001, in Zinnecker H., Mathieu R. D., eds, Proc. IAU Symp. 200, The Formation of Binary Stars. Astron. Soc. Pac., San Francisco, p. 429
 Bate M. R., 2009, MNRAS, 392, 590
 Bate M. R., 2012, MNRAS, 419, 3115
 Bate M. R., Bonnell I. A., 1997, MNRAS, 285, 33
 Bate M. R., Bonnell I. A., Price N. M., 1995, MNRAS, 277, 362
 Batten A. H., Fletcher J. M., 1992, JRASC, 86, 99
 Bergfors C. et al., 2010, A&A, 520, A54
 Biller B. A. et al., 2007, ApJS, 173, 143
 Boffin H. M. J., 2010, A&A, 524, A14
 Bonneau D., Foy R., 1980, A&A, 86, 295
 Bonnell I., Bastien P., 1992, ApJ, 401, 654
 Bonnell I., Martel H., Bastien P., Arcoragi J.-P., Benz W., 1991, ApJ, 377, 553
 Bonnell I. A., 1994, MNRAS, 269, 837
 Boss A. P., Bodenheimer P., 1979, ApJ, 234, 289
 Boss A. R., 1986, ApJS, 62, 519
 Brendley M., Mason B., 2006, IAU Commission on Double Stars, 160, 1
 Budaj J., 1997, A&A, 326, 655
 Burgasser A. J., Kirkpatrick J. D., Cruz K. L., Reid I. N., Leggett S. K., Liebert J., Burrows A., Brown M. E., 2006, ApJS, 166, 585
 Carquillat J.-M., Ginestet N., Prieur J. L., Debernardi Y., 2003, MNRAS, 346, 555
 Carquillat J.-M., Prieur J. L., 2007, MNRAS, 380, 1064
 Carrier F., North P., Udry S., Babel J., 2002, A&A, 394, 151
 Carson J. et al., 2013, ApJ, 763, L32
 Christou J. C., Drummond J. D., 2006, AJ, 131, 3100
 Clarke C. J., 1996, MNRAS, 283, 353
 Close L. M., Males J. R., 2009, ApJ, 709, 342
 Collins G. W. I., Smith R. C., 1985, MNRAS, 213, 519
 Conti P. S., 1970, PASP, 82, 781
 Couteau P., 1960, ApJ, 43, 41
 da Silva L., Torres C. A. O., de la Reza R., Quast G. R., Melo C. H. F., Sterzik M. F., 2009, A&A, 508, 833
 De Rosa R. J. et al., 2011, MNRAS, 415, 854
 De Rosa R. J. et al., 2012, MNRAS, 422, 2765
 Debernardi Y., Mermilliod J.-C., Carquillat J.-M., Ginestet N., 2000, A&A, 354, 881
 Dent W. R. F., Torrelles J. M., Osorio M., Calvet N., Anglada G., 2006, MNRAS, 365, 1283
 Doyon R., Nadeau D., Vallee P., Starr B. M., Cuillandre J. C., Beuzit J.-L., Beigbeder F., Brau-Nogue S., 1998, Proc. SPIE, 3354, 760
 Duchêne G., 1999, A&A, 341, 547
 Duerbeck H. W., Haenel A., 1979, A&AS, 38, 155
 Duquennoy A., Mayor M., 1991, A&A, 248, 485
 Durisen R. H., Sterzik M. F., Pickett B. K., 2001, A&A, 371, 952
 Eggen O. J., 1946, AJ, 52, 81
 Eggleton P., 2006, Evolutionary Processes in Binary and Multiple Stars. Cambridge University Press, Cambridge, UK
 ESA 1997, The Hipparcos and Tycho Catalogues, ESA SP-1200
 Fekel F. C., Tomkin J., Williamson M. H., 2009, ApJ, 137, 3900
 Fekel F. C., Tomkin J., Williamson M. H., Pourbaix D., 2011, AJ, 142, 69
 Fekel F. C., Williamson M., Buggs C., Onuoha G., Smith B., 2006, AJ, 132, 1490
 Figueras F., Blasi F., 1998, A&A, 329, 957
 Fischer D. A., Marcy G. W., 1992, ApJ, 396, 178

- Frost E. B., 1924, ApJ, 60, 319
- Fukagawa M. et al., 2010, PASJ, 62, 347
- Gerbaldi M., Faraggiana R., Burnage R., Delmas F., Gómez A. E., Grenier S., 1999, ApJ, 137, 273
- Ghez A. M., McCarthy D. W., Patience J. L., Beck T. L., 1997, ApJ, 481, 378
- Goodwin S. P., Whitworth A. P., Ward-Thompson D., 2004, A&A, 423, 169
- Gray D. F., 1992, The observation and analysis of stellar photospheres.. Camb. Astrophys. Ser., Vol. 20, Cambridge, UK
- Gray R. O., 2007, The Future of Photometric, Spectrophotometric and Polarimetric Standardization, 364, 305
- Gutmann F., 1965, PDAO, 12, 391
- Halbwachs J. L., 1986, A&AS, 66, 131
- Halbwachs J. L., Mayor M., Udry S., 2012, MNRAS, 422, 14
- Hambly N. C. et al., 2001, MNRAS, 326, 1279
- Hamidouche M., Looney L. W., Mundy L. G., 2006, ApJ, 651, 321
- Harper W. H., 1935, PDAO, 6, 207
- Hartkopf W. I., Mason B. D., Gies D. R., ten Brummelaar T., McAlister H. A., Moffat A. F. J., Shara M. M., Wallace D. J., 1999, AJ, 118, 509
- Hartkopf W. I., Mason B. D., McAlister H. A., 1996, AJ, 111, 370
- Hayward T. L., Brandl B., Pirger B., Blacken C., Gull G. E., Schoenwald J., Houck J. R., 2001, PASP, 113, 105
- Heintz W. D., Strom C., 1993, PASP, 105, 293
- Hodapp K. W. et al., 2003, PASP, 115, 1388
- Høg E. et al., 2000, A&A, 355, L27
- Hopmann J., 1974, OAWMN, 183, 387
- Horch E. P., Bahi L. A. P., Gaulin J. R., Howell S. B., Sherry W. H., Baena Gallé R., van Altena W. F., 2011, AJ, 143, 10
- Horch E. P., Meyer R. D., van Altena W. F., 2004, AJ, 127, 1727
- Horch E. P., van Altena W. F., Cyr W. M., Kinsman-Smith L., Srivastava A., Zhou J., 2008, AJ, 136, 312
- Hubber D. A., Whitworth A. P., 2005, A&A, 437, 113
- Isobe S., Norimoto Y., Noguchi M., Ohtsubo J., Baba N., 1990, PNAOJ, 1, 217
- Janson M., Bonavita M., Klahr H., Lafrenière D., Jayawardhana R., Zinnecker H., 2011, ApJ, 736, 89
- Janson M. et al., 2012, ApJS, 754, 44
- Jones R. B., 1931, Lick Observatory Bulletin, 15, 117
- Kalas P. et al., 2008, Science, 322, 1345
- Kasper M., Apai D., Janson M., Brandner W., 2007, A&A, 472, 321
- Kaufmann J. P., Klippen E., 1973, A&A, 27, 469
- King R. R., Parker R. J., Patience J., Goodwin S. P., 2012, MNRAS, 421, 2025
- Kiyaeva O. V., 2006, SvAL, 32, 836
- Kley W., Nelson R. P., 2008, A&A, 486, 617
- Köhler R., Petr-Gotzens M. G., McCaughrean M. J., Bouvier J., Duchêne G., Quirrenbach A., Zinnecker H., 2006, A&A, 458, 461
- Köhler R., Ratzka T., Leinert C., 2012, A&A, 541, A29
- Kouwenhoven M. B. N., Brown A. G. A., Zinnecker H., Kaper L., Portegies Zwart S. F., 2005, A&A, 430, 137
- Kratter K. M., 2011, in Montmerle T., André P., eds, From Darkness to Light: Origin and Evolution of Young Stellar Clusters. Astron. Soc. Pac., San Francisco, p. 47
- Kratter K. M., Matzner C. D., Krumholz M. R., Klein R. I., 2010, ApJ, 708, 1585
- Kratter K. M., Murray-Clay R. A., Youdin A. N., 2010, ApJ, 710, 1375
- Kraus A. L., Ireland M. J., Martinache F., Hillenbrand L. A., 2011, ApJ, 731, 8
- Krumholz M. R., Klein R. I., McKee C. F., 2012, ApJ, 754, 71
- Kuiper G. P., 1935, PASP, 47, 15
- Lada C. J., 2006, ApJ, 640, L63
- Lafrenière D. et al., 2007, ApJ, 670, 1367
- Lafrenière D., Jayawardhana R., Brandeker A., Ahmic M., van Kerwijk M. H., 2008, ApJ, 683, 844
- Lagrange A.-M. et al., 2009, A&A, 493, L21
- Lane B. F. et al., 2007, ApJ, 669, 1209
- Laureijs R. J., Jourdain de Muizon M., Leech K., Siebenmorgen R., Dominik C., Habing H. J., Trams N., Kessler M. F., 2002, ApJ, 387, 285
- Lee O. J., 1910, ApJ, 32, 300
- Lenzen R. et al., 2003, Proc. SPIE, 4841, 944
- Lépine S., Bongiorno B., 2007, AJ, 133, 889
- Lloyd C., 1981, MNRAS, 195, 805
- Lloyd J. P., Liu M. C., Macintosh B. A., Severson S. A., Deich W. T., Graham J. R., 2000, Proc. SPIE, 4008, 814
- Lucy L. B., Sweeney M. A., 1971, AJ, 76, 544
- Luyten W. J., 1938, AJ, 47, 115
- McAlister H. A., Hartkopf W. I., Hutter D. J., Shara M. M., Franz O. G., 1987, AJ, 93, 183
- McAlister H. A., Hartkopf W. I., Sowell J. R., Dombrowski E. G., Franz O. G., 1989, AJ, 97, 510
- McAlister H. A., Mason B. D., Hartkopf W. I., Shara M. M., 1993, AJ, 106, 1639
- McCaughrean M. J., Stauffer J. R., 1994, AJ, 108, 1382
- Malkov O. Y., Tamazian V. S., Docobo J. A., Chulkov D. A., 2012, A&A, 546, A69
- Mamajek E. E. et al., 2013, eprint arXiv:1310.0764
- Mamajek E. E., Hillenbrand L. A., 2008, ApJ, 687, 1264
- Mannino G., Grubisich C., 1955, MmSAI, 27, 65
- Margoni R., Munari U., Stagni R., 1992, A&AS, 93, 545
- Marois C., Lafrenière D., Doyon R., Macintosh B., Nadeau D., 2006, ApJ, 641, 556
- Marois C., Macintosh B., Barman T., Zuckerman B., Song I., Patience J., Lafrenière D., Doyon R., 2008, Science, 322, 1348
- Marois C., Zuckerman B., Konopacky Q. M., Macintosh B., Barman T., 2010, Nature, 468, 1080
- Mason B. D., Hartkopf W. I., Gies D. R., Henry T. J., Helsel J. W., 2009, AJ, 137, 3358
- Mason B. D. et al., 1999, AJ, 117, 1890
- Mason B. D., ten Brummelaar T., Gies D. R., Hartkopf W. I., Thaller M. L., 1997, AJ, 114, 2112
- Mason B. D., Wycoff G. L., Hartkopf W. I., Douglass G. G., Worley C. E., 2001, AJ, 122, 3466
- Michaud G., 1980, AJ, 85, 589
- Michaud G., Tarasick D., Charland Y., Pelletier C., 1983, ApJ, 269, 239
- Moeckel N., Bate M. R., 2010, MNRAS, 404, 721
- Moore F. C., 1931, Lick Observatory Bulletin, 15, 144
- Morgan B. L., Beddoes D. R., Scaddan R. J., Dainty J. C., 1978, MNRAS, 183, 701
- Muterspaugh M. W. et al., 2010, AJ, 140, 1623
- Muterspaugh M. W. et al., 2008, AJ, 135, 766
- Nelson A. F., 2000, ApJ, 537, L65
- Neubauer F. J., 1944, ApJ, 99, 134
- Nielsen E. L. et al., 2013, ApJ, 776, 4
- Patience J., Ghez A. M., Reid I. N., Matthews K., 2002, AJ, 123, 1570
- Paunzen E., 1997, ApJ, 326, L29

- Perryman M. A. C. et al., 1998, *A&A*, 331, 81
 Peterson D. M., Baron R. L., Dunham E., Mink D., Elliot J. L., Weekes T. C., 1981, *AJ*, 86, 280
 Petrie R. M., 1926, *PDAO*, 3, 331
 Plavchan P., Werner M. W., Chen C. H., Stapelfeldt K. R., Su K. Y. L., Stauffer J. R., Song I., 2009, *ApJ*, 698, 1068
 Pourbaix D., 2000, *A&AS*, 145, 215
 Pourbaix D. et al., 2004, *A&A*, 424, 727
 Raghavan D. et al., 2010, *ApJS*, 190, 1
 Rameau J. et al., 2013, *ApJ*, 772, L15
 Reid I. N., Cruz K. L., Burgasser A. J., C Liu M., 2008, *AJ*, 135, 580
 Reipurth B., Zinnecker H., 1993, *A&A*, 278, 81
 Rhee J. H., Song I., Zuckerman B., McElwain M., 2007, *ApJ*, 660, 1556
 Rieke G. H. et al., 2005, *ApJ*, 620, 1010
 Roberts L. C., Turner N. H., ten Brummelaar T. A., 2007, *AJ*, 133, 545
 Roeser S., Demleitner M., Schilbach E., 2010, *AJ*, 139, 2440
 Roman N. G., Morgan W. W., Eggen O. J., 1948, *ApJ*, 107, 107
 Rousset G. et al., 2003, *Proc. SPIE*, 4839, 140
 Rucinski S. M. et al., 2005, *AJ*, 130, 767
 Samus N. N., Durlevich O. V., et al., 2009, *VizieR Online Data Catalog*, 1, 02025
 Sana H. et al., 2013, *A&A*, 550, A107
 Sana H., Evans C. J., 2011, in *Proc. IAU Symp. 272, Active OB stars: structure, evolution, mass loss, and critical limits*. Cambridge University Press, Cambridge, UK, p. 474
 Shaya E. J., Olling R. P., 2010, *ApJS*, 192, 2
 Siess L., Dufour E., Forestini M., 2000, *A&A*, 358, 593
 Song I., Caillault J.-P., Navascues D. B. y., Stauffer J. R., 2001, *ApJ*, 546, 352
 Stamatellos D., Maury A., Whitworth A., André P., 2011, *MNRAS*, 413, 1787
 Stauffer J. R., 1980, *AJ*, 85, 1341
 Stauffer J. R., Hartmann L. W., Barrado y Navascues D., 1995, *ApJ*, 454, 910
 Sterzik M. F., Durisen R. H., 1998, *A&A*, 339, 95
 Sterzik M. F., Durisen R. H., 2003, *A&A*, 400, 1031
 Stickland D. J., 1990, *The Observatory*, 110, 43
 Su K. Y. L. et al., 2006, *ApJ*, 653, 675
 Talon S., Richard O., Michaud G., 2006, *ApJ*, 645, 634
 Tetzlaff N., Neuhäuser R., Hohle M. M., 2010, *ApJ*, 410, 190
 Tokovinin A., 2008, *MNRAS*, 389, 925
 Tokovinin A., 2012, *AJ*, 144, 56
 Tokovinin A., Lépine S., 2012, *AJ*, 144, 102
 Torres C. A. O., Quast G. R., Melo C. H. F., Sterzik M. F., 2008, *Handbook of Star Forming Regions: Volume II, The Southern Sky*, Astron. Soc. Pac., San Francisco, p. 757
 Torres G., Stefanik R. P., Latham D. W., 1997, *ApJ*, 485, 167
 van den Bos W. H., 1927, *Bull. Astron. Inst. Netherlands*, 3, 259
 van Leeuwen F., 2007, *A&A*, 474, 653
 Vigan A. et al., 2012, *A&A*, 544, A9
 Westin T. N. G., 1985, *A&AS*, 60, 99
 Whitworth A. P., Stamatellos D., 2006, *A&A*, 458, 817
 Woodward J. W., Tohline J. E., Hachisu I., 1994, *ApJ*, 420, 247
 Young R. K., 1910, *Lick Observatory Bulletin*, 6, 160
 Zacharias N., Finch C. T., Girard T. M., Henden A., Bartlett J. L., Monet D. G., Zacharias M. I., 2012, *VizieR Online Data Catalog*, 1322, 0
 Zhuchkov R. Y., Malogolovets E. V., Kiyaeva O. V., Orlov V. V., Bikmaev I. F., Balega Y. Y., 2012, *Astron. Rep.*, 56, 512
 Zuckerman B., Rhee J. H., Song I., Bessell M. S., 2011, *ApJ*, 732, 61
 Zuckerman B., Song I., 2004, *ARA&A*, 42, 685
 Zuckerman B., Song I., Bessell M. S., Webb R. A., 2001, *ApJ*, 562, L87

Table 1: The VAST sample

HIP	Spectral type	Distance (pc)	B_T (mag)	V_T (mag)	J (mag)	H (mag)	K_S (mag)	Age ^a (Myrs)	Age Ref.	Mass (M_\odot)	Separation coverage ($\log a$ [au])		
											Adaptive optics	CPM search	
128	Am...	70.8±1.7	6.73±0.01	6.52±0.01	6.10±0.02	6.06±0.04	6.02±0.02	180	1	1.84	1.50 ≤ log a < 2.90	3.60 ≤ log a < 4.65	
159	A3	62.5±2.1	7.26±0.01	6.96±0.01	6.33±0.02	6.27±0.02	6.21±0.02	60	1	1.59	1.50 ≤ log a < 2.90	–	
1473	A2V	41.3±0.4	4.59±0.01	4.51±0.01	4.34±0.27	4.42±0.18	4.46±0.29	200	1	2.26	1.50 ≤ log a < 2.55	3.60 ≤ log a < 4.65	
2355	A7III	62.8±1.7	5.52±0.01	5.25±0.01	4.86±0.25	4.69±0.19	4.46±0.03	710	1	2.20	1.50 ≤ log a < 2.90	3.60 ≤ log a < 4.65	
2381	A3V	53.1±0.8	5.32±0.01	5.18±0.01	5.28±0.24	4.88±0.08	4.83±0.02	450	1	2.09	1.50 ≤ log a < 2.90	–	
2472	A0V	53.0±0.7	4.79±0.01	4.75±0.01	4.67±0.04	4.77±0.07	4.70±0.03	320	1	2.37	1.50 ≤ log a < 2.90	–	
2578	A0V	45.6±0.4	5.12±0.01	5.07±0.01	5.06±0.04	5.16±0.08	4.99±0.02	30	2	2.23	1.50 ≤ log a < 2.90	–	
2852	A5m...	48.9±0.8	6.39±0.01	6.09±0.01	5.56±0.02	5.51±0.04	5.42±0.02	500	1	1.66	1.50 ≤ log a < 2.55	–	
3277	Ap...	67.0±1.6	5.96±0.01	5.72±0.01	5.59±0.02	5.58±0.02	5.57±0.03	250	1	2.14	1.50 ≤ log a < 2.90	–	
3414	A5V	53.7±0.9	5.16±0.01	4.97±0.01	4.91±0.26	4.76±0.24	4.58±0.02	250	1	1.90	1.50 ≤ log a < 2.90	–	
3521	F0V	64.4±1.7	6.27±0.01	5.96±0.01	5.36±0.02	5.27±0.03	5.18±0.02	890	1	1.92	1.50 ≤ log a < 2.90	–	
3965	F2IV	67.3±2.1	6.72±0.01	6.40±0.01	5.83±0.03	5.82±0.06	5.71±0.02	790	1	1.76	–	3.25 ≤ log a < 4.65	
4436	A5V	39.8±1.4	4.03±0.01	3.87±0.01	3.62±0.26	3.65±0.18	3.64±0.21	450	1	2.39	1.50 ≤ log a < 2.90	3.60 ≤ log a < 4.65	
4852	A2V	71.2±1.6	5.62±0.01	5.51±0.01	5.39±0.03	5.29±0.04	5.22±0.02	500	1	2.21	1.50 ≤ log a < 2.90	–	
4979	F1V	60.1±1.5	6.37±0.01	6.10±0.01	5.61±0.02	5.51±0.04	5.47±0.03	710	1	1.80	1.50 ≤ log a < 2.90	3.25 ≤ log a < 4.65	
5186	A5Vn	64.9±2.0	6.77±0.01	6.55±0.01	6.07±0.02	6.03±0.03	5.98±0.02	280	1	1.73	1.50 ≤ log a < 2.90	3.25 ≤ log a < 4.65	
5300	A3IV	56.9±2.0	5.40±0.01	5.23±0.01	4.86±0.02	4.84±0.02	4.78±0.02	400	1	2.10	1.50 ≤ log a < 2.90	–	
5310	A3V	47.3±1.7	5.72±0.01	5.58±0.01	5.28±0.02	5.27±0.04	5.22±0.02	50	3	1.83	1.50 ≤ log a < 2.55	3.25 ≤ log a < 4.65	
5317	A3m	59.0±1.0	5.19±0.01	5.05±0.01	5.10±0.21	5.00±0.21	4.77±0.02	450	1	2.27	1.50 ≤ log a < 2.90	3.60 ≤ log a < 4.65	
5542	A7V	41.0±0.4	4.54±0.01	4.34±0.01	4.45±0.30	4.28±0.25	4.13±0.40	400	1	2.24	1.50 ≤ log a < 2.90	3.60 ≤ log a < 4.65	
6514	A1m	63.9±1.2	5.92±0.01	5.62±0.01	5.06±0.02	4.99±0.02	4.97±0.02	710	1	1.77	1.50 ≤ log a < 2.90	3.60 ≤ log a < 4.65	
6539	F0V	67.5±1.5	6.49±0.01	6.24±0.01	5.79±0.02	5.65±0.03	5.62±0.02	710	1	1.84	1.50 ≤ log a < 2.90	3.60 ≤ log a < 4.65	
6686	A5III-IVv	30.5±0.1	2.84±0.01	2.66±0.01	2.34±0.26	2.37±0.19	2.25±0.28	630	4	2.53	1.50 ≤ log a < 2.55	3.95 ≤ log a < 4.65	
6960	A0V	71.4±1.5	5.14±0.01	5.11±0.01	5.38±0.25	5.03±0.03	4.96±0.02	400	1	2.45	1.50 ≤ log a < 2.90	–	
7345	A1V	59.4±1.0	5.69±0.01	5.62±0.01	5.49±0.02	5.53±0.02	5.46±0.02	20	4	2.37	1.50 ≤ log a < 2.90	3.60 ≤ log a < 4.65	
7447	F0IV	58.1±1.2	6.25±0.01	5.98±0.01	5.41±0.04	5.36±0.06	5.34±0.02	790	1	1.81	1.50 ≤ log a < 2.90	3.25 ≤ log a < 4.65	
8122	A3	69.3±1.8	7.01±0.01	6.75±0.01	6.26±0.02	6.19±0.02	6.17±0.02	100	4	1.74	1.50 ≤ log a < 2.90	3.60 ≤ log a < 4.65	
8241	A1V	62.0±0.7	5.08±0.01	5.04±0.01	4.99±0.04	5.03±0.03	4.96±0.03	200	4	2.65	1.50 ≤ log a < 2.90	3.60 ≤ log a < 4.65	
8588	F2Vw	42.0±0.8	6.28±0.01	5.96±0.01	5.29±0.02	5.19±0.03	5.10±0.02	890	1	1.57	–	3.25 ≤ log a < 4.65	
8847	A5m	70.8±2.3	6.67±0.01	6.46±0.01	6.13±0.02	6.09±0.02	6.07±0.02	100	1	1.87	1.50 ≤ log a < 2.90	–	
8903	A5V	18.0±0.2	2.83±0.01	2.65±0.01	2.34±0.23	2.35±0.16	2.27±0.24	630	6	2.01	1.50 ≤ log a < 2.20	3.60 ≤ log a < 4.65	
9153	F0V	39.5±0.5	5.11±0.01	4.80±0.01	4.57±0.24	4.34±0.19	4.35±0.30	450	1	1.97	1.50 ≤ log a < 2.55	3.60 ≤ log a < 4.65	
9480	A3IV	35.3±0.5	4.79±0.01	4.65±0.01	4.35±0.25	4.12±0.04	4.25±0.27	40	1	1.93	1.50 ≤ log a < 2.55	–	
9836	A2m	55.7±1.1	5.19±0.01	5.04±0.01	5.22±0.31	4.74±0.04	4.74±0.02	500	1	2.20	1.50 ≤ log a < 2.90	–	
9977	A5IV-V	58.7±0.9	4.93±0.01	4.80±0.01	4.62±0.24	4.57±0.23	4.42±0.02	500	1	2.36	1.50 ≤ log a < 2.90	3.60 ≤ log a < 4.65	
10054	A1V	70.6±1.2	6.18±0.01	6.05±0.01	5.75±0.02	5.76±0.02	5.69±0.03	200	4	2.20	1.50 ≤ log a < 2.90	–	
10064	A5III	38.9±0.5	3.20±0.01	3.02±0.01	2.74±0.32	2.77±0.25	2.68±0.35	400	1	2.80	1.50 ≤ log a < 2.55	3.60 ≤ log a < 4.65	
10069	F0IV/V	66.7±2.1	6.81±0.01	6.49±0.01	5.98±0.02	5.91±0.04	5.87±0.02	630	1	1.75	1.50 ≤ log a < 2.90	–	
10670	A1Vnn	34.4±0.3	4.03±0.01	4.00±0.01	3.80±0.27	3.86±0.23	3.96±0.03	100	4	2.57	1.50 ≤ log a < 2.20	3.60 ≤ log a < 4.65	
11090	F0III-IV	47.0±0.7	6.12±0.01	5.83±0.01	5.20±0.04	5.13±0.02	5.07±0.03	890	1	1.69	1.85 ≤ log a < 2.55	3.60 ≤ log a < 4.65	
11102	A5V	60.9±1.0	6.15±0.01	5.92±0.01	5.58±0.03	5.49±0.02	5.44±0.02	890	5	1.77	1.50 ≤ log a < 2.90	–	
11138	A5V	71.9±2.3	6.88±0.01	6.66±0.01	6.23±0.02	6.14±0.04	6.15±0.02	100	1	1.80	1.50 ≤ log a < 2.90	–	
11486	F0III	49.8±0.7	5.64±0.01	5.32±0.01	5.08±0.25	4.82±0.19	4.59±0.02	1000	4	1.80	–	3.25 ≤ log a < 4.65	
11569	A5p...	40.7±1.3	4.73±0.01	4.63±0.01	3.98±0.43	4.29±0.04	4.25±0.03	180	1	2.19	1.85 ≤ log a < 2.90	–	
11678	A9V	66.1±2.0	6.43±0.01	6.16±0.01	5.60±0.02	5.54±0.02	5.49±0.02	790	1	1.84	–	3.60 ≤ log a < 4.65	
12489	A3V	71.0±1.6	5.40±0.01	5.31±0.01	5.11±0.02	5.12±0.03	5.07±0.02	450	1	2.32	–	3.60 ≤ log a < 4.65	

Table 1: The VAST sample

HIP	Spectral type	Distance (pc)	B_T (mag)	V_T (mag)	J (mag)	H (mag)	K_S (mag)	Age ^a (Myrs)	Age Ref.	Mass (M_\odot)	Separation coverage ($\log a$ [au])		
											Adaptive optics	CPM search	
12706	A3V	24.4±0.4	3.64±0.01	3.55±0.01	3.24±0.26	3.10±0.21	3.08±0.26	350	1	2.09	$1.50 \leq \log a < 2.20$	$3.60 \leq \log a < 4.65$	
12828	F0IV	25.8±0.2	4.63±0.01	4.30±0.01	3.66±0.25	3.44±0.21	3.46±0.19	1000	1	1.78	–	$3.60 \leq \log a < 4.65$	
12832	A7III-IV	36.3±0.5	5.44±0.01	5.21±0.01	–	–	4.56±0.03	630	1	1.73	$1.50 \leq \log a < 2.55$	$3.25 \leq \log a < 4.65$	
13133	A3Vv+...	64.8±1.6	6.44±0.01	6.28±0.01	5.71±0.02	5.54±0.02	5.47±0.02	10	3	2.59	$1.50 \leq \log a < 2.90$	–	
13141	A2V	50.5±0.5	5.38±0.01	5.27±0.01	5.14±0.04	5.16±0.08	4.97±0.02	100	4	2.39	$1.50 \leq \log a < 2.90$	–	
13717	A3V	57.2±0.8	5.26±0.01	5.17±0.01	5.02±0.03	4.98±0.04	4.86±0.02	500	1	2.17	$1.50 \leq \log a < 2.90$	–	
13782	A5IV/V	47.7±0.8	5.73±0.01	5.46±0.01	5.06±0.04	5.01±0.03	4.92±0.02	560	1	1.86	$1.50 \leq \log a < 2.55$	–	
14146	A3IV-V	27.2±0.1	4.28±0.01	4.09±0.01	3.66±0.27	3.54±0.22	3.57±0.24	350	6	2.07	$1.50 \leq \log a < 2.55$	–	
14232	F0V	46.0±1.0	6.72±0.01	6.40±0.01	5.72±0.02	5.65±0.05	5.55±0.02	400	1	1.53	–	$3.25 \leq \log a < 4.65$	
14293	A8V	41.6±0.7	5.49±0.01	5.28±0.01	4.87±0.05	4.83±0.04	4.74±0.02	500	1	1.83	$1.50 \leq \log a < 2.90$	$3.25 \leq \log a < 4.65$	
14551	A5V	54.6±1.5	6.38±0.01	6.19±0.01	5.89±0.02	5.85±0.05	5.77±0.02	30	2	1.67	$1.50 \leq \log a < 2.90$	–	
14862	A2Vnn	50.7±0.5	4.89±0.01	4.84±0.01	5.07±0.27	4.78±0.02	4.71±0.02	320	1	2.26	$1.50 \leq \log a < 2.55$	$3.60 \leq \log a < 4.65$	
15197	kA4hA9mA9V	33.6±0.3	5.07±0.01	4.82±0.01	4.42±0.25	4.25±0.22	4.22±0.02	400	4	1.88	$1.50 \leq \log a < 2.55$	–	
15353	A3V	54.9±0.9	6.20±0.01	6.04±0.01	5.78±0.02	5.75±0.03	5.69±0.03	60	2	1.71	$1.50 \leq \log a < 2.90$	–	
15648	A3V	46.2±0.7	5.03±0.01	4.95±0.01	4.80±0.04	4.86±0.02	4.78±0.02	250	1	2.11	$1.85 \leq \log a < 2.55$	–	
16285	A5V	65.4±1.3	6.00±0.01	5.78±0.01	5.35±0.04	5.24±0.04	5.18±0.04	710	1	2.00	$1.50 \leq \log a < 2.90$	–	
16292	A1V	60.9±1.1	5.14±0.01	5.10±0.01	4.72±0.19	5.06±0.04	5.00±0.02	350	1	2.32	$1.50 \leq \log a < 2.90$	–	
16591	A3V	56.1±1.4	5.95±0.01	5.79±0.01	5.50±0.02	5.50±0.01	5.49±0.02	40	1	1.77	$1.50 \leq \log a < 2.90$	–	
16599	A3V	74.4±2.1	6.11±0.01	5.98±0.01	5.72±0.03	5.71±0.03	5.68±0.02	400	1	2.08	$1.50 \leq \log a < 2.90$	–	
17395	A5m	42.4±0.9	5.85±0.01	5.62±0.01	5.21±0.02	5.17±0.06	5.08±0.02	130	1	1.75	$1.50 \leq \log a < 2.90$	–	
17954	A2V+...	56.5±1.8	5.50±0.01	5.26±0.01	4.84±0.04	4.90±0.02	4.81±0.02	250	1	1.94	$1.50 \leq \log a < 2.90$	$3.60 \leq \log a < 4.65$	
18217	A5m	50.5±1.0	6.01±0.01	5.81±0.01	5.45±0.02	5.41±0.02	5.37±0.02	50	1	1.75	$1.50 \leq \log a < 2.55$	$3.60 \leq \log a < 4.65$	
18481	A2Vn	70.2±2.1	6.16±0.01	6.08±0.01	5.97±0.02	5.97±0.03	5.92±0.02	100	1	2.05	–	$3.60 \leq \log a < 4.65$	
18547	A8V	61.2±1.7	6.79±0.01	6.56±0.01	6.07±0.02	6.02±0.02	5.98±0.02	100	1	1.70	$1.50 \leq \log a < 2.90$	–	
18907	A0.5Va	35.9±0.2	3.94±0.01	3.89±0.01	3.75±0.20	3.84±0.19	3.78±0.30	350	1	2.35	$1.50 \leq \log a < 2.90$	–	
19893	F1V	20.5±0.2	4.61±0.01	4.29±0.01	3.68±0.25	3.47±0.21	3.51±0.22	320	4	1.70	–	$3.25 \leq \log a < 4.65$	
19990	A3m	28.9±0.3	5.23±0.01	4.95±0.01	4.79±0.27	4.58±0.26	4.36±0.02	10	3	1.41	$1.50 \leq \log a < 2.55$	$3.25 \leq \log a < 4.65$	
20087	F0V	54.1±1.5	5.97±0.01	5.66±0.01	5.06±0.04	4.94±0.06	4.90±0.02	630	7	1.75	$1.50 \leq \log a < 2.90$	–	
20156	A7V	74.5±2.1	5.73±0.01	5.48±0.01	5.13±0.25	4.78±0.03	4.74±0.03	710	1	2.20	–	$3.60 \leq \log a < 4.65$	
20219	F0IV	45.7±0.8	5.91±0.01	5.61±0.01	5.00±0.04	4.93±0.05	4.85±0.01	630	7	1.83	$1.85 \leq \log a < 2.55$	–	
20261	F0IV-V	46.9±0.9	5.52±0.01	5.28±0.01	4.75±0.05	4.97±0.28	4.69±0.02	630	7	1.93	$1.50 \leq \log a < 2.90$	–	
20507	A2V	64.1±1.0	5.26±0.01	5.17±0.01	5.08±0.02	5.06±0.02	4.93±0.02	450	1	2.29	$1.50 \leq \log a < 2.90$	–	
20542	A7V	49.5±1.0	5.00±0.01	4.81±0.01	4.56±0.27	4.51±0.21	4.41±0.02	630	7	2.09	$1.50 \leq \log a < 2.90$	–	
20635	A7IV-V	47.2±0.5	4.38±0.01	4.21±0.01	4.09±0.28	4.06±0.23	4.08±0.47	630	7	2.18	–	–	
20641	A7V	45.4±0.7	5.56±0.01	5.29±0.01	5.09±0.25	4.92±0.23	4.61±0.02	630	7	1.94	$1.50 \leq \log a < 2.90$	–	
20648	A2IV	45.5±1.1	4.32±0.01	4.26±0.01	4.34±0.32	4.38±0.24	4.10±0.03	630	7	2.11	$1.50 \leq \log a < 2.90$	–	
20711	A8Vn	47.1±0.6	4.60±0.01	4.30±0.01	3.86±0.25	3.79±0.23	3.76±0.35	630	7	2.31	$2.20 \leq \log a < 2.55$	–	
20713	F0V	49.1±1.4	4.78±0.01	4.50±0.01	4.17±0.25	3.95±0.24	4.03±0.24	630	7	2.24	$1.50 \leq \log a < 2.90$	–	
20842	Am	47.1±0.9	6.04±0.01	5.75±0.01	5.16±0.02	5.10±0.02	5.05±0.02	630	7	1.77	$1.50 \leq \log a < 2.90$	–	
20894	A7III	46.1±1.0	3.62±0.01	3.41±0.01	2.99±0.21	3.00±0.21	2.88±0.26	630	7	2.47	$1.50 \leq \log a < 2.90$	–	
20901	A7V	48.9±0.7	5.28±0.01	5.03±0.01	4.79±0.20	4.66±0.20	4.53±0.03	630	7	2.03	$1.50 \leq \log a < 2.55$	–	
21029	A6IV	43.2±0.6	4.98±0.01	4.79±0.01	4.77±0.22	4.68±0.20	4.36±0.04	630	7	2.00	$1.50 \leq \log a < 2.90$	–	
21036	F0V	45.2±0.7	5.71±0.01	5.42±0.01	5.22±0.31	4.83±0.04	4.75±0.02	630	7	1.87	$1.50 \leq \log a < 2.90$	–	
21039	Am	44.9±1.0	5.76±0.01	5.48±0.01	5.46±0.24	4.97±0.04	4.90±0.02	630	7	1.79	$1.50 \leq \log a < 2.90$	–	
21238	F0	70.8±3.2	7.04±0.02	6.83±0.01	6.39±0.02	6.38±0.03	6.32±0.03	60	1	1.74	–	$3.60 \leq \log a < 4.65$	
21273	A8V	48.5±1.3	4.93±0.01	4.67±0.01	4.31±0.26	4.29±0.23	4.07±0.04	630	7	2.21	–	–	

Table 1: The VAST sample

HIP	Spectral type	Distance (pc)	B_T (mag)	V_T (mag)	J (mag)	H (mag)	K_S (mag)	Age ^a (Myrs)	Age Ref.	Mass (M_\odot)	Separation coverage ($\log a$ [au])		
											Adaptive optics	CPM search	
21402	A5m	47.9±2.2	4.45±0.01	4.27±0.01	3.70±0.23	3.88±0.04	3.69±0.25	500	1	2.50	–	–	
21547	F0V	29.4±0.3	5.55±0.01	5.24±0.01	4.74±0.04	4.77±0.08	4.54±0.02	10	2	1.39	$1.50 \leq \log a < 2.55$	$3.25 \leq \log a < 4.65$	
21589	A6V	47.1±1.2	4.42±0.01	4.28±0.01	4.12±0.26	4.08±0.23	4.11±0.33	630	7	2.17	–	–	
21644	A0V	71.3±2.7	5.09±0.01	5.01±0.01	5.31±0.20	4.88±0.02	4.76±0.02	400	1	2.41	–	$3.60 \leq \log a < 4.65$	
21670	A5m	49.2±0.8	5.68±0.01	5.40±0.01	5.18±0.25	4.93±0.03	4.81±0.02	630	7	1.92	$1.50 \leq \log a < 2.55$	–	
21673	A4m	45.1±1.9	5.24±0.01	5.09±0.01	4.82±0.02	4.86±0.04	4.80±0.02	280	1	2.01	$1.50 \leq \log a < 2.90$	$3.25 \leq \log a < 4.65$	
21683	A5Vn	47.7±0.6	4.87±0.01	4.69±0.01	4.68±0.29	4.55±0.22	4.23±0.04	630	7	2.13	$1.50 \leq \log a < 2.90$	–	
22044	F0V	45.8±0.6	5.69±0.01	5.41±0.01	4.96±0.25	4.73±0.03	4.73±0.02	630	7	1.89	$1.50 \leq \log a < 2.55$	–	
22192	A3IV	56.2±1.0	6.39±0.01	6.20±0.01	5.80±0.02	5.73±0.04	5.71±0.02	10	3	1.43	$1.50 \leq \log a < 2.90$	–	
22287	A3m	52.8±1.4	5.57±0.01	5.31±0.01	5.11±0.24	4.77±0.04	4.72±0.02	560	1	2.01	–	$3.60 \leq \log a < 4.65$	
22300	F0	52.4±1.3	6.67±0.01	6.35±0.01	5.66±0.02	5.58±0.03	5.53±0.02	890	1	1.61	–	$3.25 \leq \log a < 4.65$	
22361	A9IV	47.1±0.6	6.29±0.01	5.99±0.01	5.35±0.02	5.29±0.02	5.22±0.02	790	1	1.64	$1.85 \leq \log a < 2.20$	$3.25 \leq \log a < 4.65$	
22565	A7IV-V	51.3±1.9	5.34±0.01	5.12±0.01	4.97±0.26	4.57±0.04	4.49±0.02	630	7	2.09	$1.50 \leq \log a < 2.55$	–	
22845	A0V	35.7±0.3	4.75±0.01	4.66±0.01	4.85±0.25	4.52±0.05	4.42±0.05	100	4	2.16	$1.85 \leq \log a < 2.20$	$3.25 \leq \log a < 4.65$	
23179	A1V	52.3±2.2	5.02±0.01	5.00±0.01	4.90±0.47	4.98±0.02	4.92±0.03	30	2	2.39	$1.50 \leq \log a < 2.90$	$3.60 \leq \log a < 4.65$	
23296	A8IV	49.6±1.3	6.64±0.01	6.34±0.01	5.76±0.02	5.62±0.02	5.58±0.02	450	1	1.59	$1.50 \leq \log a < 2.55$	–	
23497	A7V	53.0±0.8	4.83±0.01	4.63±0.01	4.33±0.32	4.38±0.21	4.25±0.02	630	7	2.22	$1.50 \leq \log a < 2.55$	–	
23554	A2IV	58.2±1.0	5.71±0.01	5.60±0.01	5.43±0.06	5.40±0.04	5.34±0.02	280	1	2.04	$1.50 \leq \log a < 2.90$	–	
23585	A2	61.3±2.0	6.78±0.01	6.54±0.01	6.09±0.02	6.02±0.03	5.98±0.02	10	3	1.42	$1.50 \leq \log a < 2.90$	$3.25 \leq \log a < 4.65$	
23871	A5V	58.1±1.3	5.43±0.01	5.30±0.01	5.11±0.04	5.08±0.03	5.05±0.02	400	1	2.15	$1.50 \leq \log a < 2.90$	–	
23875	A3III	27.4±0.3	2.95±0.01	2.78±0.01	2.47±0.26	2.44±0.20	2.40±0.22	500	1	2.44	–	$3.60 \leq \log a < 4.65$	
23983	A2m	54.7±1.1	5.73±0.01	5.45±0.01	4.96±0.03	4.93±0.02	4.86±0.02	630	7	2.00	$1.50 \leq \log a < 2.90$	–	
24340	A4m	46.9±1.8	5.07±0.01	4.85±0.01	4.38±0.19	4.39±0.04	4.40±0.03	560	1	2.09	$1.50 \leq \log a < 2.90$	$3.25 \leq \log a < 4.65$	
25280	A0V	68.3±1.6	5.63±0.01	5.63±0.01	5.65±0.02	5.68±0.04	5.65±0.02	140	1	2.29	$1.50 \leq \log a < 2.90$	–	
26309	A2III-IV	52.8±1.2	6.45±0.01	6.28±0.01	5.96±0.02	5.94±0.03	5.86±0.02	30	2	1.55	$1.50 \leq \log a < 2.55$	–	
26382	F0V	48.6±0.9	5.80±0.01	5.55±0.01	5.06±0.02	5.00±0.02	4.93±0.03	630	7	1.86	$1.50 \leq \log a < 2.55$	–	
26395	A2V	62.9±1.7	6.16±0.01	6.10±0.01	5.99±0.02	5.99±0.02	5.97±0.02	10	3	1.43	$1.50 \leq \log a < 2.90$	–	
26563	A4V	44.6±0.9	4.95±0.01	4.79±0.01	4.69±0.19	4.54±0.08	4.42±0.02	500	1	2.11	$1.50 \leq \log a < 2.90$	–	
26624	A8Vs	42.6±0.7	6.32±0.01	6.01±0.01	5.42±0.04	5.36±0.05	5.21±0.02	710	1	1.58	$1.50 \leq \log a < 2.90$	–	
27249	A4Vn	60.8±1.6	6.11±0.01	5.95±0.01	5.54±0.02	5.53±0.02	5.51±0.02	350	1	1.92	$2.20 \leq \log a < 2.55$	–	
27288	A2IV-V(n)	21.6±0.1	3.67±0.01	3.54±0.01	3.39±0.28	3.31±0.25	3.29±0.28	200	8	2.03	$1.50 \leq \log a < 2.55$	–	
27321	A6V	19.4±0.0	4.06±0.01	3.87±0.01	3.67±0.24	3.54±0.20	3.53±0.22	10	2	1.41	$1.50 \leq \log a < 2.20$	–	
27947	F1V	34.7±0.2	5.62±0.01	5.32±0.01	4.99±0.27	4.69±0.02	4.57±0.03	790	1	1.65	–	$3.25 \leq \log a < 4.65$	
28614		47.5±1.5	4.33±0.01	4.15±0.01	3.73±0.31	3.60±0.28	3.64±0.26	710	9	2.19	$1.50 \leq \log a < 2.55$	–	
28910	A0V	53.0±1.5	4.72±0.01	4.67±0.01	4.74±0.23	4.59±0.24	4.52±0.02	400	1	2.35	$1.50 \leq \log a < 2.55$	–	
29711	A5IVs	65.1±1.8	6.09±0.01	6.01±0.01	5.87±0.02	5.90±0.04	5.86±0.02	40	1	1.80	$1.50 \leq \log a < 2.90$	–	
29850	A2V	69.1±1.6	5.51±0.01	5.40±0.01	5.34±0.25	5.18±0.02	5.11±0.03	220	1	2.06	$1.50 \leq \log a < 2.90$	–	
29852	A2V	61.9±1.0	6.06±0.01	5.89±0.01	5.57±0.02	5.52±0.03	5.44±0.02	280	1	1.95	$1.50 \leq \log a < 2.90$	–	
29997	A0Vn	53.6±0.7	4.78±0.01	4.76±0.01	4.97±0.21	4.77±0.04	4.67±0.02	110	10	2.80	$1.50 \leq \log a < 2.90$	$3.60 \leq \log a < 4.65$	
30060	A2Vs	48.0±0.9	4.47±0.01	4.44±0.01	4.28±0.27	4.29±0.19	4.35±0.02	350	1	2.39	$1.50 \leq \log a < 2.90$	–	
30167	A5	63.1±1.9	7.04±0.01	6.78±0.01	6.28±0.02	6.16±0.03	6.14±0.02	40	1	1.65	$1.85 \leq \log a < 2.90$	–	
30419	A5IV	37.5±1.3	4.63±0.01	4.42±0.01	3.87±0.25	3.72±0.19	3.92±0.04	630	1	2.05	$1.50 \leq \log a < 2.90$	–	
30666	A3Vn	72.5±1.6	5.95±0.01	5.86±0.01	5.70±0.02	5.70±0.03	5.64±0.02	350	1	2.12	$1.50 \leq \log a < 2.90$	–	
31119	A3V	63.7±1.5	5.43±0.01	5.23±0.01	4.92±0.04	4.86±0.07	4.77±0.04	560	1	2.20	$1.50 \leq \log a < 2.90$	–	
31167	F0Vnn	41.8±0.4	5.90±0.01	5.63±0.01	5.12±0.02	5.01±0.02	4.91±0.02	710	1	1.68	$1.50 \leq \log a < 2.55$	–	
32104	A2V	43.6±1.3	5.30±0.01	5.22±0.01	5.03±0.04	5.07±0.02	5.01±0.02	30	2	1.94	$1.85 \leq \log a < 2.55$	$3.25 \leq \log a < 4.65$	

Table 1: The VAST sample

HIP	Spectral type	Distance (pc)	B_T (mag)	V_T (mag)	J (mag)	H (mag)	K_S (mag)	Age ^a (Myrs)	Age Ref.	Mass (M_\odot)	Separation coverage (log a [au])	
											Adaptive optics	CPM search
32617	F1V	40.0±0.5	6.08±0.01	5.77±0.01	5.40±0.28	5.13±0.03	5.01±0.02	630	1	1.61	1.50 ≤ log a < 2.55	–
32938	A3V	55.2±0.7	6.17±0.01	5.96±0.01	5.58±0.02	5.54±0.03	5.51±0.02	200	1	1.84	1.50 ≤ log a < 2.90	–
33018	A3III	58.0±0.6	3.73±0.01	3.60±0.01	3.25±0.22	3.23±0.19	3.16±0.30	500	1	2.50	1.85 ≤ log a < 2.90	–
33024	F0Vn	62.3±1.3	6.05±0.01	5.77±0.01	5.31±0.02	5.23±0.06	5.09±0.02	790	1	1.96	1.85 ≤ log a < 2.90	–
33202	F0Vp	25.6±1.0	5.06±0.01	4.75±0.01	3.90±0.41	3.71±0.43	3.89±0.04	1000	1	1.61	–	3.60 ≤ log a < 4.65
33485	A2Vn	73.9±1.3	4.93±0.01	4.90±0.01	5.05±0.27	4.94±0.23	4.79±0.03	350	1	2.64	1.50 ≤ log a < 2.90	–
34059	A4IV	60.6±1.5	5.08±0.01	4.94±0.01	4.86±0.25	4.72±0.08	4.57±0.02	500	1	2.34	–	3.60 ≤ log a < 4.65
34897	A5	66.8±2.6	7.08±0.01	6.78±0.01	6.14±0.02	6.04±0.02	5.99±0.02	890	1	1.63	1.50 ≤ log a < 2.90	3.60 ≤ log a < 4.65
35350	A3V	30.9±0.2	3.71±0.01	3.58±0.01	3.54±0.33	3.50±0.28	3.54±0.26	320	1	2.39	1.50 ≤ log a < 2.55	–
36393	A4V	54.0±0.7	5.22±0.01	5.08±0.01	4.82±0.04	4.79±0.02	4.74±0.02	500	1	2.16	1.50 ≤ log a < 2.90	3.60 ≤ log a < 4.65
38235	A9V	61.2±1.9	7.07±0.01	6.75±0.01	6.06±0.02	5.93±0.05	5.86±0.02	1120	1	1.57	1.85 ≤ log a < 2.90	–
38723	A3p	59.0±1.7	6.54±0.01	6.25±0.01	5.55±0.02	5.44±0.02	5.40±0.02	1120	1	1.70	1.50 ≤ log a < 2.90	3.60 ≤ log a < 4.65
39567	A1V	65.8±1.4	5.15±0.01	5.14±0.01	5.11±0.04	5.12±0.02	5.10±0.02	320	1	2.42	–	3.60 ≤ log a < 4.65
40878	F0IV	59.4±1.4	6.84±0.01	6.53±0.01	5.90±0.03	5.82±0.03	5.79±0.02	710	1	1.64	–	3.60 ≤ log a < 4.65
41081	A0V	70.0±1.1	5.91±0.01	5.89±0.01	5.86±0.02	5.87±0.03	5.87±0.02	10	11	2.30	1.50 ≤ log a < 2.90	–
41152	A3V	50.4±0.7	5.66±0.01	5.52±0.01	5.25±0.02	5.29±0.03	5.25±0.02	200	4	1.91	1.85 ≤ log a < 2.55	3.60 ≤ log a < 4.65
41375	A5III-IV	50.0±1.0	5.86±0.01	5.62±0.01	5.16±0.04	5.13±0.05	4.99±0.02	710	1	1.83	1.85 ≤ log a < 2.90	3.25 ≤ log a < 4.65
42080	A2m	46.8±0.9	5.70±0.01	5.48±0.01	5.04±0.04	5.02±0.03	4.93±9.99	560	1	1.84	1.85 ≤ log a < 2.55	3.25 ≤ log a < 4.65
42313	A1Vnn	49.2±1.5	4.15±0.01	4.13±0.01	4.15±0.28	4.13±0.26	4.03±0.04	350	1	2.59	1.50 ≤ log a < 2.90	3.60 ≤ log a < 4.65
42425	A0V	73.6±1.1	5.19±0.01	5.18±0.01	5.24±0.04	5.12±0.04	5.07±0.02	100	10	3.11	1.50 ≤ log a < 2.90	–
42806	A1IV	55.6±0.6	4.68±0.01	4.65±0.01	4.80±0.18	4.79±0.19	4.64±0.02	320	1	2.49	1.85 ≤ log a < 2.90	3.60 ≤ log a < 4.65
42895	A4V	58.6±0.9	6.28±0.01	6.05±0.01	5.63±0.02	5.52±0.03	5.47±0.02	630	1	1.81	1.50 ≤ log a < 2.90	–
43121	A1V	54.0±1.3	6.03±0.01	5.90±0.01	5.65±0.04	5.64±0.04	5.55±0.02	50	1	1.88	1.50 ≤ log a < 2.90	3.60 ≤ log a < 4.65
43584	A8ms	64.5±1.7	5.92±0.01	5.69±0.01	5.48±0.32	5.19±0.04	5.15±0.02	630	1	2.03	2.20 ≤ log a < 2.55	–
43932	A7IV	59.6±1.0	5.63±0.01	5.46±0.01	5.31±0.26	5.08±0.02	5.02±0.02	500	1	2.06	2.20 ≤ log a < 2.55	–
43970	A5III	45.7±0.5	5.41±0.01	5.24±0.01	4.91±0.04	4.97±0.22	4.87±0.02	400	4	1.90	1.50 ≤ log a < 2.90	3.60 ≤ log a < 4.65
44001	F0IV	46.1±0.7	5.94±0.01	5.71±0.01	5.27±0.02	5.21±0.02	5.16±0.02	320	4	1.77	1.50 ≤ log a < 2.90	3.25 ≤ log a < 4.65
44127	A7V	14.5±0.0	3.36±0.01	3.13±0.01	2.78±0.23	2.76±0.18	2.66±0.24	630	6	1.69	1.50 ≤ log a < 2.20	3.60 ≤ log a < 4.65
44342	A8Vn	58.0±1.3	6.34±0.01	6.08±0.01	5.54±0.02	5.52±0.03	5.43±0.02	710	1	1.78	–	3.25 ≤ log a < 4.65
44574	A8V	72.8±2.4	6.74±0.01	6.48±0.01	5.95±0.03	5.89±0.02	5.87±0.02	710	1	1.81	–	3.25 ≤ log a < 4.65
44901	A1m	28.8±0.2	4.79±0.01	4.48±0.01	4.15±0.28	4.04±0.24	4.04±0.28	220	1	1.86	1.50 ≤ log a < 2.55	3.60 ≤ log a < 4.65
45001	A4IV-V	65.0±1.3	5.81±0.01	5.62±0.01	5.29±0.02	5.23±0.03	5.14±0.02	560	1	2.07	1.50 ≤ log a < 2.90	–
45493	A5V	35.8±0.3	5.04±0.01	4.83±0.01	4.48±0.20	4.35±0.18	4.29±0.02	560	1	1.87	1.50 ≤ log a < 2.55	3.60 ≤ log a < 4.65
45510	A3	74.3±3.2	7.38±0.01	7.06±0.01	6.36±0.02	6.26±0.03	6.22±0.02	1000	1	1.61	–	3.25 ≤ log a < 4.65
45688	A3V	38.3±1.1	3.96±0.01	3.92±0.01	3.48±0.28	3.46±0.26	3.42±0.35	560	1	2.19	1.50 ≤ log a < 2.55	3.60 ≤ log a < 4.65
47204	A2.5V	71.5±2.1	5.68±0.01	5.54±0.01	5.16±0.02	5.12±0.03	5.05±0.02	450	1	1.91	1.50 ≤ log a < 2.90	–
47300	F0V	37.6±0.5	5.55±0.01	5.30±0.01	4.97±0.23	4.84±0.04	4.75±0.02	280	1	1.76	1.50 ≤ log a < 2.55	–
47479	A3IV	72.6±2.2	5.54±0.01	5.33±0.01	5.37±0.31	5.05±0.34	4.80±0.02	560	1	2.18	1.50 ≤ log a < 2.90	–
47701	A2IV	49.0±0.9	5.77±0.01	5.64±0.01	5.39±0.02	5.44±0.02	5.39±0.02	10	3	1.44	–	3.25 ≤ log a < 4.65
47777	F0	73.4±2.1	7.13±0.01	6.81±0.01	6.11±0.02	5.98±0.02	5.96±0.02	1120	1	1.67	–	3.60 ≤ log a < 4.65
48319	F2IV	35.6±0.3	4.12±0.01	3.80±0.01	3.27±0.23	3.12±0.25	3.15±0.27	710	1	2.20	1.50 ≤ log a < 2.90	3.60 ≤ log a < 4.65
48341	A8III	63.6±1.2	6.22±0.01	6.04±0.01	5.73±0.02	5.68±0.04	5.64±0.02	320	12	1.91	1.50 ≤ log a < 2.20	–
48763	A4V	67.5±2.5	6.53±0.01	6.31±0.01	5.85±0.02	5.77±0.03	5.69±0.02	500	1	1.82	1.50 ≤ log a < 2.55	–
49593	A7V	28.2±0.1	4.71±0.01	4.50±0.01	4.27±0.25	4.05±0.04	4.00±0.04	320	12	1.82	1.50 ≤ log a < 2.55	–
50372	A2IV	42.2±1.4	3.48±0.01	3.43±0.01	3.44±0.28	3.46±0.21	3.42±0.33	320	1	2.83	1.50 ≤ log a < 2.55	3.95 ≤ log a < 4.65
51056	F0V	71.5±1.1	5.04±0.01	4.75±0.01	4.55±0.35	4.26±0.34	3.97±0.02	710	1	2.20	–	3.60 ≤ log a < 4.65

Table 1: The VAST sample

HIP	Spectral type	Distance (pc)	B_T (mag)	V_T (mag)	J (mag)	H (mag)	K_S (mag)	Age ^a (Myrs)	Age Ref.	Mass (M_\odot)	Separation coverage ($\log a$ [au])	
											Adaptive optics	CPM search
51194	A2V	68.4±1.2	6.12±0.01	6.00±0.01	5.84±0.02	5.86±0.04	5.79±0.02	200	1	2.04	$1.50 \leq \log a < 2.90$	–
51200	A2V	66.1±1.5	6.19±0.01	6.03±0.01	5.63±0.02	5.58±0.02	5.53±0.02	400	1	1.96	$1.50 \leq \log a < 2.90$	$3.60 \leq \log a < 4.65$
51384	F0IV	40.6±0.6	5.80±0.01	5.55±0.01	4.95±0.04	4.93±0.03	4.85±0.02	710	1	1.69	$1.50 \leq \log a < 2.55$	$3.60 \leq \log a < 4.65$
51658	A7IV	34.6±0.6	4.97±0.01	4.74±0.01	4.12±0.23	4.06±0.23	4.20±0.01	200	4	2.15	$1.50 \leq \log a < 2.55$	$3.60 \leq \log a < 4.65$
51907	F0V	61.5±2.0	6.90±0.01	6.60±0.01	6.05±0.02	5.93±0.03	5.88±0.02	630	1	1.64	$1.50 \leq \log a < 2.90$	–
51974	F0V	74.4±2.5	6.86±0.01	6.55±0.01	5.95±0.02	5.83±0.02	5.80±0.02	890	1	1.80	–	$3.25 \leq \log a < 4.65$
52457	A3Vn	70.3±1.2	5.12±0.01	5.08±0.01	4.94±0.04	4.93±0.02	4.92±0.02	400	1	2.46	–	$3.60 \leq \log a < 4.65$
52513	A5V	66.9±1.4	6.49±0.01	6.29±0.01	5.84±0.02	5.83±0.02	5.77±0.03	450	1	1.84	–	$3.60 \leq \log a < 4.65$
53824	A5III	46.4±0.6	5.17±0.01	5.00±0.01	4.86±0.24	4.70±0.02	4.61±0.02	450	1	2.04	$1.50 \leq \log a < 2.55$	$3.60 \leq \log a < 4.65$
53954	A1m	38.9±0.3	4.47±0.01	4.41±0.01	4.32±0.23	4.32±0.18	4.32±0.04	250	1	2.22	$1.50 \leq \log a < 2.55$	–
54027	F0V	55.9±1.4	6.43±0.01	6.15±0.01	5.63±0.03	5.49±0.05	5.45±0.02	790	1	1.72	$1.85 \leq \log a < 2.90$	$3.25 \leq \log a < 4.65$
54063	A5	61.4±2.3	7.29±0.01	7.01±0.01	6.37±0.02	6.29±0.02	6.27±0.02	20	3	1.29	$1.50 \leq \log a < 2.90$	$3.25 \leq \log a < 4.65$
54214	F0Vn	59.7±1.2	6.42±0.01	6.12±0.01	5.52±0.02	5.36±0.04	5.30±0.02	1000	1	1.74	–	$3.25 \leq \log a < 4.65$
54477	A1V	55.6±1.6	5.51±0.01	5.43±0.01	5.31±0.03	5.35±0.03	5.24±0.02	250	1	2.09	$1.50 \leq \log a < 2.90$	–
54688	A5V	56.2±1.1	6.57±0.01	6.32±0.01	5.84±0.02	5.83±0.04	5.76±0.02	60	1	1.72	$1.50 \leq \log a < 2.90$	$3.25 \leq \log a < 4.65$
54746	A3IV-V	50.4±2.2	5.57±0.01	5.39±0.01	5.06±0.02	5.04±0.03	4.97±0.02	400	1	1.96	$1.50 \leq \log a < 2.90$	–
54872	A4V	17.9±0.1	2.71±0.01	2.54±0.01	2.24±0.26	2.19±0.19	2.14±0.21	710	13	2.07	$1.50 \leq \log a < 2.20$	$3.60 \leq \log a < 4.65$
54879	A2V	50.6±0.4	3.32±0.01	3.30±0.01	3.12±0.28	3.19±0.24	3.08±0.31	320	1	3.00	–	$3.95 \leq \log a < 4.65$
55033	F0V	66.6±2.3	7.00±0.01	6.68±0.01	6.05±0.02	5.96±0.03	5.90±0.02	890	1	1.66	–	$3.60 \leq \log a < 4.65$
55084	A7IVn	56.5±0.8	4.70±0.01	4.48±0.01	4.32±0.30	4.19±0.24	4.13±0.28	500	1	2.40	$1.50 \leq \log a < 2.90$	$3.60 \leq \log a < 4.65$
55266	A2V	58.8±1.2	4.90±0.01	4.77±0.01	4.66±0.23	4.52±0.04	4.46±0.04	500	1	2.33	$1.50 \leq \log a < 2.90$	$3.60 \leq \log a < 4.65$
55488	A2	72.8±3.3	7.04±0.01	6.73±0.01	6.10±0.03	6.01±0.04	5.93±0.02	1000	1	1.70	–	$3.60 \leq \log a < 4.65$
55705	A7V(n)	25.2±0.1	4.30±0.01	4.09±0.01	3.65±0.43	3.52±0.57	3.55±0.53	630	9	1.81	$1.50 \leq \log a < 2.55$	$3.25 \leq \log a < 4.65$
56034	A2V	65.2±2.3	5.37±0.01	5.35±0.01	5.26±0.02	5.32±0.02	5.31±0.02	280	1	2.32	$1.50 \leq \log a < 2.90$	–
56083	A4m	67.2±1.7	6.48±0.01	6.30±0.01	5.97±0.02	5.97±0.03	5.93±0.02	140	1	1.88	$1.50 \leq \log a < 2.90$	$3.60 \leq \log a < 4.65$
56253	A2m	59.2±0.9	6.44±0.01	6.15±0.01	5.66±0.03	5.60±0.02	5.56±0.02	320	4	1.86	–	$3.25 \leq \log a < 4.65$
56920	A3	68.3±2.8	7.22±0.01	6.90±0.01	6.25±0.02	6.15±0.02	6.15±0.02	710	1	1.62	–	$3.25 \leq \log a < 4.65$
57013	A0V	65.5±1.4	5.58±0.01	5.54±0.01	5.49±0.03	5.51±0.05	5.44±0.02	180	11	2.35	$1.50 \leq \log a < 2.90$	–
57328	A4V	37.4±0.3	5.04±0.01	4.86±0.01	4.63±0.20	4.54±0.08	4.41±0.05	400	1	1.93	$1.50 \leq \log a < 2.90$	–
57562	A1	59.2±1.0	5.35±0.01	5.32±0.01	5.28±0.02	5.30±0.04	5.25±0.02	220	1	2.24	$1.50 \leq \log a < 2.90$	–
57606	F0V	59.7±2.1	6.25±0.01	5.97±0.01	5.27±0.02	5.16±0.02	5.12±0.02	1000	1	1.85	–	$3.25 \leq \log a < 4.65$
57646	A3m	63.0±1.5	6.37±0.01	6.07±0.01	5.49±0.02	5.45±0.03	5.35±0.02	890	1	1.83	$1.50 \leq \log a < 2.90$	$3.25 \leq \log a < 4.65$
57779	A5m	51.6±1.1	6.69±0.01	6.40±0.01	5.80±0.02	5.75±0.02	5.71±0.02	70	1	1.63	–	$3.25 \leq \log a < 4.65$
58001	A0Ve	25.5±0.3	2.46±0.01	2.40±0.01	2.38±0.29	2.49±0.17	2.43±0.29	320	12	2.78	$1.50 \leq \log a < 2.55$	$3.95 \leq \log a < 4.65$
58684	A7m	34.3±0.9	5.53±0.01	5.24±0.01	4.71±0.18	4.84±0.04	4.55±0.02	630	1	1.67	$1.50 \leq \log a < 2.55$	$3.25 \leq \log a < 4.65$
58758	Am	72.0±0.8	4.62±0.01	4.35±0.01	3.50±0.26	3.26±0.25	3.23±0.29	710	1	2.20	–	$3.95 \leq \log a < 4.65$
59394	A1V	58.8±1.9	5.51±0.01	5.45±0.01	5.34±0.02	5.36±0.04	5.32±0.02	220	1	2.15	$1.50 \leq \log a < 2.90$	–
59608	A2m	50.2±0.7	6.15±0.01	5.86±0.01	5.41±0.02	5.33±0.04	5.24±0.02	630	1	1.75	$1.50 \leq \log a < 2.90$	$3.25 \leq \log a < 4.65$
59774	A3V	24.7±0.1	3.41±0.01	3.30±0.01	3.32±0.25	3.31±0.25	3.10±0.34	320	12	2.31	$1.50 \leq \log a < 2.55$	$3.25 \leq \log a < 4.65$
59819	A3V	60.9±0.7	5.17±0.01	5.09±0.01	5.17±0.25	4.95±0.08	4.89±0.02	400	1	2.29	$1.50 \leq \log a < 2.90$	$3.60 \leq \log a < 4.65$
59923	A4m...	54.9±1.1	5.91±0.01	5.72±0.01	5.37±0.02	5.37±0.02	5.36±0.02	250	1	1.94	$1.50 \leq \log a < 2.90$	–
60018	A9.5III	59.4±1.6	6.58±0.01	6.26±0.01	5.53±0.02	5.45±0.02	5.36±0.02	1120	1	1.72	–	$3.25 \leq \log a < 4.65$
60595	A1V	70.5±1.4	5.99±0.01	5.93±0.01	5.89±0.02	5.91±0.02	5.83±0.02	140	1	2.13	$1.50 \leq \log a < 2.90$	–
61498	A0	72.8±1.7	5.79±0.01	5.78±0.01	5.78±0.02	5.79±0.04	5.77±0.02	10	14	2.53	$1.50 \leq \log a < 2.90$	–
61558	A3V	69.0±1.6	5.96±0.01	5.88±0.01	5.78±0.02	5.77±0.05	5.70±0.02	220	1	2.10	$1.50 \leq \log a < 2.90$	–
61622	A2V	40.2±0.9	3.91±0.01	3.85±0.01	3.80±0.25	3.68±0.23	3.71±0.26	400	1	2.45	–	$3.60 \leq \log a < 4.65$

Table 1: The VAST sample

HIP	Spectral type	Distance (pc)	B_T (mag)	V_T (mag)	J (mag)	H (mag)	K_S (mag)	Age ^a (Myrs)	Age Ref.	Mass (M_\odot)	Separation coverage ($\log a$ [au])		
											Adaptive optics	CPM search	
61688	F0V	67.3±1.6	6.34±0.01	6.02±0.01	5.37±0.02	5.25±0.04	5.16±0.02	1000	1	1.90	–	3.60 ≤ $\log a$ < 4.65	
61692	A7Vn	67.8±2.0	6.59±0.01	6.38±0.01	5.94±0.03	5.82±0.04	5.81±0.02	560	1	1.81	1.50 ≤ $\log a$ < 2.90	–	
61932	A1IV+	39.9±0.4	2.84±0.01	2.82±0.01	2.05±0.29	2.18±0.25	2.10±0.28	500	1	2.61	–	4.30 ≤ $\log a$ < 4.65	
61937	A7Vn	62.9±1.1	6.46±0.01	6.24±0.01	5.80±0.02	5.71±0.05	5.65±0.02	630	1	1.79	1.50 ≤ $\log a$ < 2.90	3.25 ≤ $\log a$ < 4.65	
61960	A0V	36.3±0.3	4.96±0.01	4.88±0.01	4.99±0.27	4.76±0.02	4.68±0.02	100	4	1.79	1.50 ≤ $\log a$ < 2.90	3.25 ≤ $\log a$ < 4.65	
62788	A0III	67.0±1.7	6.41±0.01	6.17±0.01	5.57±0.02	5.44±0.03	5.40±0.03	220	15	2.36	1.50 ≤ $\log a$ < 2.90	–	
62933	A7III	60.9±3.0	6.58±0.01	6.28±0.01	5.61±0.02	5.52±0.02	5.47±0.01	320	12	1.99	1.50 ≤ $\log a$ < 2.90	3.60 ≤ $\log a$ < 4.65	
62983	A2V	68.5±1.7	6.08±0.01	5.99±0.01	5.87±0.02	5.85±0.04	5.83±0.02	50	1	1.66	1.50 ≤ $\log a$ < 2.90	3.60 ≤ $\log a$ < 4.65	
63320	A5	70.4±2.7	7.21±0.01	6.96±0.01	6.49±0.04	6.39±0.05	6.39±0.03	40	1	1.69	–	3.25 ≤ $\log a$ < 4.65	
63491	A9V	56.2±1.3	6.92±0.01	6.61±0.01	5.96±0.02	5.87±0.03	5.78±0.02	790	1	1.57	1.50 ≤ $\log a$ < 2.90	–	
64246	A9III-IV	63.3±1.6	6.27±0.01	5.95±0.01	5.25±0.03	5.17±0.02	5.10±0.02	1000	1	1.88	2.20 ≤ $\log a$ < 2.55	3.60 ≤ $\log a$ < 4.65	
64692	A7V	74.1±2.4	6.01±0.01	5.80±0.01	5.34±0.02	5.29±0.03	5.22±0.02	560	1	2.10	–	3.60 ≤ $\log a$ < 4.65	
64979	F0IV	63.0±1.3	6.32±0.01	6.04±0.01	5.46±0.04	5.35±0.02	5.29±0.02	890	1	1.86	1.50 ≤ $\log a$ < 2.90	–	
65109	kA15hA3mA3va	18.0±0.1	2.81±0.01	2.73±0.01	2.71±0.28	2.74±0.21	2.76±0.26	350	6	2.02	–	3.25 ≤ $\log a$ < 4.65	
65241	A2m	65.9±1.4	6.02±0.01	5.89±0.01	5.69±0.02	5.67±0.03	5.62±0.02	220	1	2.05	1.50 ≤ $\log a$ < 2.90	3.60 ≤ $\log a$ < 4.65	
65477	A5V+M3-4V	25.1±0.1	4.20±0.01	4.01±0.01	3.29±0.23	3.29±0.23	3.15±0.24	320	12	2.30	1.50 ≤ $\log a$ < 2.55	3.60 ≤ $\log a$ < 4.65	
65728	A1Vn	71.4±1.0	5.46±0.01	5.46±0.01	5.43±0.02	5.46±0.03	5.43±0.02	280	1	2.37	1.85 ≤ $\log a$ < 2.90	3.60 ≤ $\log a$ < 4.65	
66065	A0/A1V	71.6±1.5	5.75±0.01	5.70±0.01	5.63±0.02	5.67±0.03	5.59±0.02	280	1	2.23	1.50 ≤ $\log a$ < 2.90	–	
66200	A1p...	56.7±0.6	4.97±0.01	4.92±0.01	5.18±0.28	4.98±0.27	4.88±0.02	320	1	2.38	1.50 ≤ $\log a$ < 2.55	–	
66223	F0IV	69.8±2.0	6.64±0.01	6.40±0.01	5.93±0.02	5.90±0.02	5.88±0.02	400	1	1.84	1.50 ≤ $\log a$ < 2.90	–	
66234	A5V	55.3±0.6	4.84±0.01	4.68±0.01	4.53±0.26	4.46±0.02	4.27±0.04	500	1	2.38	1.50 ≤ $\log a$ < 2.55	3.60 ≤ $\log a$ < 4.65	
66249	A3V	22.7±0.1	3.52±0.01	3.38±0.01	3.26±0.27	3.15±0.28	3.22±0.27	250	1	2.14	1.50 ≤ $\log a$ < 2.55	3.60 ≤ $\log a$ < 4.65	
66458	A7III	60.9±2.0	5.21±0.01	4.98±0.01	4.04±0.29	4.03±0.25	4.15±0.01	710	1	2.23	1.50 ≤ $\log a$ < 2.90	3.60 ≤ $\log a$ < 4.65	
66634	A3Vn	53.6±0.8	5.60±0.01	5.47±0.01	5.22±0.02	5.20±0.02	5.17±0.02	320	1	2.02	1.50 ≤ $\log a$ < 2.90	3.60 ≤ $\log a$ < 4.65	
66798	A2V	68.2±1.1	5.94±0.01	5.85±0.01	5.65±0.02	5.69±0.03	5.65±0.02	280	1	2.09	1.50 ≤ $\log a$ < 2.90	–	
67194	A5V	52.5±1.0	6.13±0.01	5.90±0.01	5.43±0.02	5.37±0.02	5.34±0.02	500	1	1.78	1.50 ≤ $\log a$ < 2.90	3.25 ≤ $\log a$ < 4.65	
67483	A7IV-V	62.5±1.9	6.72±0.01	6.46±0.01	5.87±0.02	5.78±0.02	5.62±0.99	1120	1	1.67	1.50 ≤ $\log a$ < 2.90	3.25 ≤ $\log a$ < 4.65	
67782	A7V	65.7±1.6	6.15±0.01	5.93±0.01	5.54±0.02	5.50±0.03	5.46±0.02	500	1	1.97	1.50 ≤ $\log a$ < 2.90	3.60 ≤ $\log a$ < 4.65	
69483	A8IV	50.1±1.6	4.75±0.01	4.54±0.01	4.21±0.29	4.16±0.24	4.10±0.30	500	1	2.38	1.50 ≤ $\log a$ < 2.90	–	
69592	A7V	59.9±1.6	6.62±0.01	6.40±0.01	5.93±0.02	5.90±0.02	5.88±0.02	60	1	1.75	1.50 ≤ $\log a$ < 2.90	–	
69713	A7V	29.1±0.2	5.00±0.01	4.76±0.01	4.64±0.20	4.32±0.04	4.29±0.04	50	1	1.81	1.50 ≤ $\log a$ < 2.55	3.25 ≤ $\log a$ < 4.65	
69732	A0p	30.4±0.1	4.27±0.01	4.18±0.01	3.98±0.30	4.03±0.25	3.91±0.04	200	4	2.15	1.50 ≤ $\log a$ < 2.55	3.60 ≤ $\log a$ < 4.65	
69951	A5	74.6±2.1	7.45±0.01	7.13±0.01	6.47±0.02	6.39±0.04	6.37±0.02	710	1	1.61	1.50 ≤ $\log a$ < 2.90	3.25 ≤ $\log a$ < 4.65	
69974	A1V	57.2±0.9	4.68±0.01	4.53±0.01	4.39±0.23	4.28±0.21	4.24±0.02	450	1	2.20	1.50 ≤ $\log a$ < 2.90	–	
69995	A2Vn	73.5±1.8	6.03±0.01	5.94±0.01	5.79±0.02	5.74±0.02	5.77±0.02	200	1	2.16	1.50 ≤ $\log a$ < 2.90	–	
70022	A7V	63.3±1.6	6.42±0.01	6.21±0.01	5.82±0.02	5.75±0.04	5.71±0.02	320	1	1.84	1.50 ≤ $\log a$ < 2.90	–	
70035	Am	48.4±0.8	5.55±0.01	5.24±0.01	5.06±0.22	4.79±0.05	4.67±0.02	710	1	1.94	–	3.60 ≤ $\log a$ < 4.65	
70400	A5V	48.8±0.5	5.26±0.01	5.11±0.01	4.86±0.04	4.92±0.02	4.77±0.02	450	1	2.07	1.50 ≤ $\log a$ < 2.90	3.60 ≤ $\log a$ < 4.65	
70931	A1V+...	62.3±2.8	5.44±0.01	5.38±0.01	5.30±0.02	5.31±0.05	5.20±0.02	40	1	1.77	1.50 ≤ $\log a$ < 2.90	–	
71075	A7III	26.6±0.1	3.27±0.01	3.04±0.01	2.65±0.28	2.57±0.25	2.51±0.38	1000	4	2.10	1.50 ≤ $\log a$ < 2.20	3.95 ≤ $\log a$ < 4.65	
71618	A1V	57.0±1.3	5.42±0.01	5.39±0.01	5.20±0.04	5.28±0.04	5.26±0.02	220	1	2.15	1.50 ≤ $\log a$ < 2.90	3.60 ≤ $\log a$ < 4.65	
71759	F0V	50.8±1.0	6.20±0.01	5.95±0.01	5.45±0.02	5.40±0.02	5.37±0.02	450	1	1.74	1.50 ≤ $\log a$ < 2.55	–	
71908	A7VpSrCrEu	16.6±0.0	3.47±0.01	3.19±0.01	2.54±0.28	2.47±0.20	2.42±0.22	1000	1	1.79	–	3.60 ≤ $\log a$ < 4.65	
72066	F0	61.5±1.3	7.07±0.01	6.76±0.01	6.13±0.03	6.01±0.02	5.98±0.02	630	1	1.59	1.50 ≤ $\log a$ < 2.90	–	
72220	A0V	41.2±0.3	3.72±0.01	3.72±0.01	3.68±0.24	3.63±0.20	3.65±0.19	320	16	2.71	1.50 ≤ $\log a$ < 2.20	3.60 ≤ $\log a$ < 4.65	
72622	kA2hA5mA4IV-V	23.2±0.1	2.93±0.01	2.74±0.01	2.47±0.28	2.44±0.18	2.44±0.28	500	6	2.33	1.50 ≤ $\log a$ < 2.55	3.60 ≤ $\log a$ < 4.65	

Table 1: The VAST sample

HIP	Spectral type	Distance (pc)	B_T (mag)	V_T (mag)	J (mag)	H (mag)	K_S (mag)	Age ^a (Myrs)	Age Ref.	Mass (M_\odot)	Separation coverage ($\log a$ [au])		
											Adaptive optics	CPM search	
74000	A3V	72.2±2.1	6.12±0.01	6.04±0.01	5.87±0.02	5.89±0.02	5.87±0.02	180	1	2.09	–	3.60 ≤ $\log a$ < 4.65	
74488	A2	74.3±3.3	6.92±0.01	6.66±0.01	6.21±0.02	6.16±0.06	6.08±0.03	560	1	1.77	–	3.25 ≤ $\log a$ < 4.65	
74689	A4V	46.1±0.9	5.84±0.01	5.65±0.01	5.73±0.32	5.25±0.03	5.18±0.02	50	3	1.87	1.50 ≤ $\log a$ < 2.90	3.25 ≤ $\log a$ < 4.65	
74824	A3Va	30.6±0.2	4.18±0.01	4.07±0.01	3.93±0.25	3.81±0.24	3.88±0.18	160	9	2.27	–	3.60 ≤ $\log a$ < 4.65	
75342	F0V	51.1±0.9	6.41±0.01	6.14±0.01	5.63±0.03	5.49±0.03	5.47±0.02	500	1	1.67	1.50 ≤ $\log a$ < 2.55	3.25 ≤ $\log a$ < 4.65	
75695	F0p	34.3±0.9	3.99±0.01	3.67±0.01	3.60±0.30	3.55±0.21	3.46±0.30	450	1	2.34	–	3.60 ≤ $\log a$ < 4.65	
75736	Am	65.1±1.3	6.83±0.01	6.52±0.01	5.95±0.02	5.86±0.04	5.77±0.03	890	1	1.70	–	3.60 ≤ $\log a$ < 4.65	
75761	A8IV	39.7±0.5	5.43±0.01	5.18±0.01	4.75±0.04	4.78±0.03	4.59±0.02	630	1	1.81	1.50 ≤ $\log a$ < 2.55	3.25 ≤ $\log a$ < 4.65	
76106	A2IV	70.1±1.6	5.72±0.01	5.52±0.01	5.26±0.02	5.26±0.04	5.15±0.02	500	1	2.21	1.50 ≤ $\log a$ < 2.90	–	
76291	F0III	56.4±1.3	6.88±0.01	6.58±0.01	6.00±0.03	5.93±0.02	5.85±0.02	400	1	1.61	1.50 ≤ $\log a$ < 2.90	3.25 ≤ $\log a$ < 4.65	
76852	A1V	58.3±2.3	4.58±0.01	4.51±0.01	4.41±0.23	4.48±0.22	4.30±0.02	350	1	2.22	1.50 ≤ $\log a$ < 2.90	3.60 ≤ $\log a$ < 4.65	
76878	A2m	53.1±1.1	6.04±0.01	5.82±0.01	5.37±0.02	5.33±0.02	5.30±0.02	400	1	1.84	1.50 ≤ $\log a$ < 2.55	3.60 ≤ $\log a$ < 4.65	
76952	B9IV+...	44.8±1.0	3.87±0.01	3.85±0.01	3.62±0.19	3.69±0.21	3.67±0.23	350	1	2.50	1.85 ≤ $\log a$ < 2.55	3.60 ≤ $\log a$ < 4.65	
76996	A2V	66.1±1.0	5.71±0.01	5.58±0.01	5.28±0.02	5.21±0.03	5.13±0.02	560	1	2.09	1.85 ≤ $\log a$ < 2.90	3.60 ≤ $\log a$ < 4.65	
77060	A6IV	45.7±0.5	5.68±0.01	5.44±0.01	5.04±0.04	4.98±0.08	4.82±0.02	710	1	1.82	1.50 ≤ $\log a$ < 2.55	3.25 ≤ $\log a$ < 4.65	
77233	A3V	47.6±0.6	3.75±0.01	3.65±0.01	3.44±0.29	3.54±0.28	3.55±0.32	320	12	2.87	1.50 ≤ $\log a$ < 2.55	3.95 ≤ $\log a$ < 4.65	
77464	A5IV	54.0±0.8	5.68±0.01	5.54±0.01	5.33±0.02	5.27±0.03	5.26±0.02	250	1	2.00	1.50 ≤ $\log a$ < 2.90	–	
77622	A2m	21.6±0.1	3.88±0.01	3.71±0.01	3.56±0.26	3.44±0.23	3.42±0.27	140	1	1.94	1.50 ≤ $\log a$ < 2.20	3.25 ≤ $\log a$ < 4.65	
77660	A3Vn	49.8±0.8	5.25±0.01	5.11±0.01	5.17±0.28	4.85±0.05	4.70±0.02	350	1	2.05	1.50 ≤ $\log a$ < 2.90	3.60 ≤ $\log a$ < 4.65	
77952	F1V	12.4±0.0	3.18±0.01	2.85±0.01	2.23±0.30	2.21±0.25	2.15±0.29	790	1	1.72	–	3.25 ≤ $\log a$ < 4.65	
78045	A3V	66.0±1.3	5.85±0.01	5.76±0.01	5.65±0.02	5.66±0.05	5.57±0.02	250	1	2.10	1.50 ≤ $\log a$ < 2.90	–	
78078	A2Ib/II	51.1±1.0	6.40±0.01	6.15±0.01	5.50±0.02	5.39±0.05	5.34±0.01	320	15	1.79	1.50 ≤ $\log a$ < 2.90	3.25 ≤ $\log a$ < 4.65	
78180	F0IV	33.6±0.2	5.28±0.01	4.99±0.01	4.38±0.28	4.33±0.02	4.28±0.03	790	1	1.73	1.50 ≤ $\log a$ < 2.55	3.25 ≤ $\log a$ < 4.65	
78286	F0IV	49.0±0.6	6.36±0.01	6.07±0.01	5.43±0.02	5.32±0.02	5.29±0.02	890	1	1.65	1.50 ≤ $\log a$ < 2.55	–	
78554	A3V	54.9±0.8	4.91±0.01	4.83±0.01	5.01±0.27	4.66±0.04	4.62±0.02	320	4	2.50	1.50 ≤ $\log a$ < 2.55	–	
79781	A9Vn	44.4±0.9	6.53±0.01	6.20±0.01	5.53±0.02	5.41±0.03	5.34±0.02	790	1	1.54	1.50 ≤ $\log a$ < 2.55	–	
79797	A4V	52.2±1.1	6.13±0.01	5.96±0.01	5.77±0.03	5.68±0.05	5.66±0.02	40	17	1.68	1.50 ≤ $\log a$ < 2.90	–	
79881	A0V	41.3±0.4	4.82±0.01	4.79±0.01	4.86±0.04	4.94±0.08	4.74±0.02	10	2	1.49	1.50 ≤ $\log a$ < 2.90	–	
80170	A9III	59.1±0.8	4.06±0.01	3.76±0.01	3.27±0.22	3.12±0.22	2.94±0.35	500	1	2.50	1.85 ≤ $\log a$ < 2.90	3.95 ≤ $\log a$ < 4.65	
80480	F0V	42.9±0.5	5.84±0.01	5.58±0.01	5.07±0.02	5.00±0.03	4.99±0.02	500	1	1.73	1.50 ≤ $\log a$ < 2.55	3.25 ≤ $\log a$ < 4.65	
80628	A3m	41.0±1.5	4.85±0.01	4.65±0.01	4.27±0.24	4.16±0.20	4.17±0.04	250	1	1.92	1.50 ≤ $\log a$ < 2.55	–	
80883	A0V+...	53.1±1.5	4.19±0.01	4.15±0.01	3.91±0.29	3.79±0.26	3.79±0.27	450	1	2.42	–	3.95 ≤ $\log a$ < 4.65	
80953	A4Vn	69.3±3.0	5.81±0.01	5.69±0.01	5.37±0.03	5.40±0.04	5.33±0.02	500	1	2.13	1.50 ≤ $\log a$ < 2.90	–	
80975	A7p	51.7±0.6	4.60±0.01	4.45±0.01	3.92±0.19	3.85±0.18	4.14±0.01	450	1	2.44	1.50 ≤ $\log a$ < 2.55	–	
82321	A2Vspe...	55.2±1.0	4.93±0.01	4.84±0.01	4.78±0.26	4.58±0.04	4.57±0.02	400	1	2.31	1.50 ≤ $\log a$ < 2.90	–	
82402	A3m	54.4±1.0	5.61±0.01	5.48±0.01	5.24±0.02	5.24±0.02	5.23±0.03	280	1	2.03	1.50 ≤ $\log a$ < 2.90	–	
83187	A5IV-V	51.8±0.9	5.86±0.01	5.66±0.01	5.32±0.03	5.26±0.04	5.19±0.02	350	1	1.89	1.50 ≤ $\log a$ < 2.90	–	
83317	F0IV-Vn	46.6±0.5	6.51±0.01	6.20±0.01	5.55±0.02	5.47±0.02	5.42±0.02	630	1	1.58	–	3.25 ≤ $\log a$ < 4.65	
83494	A5V	55.0±0.9	6.33±0.01	6.10±0.01	5.65±0.02	5.67±0.04	5.60±0.02	30	2	1.79	1.50 ≤ $\log a$ < 2.90	–	
83613	A4IV	40.9±0.6	5.04±0.01	4.89±0.01	5.07±0.23	4.72±0.02	4.61±0.02	280	1	2.02	1.50 ≤ $\log a$ < 2.55	–	
84012	A2IV-V	27.1±0.6	2.60±0.01	2.48±0.01	2.37±0.28	2.41±0.22	2.34±0.24	350	1	2.52	1.50 ≤ $\log a$ < 2.20	3.60 ≤ $\log a$ < 4.65	
84150	A1V	62.9±1.2	5.72±0.01	5.66±0.01	5.59±0.02	5.57±0.03	5.57±0.03	140	1	2.15	1.50 ≤ $\log a$ < 2.90	–	
84183	F0IV	43.0±0.4	5.79±0.01	5.57±0.01	5.09±0.04	5.11±0.05	5.05±0.02	100	1	1.79	1.50 ≤ $\log a$ < 2.55	–	
84379	A3IV	23.0±0.1	3.22±0.01	3.12±0.01	2.83±0.24	2.98±0.18	2.81±0.30	220	1	2.15	1.50 ≤ $\log a$ < 2.55	3.60 ≤ $\log a$ < 4.65	
84606	A2V	53.8±1.0	4.66±0.01	4.62±0.01	4.77±0.28	4.46±0.04	4.44±0.02	350	1	2.40	–	3.60 ≤ $\log a$ < 4.65	
84880	A0/A1V	62.3±1.0	4.38±0.01	4.33±0.01	4.13±0.20	4.03±0.16	4.19±0.02	350	1	2.70	1.50 ≤ $\log a$ < 2.90	–	

Table 1: The VAST sample

HIP	Spectral type	Distance (pc)	B_T (mag)	V_T (mag)	J (mag)	H (mag)	K_S (mag)	Age ^a (Myrs)	Age Ref.	Mass (M_\odot)	Separation coverage (log a [au])	
											Adaptive optics	CPM search
85157	F0IV	42.7±0.8	5.96±0.01	5.73±0.01	5.24±0.02	5.21±0.02	5.18±0.02	100	4	1.70	1.50 ≤ log a < 2.55	–
85340	kA5hA9mF1III	25.5±0.2	4.50±0.01	4.19±0.01	3.49±0.21	3.33±0.18	3.34±0.20	1000	1	1.82	1.50 ≤ log a < 2.55	–
85537	A7V	59.6±0.9	5.70±0.01	5.44±0.01	4.81±0.04	4.88±0.02	4.80±0.02	630	4	2.10	1.50 ≤ log a < 2.90	–
85699	A2m	46.9±0.4	6.03±0.01	5.79±0.01	5.34±0.02	5.31±0.02	5.29±0.02	60	1	1.80	1.50 ≤ log a < 2.55	–
85819	A6V	30.2±0.1	5.17±0.01	4.90±0.01	4.83±0.25	4.58±0.20	4.24±0.02	10	3	1.46	–	–
85822	A1Vn	52.8±0.4	4.38±0.01	4.34±0.01	4.05±0.18	4.33±0.04	4.26±0.03	350	1	2.55	1.50 ≤ log a < 2.90	–
85829	A4m	30.5±0.2	5.18±0.01	4.87±0.01	4.76±0.24	4.50±0.24	4.16±0.01	790	1	1.70	1.50 ≤ log a < 2.55	3.25 ≤ log a < 4.65
85922	A5V	48.1±0.8	5.84±0.01	5.63±0.01	5.25±0.03	5.25±0.03	5.14±0.01	320	1	1.84	1.50 ≤ log a < 2.90	3.25 ≤ log a < 4.65
86178	A5V	69.6±1.5	6.23±0.01	6.06±0.01	5.70±0.02	5.71±0.02	5.67±0.02	400	1	1.99	1.50 ≤ log a < 2.90	–
86263	A9IIIpSr:	32.3±0.2	3.85±0.01	3.55±0.01	3.06±0.24	2.91±0.18	2.91±0.24	710	1	2.20	1.50 ≤ log a < 2.90	3.95 ≤ log a < 4.65
86305	A5IV-V	44.6±0.5	5.48±0.01	5.27±0.01	4.92±0.02	4.87±0.03	4.78±0.02	50	9	2.40	1.50 ≤ log a < 2.90	–
86565	A2Va	53.1±0.7	4.34±0.01	4.24±0.01	4.25±0.25	4.18±0.17	4.11±0.25	400	1	2.53	1.50 ≤ log a < 2.55	3.60 ≤ log a < 4.65
87108	A0V	31.5±0.2	3.79±0.01	3.74±0.01	3.59±0.23	3.66±0.21	3.62±0.23	180	9	2.58	1.50 ≤ log a < 2.55	3.60 ≤ log a < 4.65
87212	A2V	66.5±1.9	5.06±0.01	5.02±0.01	4.91±0.04	4.95±0.03	4.88±0.02	400	1	2.42	1.50 ≤ log a < 2.90	3.60 ≤ log a < 4.65
87813	A0V	74.0±2.5	5.98±0.01	5.93±0.01	5.80±0.03	5.79±0.05	5.70±0.02	350	1	2.11	1.50 ≤ log a < 2.90	–
87836	A7V:	51.3±1.0	6.01±0.01	5.79±0.01	5.34±0.02	5.31±0.03	5.26±0.02	400	1	1.82	1.50 ≤ log a < 2.90	–
88528	F0IV-V	61.6±2.3	6.69±0.01	6.37±0.01	5.66±0.02	5.57±0.02	5.51±0.02	1120	1	1.69	–	3.25 ≤ log a < 4.65
88565	F0V	54.7±1.9	6.70±0.01	6.41±0.01	5.76±0.02	5.69±0.02	5.64±0.02	710	1	1.62	1.50 ≤ log a < 2.90	3.25 ≤ log a < 4.65
88726	A5V	41.8±1.2	5.89±0.01	5.65±0.01	4.68±0.25	4.49±0.04	4.39±0.02	10	2	1.43	1.50 ≤ log a < 2.55	–
88771	A4IVs	26.6±0.1	3.88±0.01	3.72±0.01	3.51±0.23	3.43±0.22	3.41±0.19	400	1	2.08	1.50 ≤ log a < 2.90	3.60 ≤ log a < 4.65
88866	A7sp...	39.9±0.3	4.62±0.01	4.36±0.01	3.98±0.25	3.80±0.26	3.80±0.29	630	1	2.15	–	3.60 ≤ log a < 4.65
89925	A5m	56.2±0.9	5.89±0.01	5.63±0.01	5.12±0.03	5.04±0.02	4.99±0.02	280	1	1.80	1.50 ≤ log a < 2.90	–
90156	A1V	56.5±1.1	5.13±0.01	5.06±0.01	4.94±0.44	4.87±0.02	4.78±0.02	350	1	2.23	1.50 ≤ log a < 2.90	3.60 ≤ log a < 4.65
90806	B9.2/A0V	68.4±1.3	5.13±0.01	5.12±0.01	5.08±0.04	5.18±0.03	5.07±0.02	280	11	2.58	1.50 ≤ log a < 2.90	–
90991	A0/A1V	69.6±1.4	5.78±0.01	5.74±0.01	5.65±0.02	5.69±0.04	5.63±0.02	220	1	2.19	1.50 ≤ log a < 2.90	–
91196	F0V	66.4±1.5	6.39±0.01	6.08±0.01	5.43±0.03	5.40±0.04	5.31±0.02	890	1	1.89	1.50 ≤ log a < 2.90	3.25 ≤ log a < 4.65
91919	A3	49.8±1.9	5.15±0.01	5.01±0.01	4.20±0.22	4.30±0.03	4.23±0.02	400	1	2.13	1.50 ≤ log a < 2.55	–
91926	A5	47.7±1.1	5.43±0.01	5.25±0.01	4.03±0.24	4.21±0.03	4.16±0.02	350	1	1.99	1.50 ≤ log a < 2.55	–
91971	Am	47.9±0.4	4.57±0.01	4.34±0.01	4.06±0.28	4.01±0.22	3.97±0.23	500	1	2.36	1.50 ≤ log a < 2.90	–
91973	F0IVv	47.7±0.5	5.93±0.01	5.62±0.01	5.10±0.04	5.05±0.04	4.96±0.02	790	1	1.78	1.50 ≤ log a < 2.90	–
92024	A7V	28.5±0.2	5.01±0.01	4.79±0.01	4.38±0.26	4.25±0.21	4.30±0.03	10	2	1.42	1.50 ≤ log a < 2.55	–
92161	A5III	28.9±0.4	4.50±0.01	4.36±0.01	4.50±0.32	4.45±0.23	4.08±0.03	110	1	1.94	1.50 ≤ log a < 2.55	3.60 ≤ log a < 4.65
92269	A7III	60.1±0.9	6.38±0.01	6.14±0.01	5.66±0.02	5.61±0.02	5.60±0.02	450	1	1.81	1.50 ≤ log a < 2.90	–
92405	A3V	71.0±1.3	5.35±0.01	5.24±0.01	4.93±0.02	5.00±0.05	4.90±0.02	500	1	2.32	1.50 ≤ log a < 2.90	–
93408	A7V	37.4±0.2	5.24±0.01	5.03±0.01	4.78±0.28	4.58±0.04	4.50±0.02	320	12	1.90	1.50 ≤ log a < 2.90	3.60 ≤ log a < 4.65
93506	A2.5V _a	27.0±0.6	2.72±0.01	2.60±0.01	2.32±0.24	2.32±0.20	2.29±0.23	450	1	2.51	1.50 ≤ log a < 2.20	–
93580	A4V	54.9±0.9	6.04±0.01	5.84±0.01	5.46±0.02	5.36±0.02	5.32±0.02	60	2	2.28	1.50 ≤ log a < 2.55	3.25 ≤ log a < 4.65
93747	A0Vn	25.5±0.1	2.99±0.01	2.96±0.01	3.08±0.33	3.05±0.28	2.88±0.36	130	10	2.93	1.50 ≤ log a < 2.55	3.60 ≤ log a < 4.65
93843	F0III	40.0±0.5	5.86±0.01	5.55±0.01	5.05±0.04	5.00±0.04	4.81±0.02	790	1	1.67	1.50 ≤ log a < 2.90	3.25 ≤ log a < 4.65
94083	A7V	27.3±0.1	5.46±0.01	5.14±0.01	4.34±0.22	4.26±0.14	4.31±0.02	320	12	1.60	–	3.25 ≤ log a < 4.65
95077	F0III:	55.4±1.1	5.91±0.01	5.61±0.01	5.10±0.04	5.05±0.02	4.92±0.02	890	1	1.87	1.50 ≤ log a < 2.90	–
95081	A0III	70.2±0.6	4.63±0.01	4.58±0.01	4.55±0.18	4.58±0.17	4.45±0.02	350	1	2.70	1.50 ≤ log a < 2.90	–
95168	A9IV	38.9±0.3	4.18±0.01	3.94±0.01	3.61±0.24	3.41±0.22	3.41±0.24	630	1	2.20	1.50 ≤ log a < 2.90	–
95793	A0V	61.2±1.3	5.89±0.01	5.79±0.01	5.60±0.03	5.59±0.05	5.53±0.02	10	15	2.36	1.50 ≤ log a < 2.90	–
95853	A5V	37.2±0.2	3.94±0.01	3.77±0.01	3.73±0.29	3.69±0.23	3.60±0.28	450	6	2.34	1.50 ≤ log a < 2.55	3.60 ≤ log a < 4.65
96313	A3	60.6±1.9	7.06±0.01	6.76±0.01	6.19±0.02	6.13±0.02	6.14±0.02	10	3	1.42	1.50 ≤ log a < 2.90	3.25 ≤ log a < 4.65

Table 1: The VAST sample

HIP	Spectral type	Distance (pc)	B_T (mag)	V_T (mag)	J (mag)	H (mag)	K_S (mag)	Age ^a (Myrs)	Age Ref.	Mass (M_\odot)	Separation coverage ($\log a$ [au])		
											Adaptive optics	CPM search	
97229	A3IV	53.6±1.2	6.10±0.01	5.91±0.01	5.57±0.02	5.47±0.04	5.46±0.02	180	1	1.84	1.50 ≤ log a < 2.55	–	
97319	A7IV	59.6±1.8	6.99±0.01	6.69±0.01	6.04±0.02	5.96±0.03	5.93±0.03	560	1	1.60	1.50 ≤ log a < 2.90	3.60 ≤ log a < 4.65	
97421	A7III-IV	49.6±0.7	5.56±0.01	5.36±0.01	5.01±0.04	4.98±0.03	4.90±0.02	450	1	1.96	1.50 ≤ log a < 2.90	3.95 ≤ log a < 4.65	
97423	A6IIIIm	65.5±1.5	6.33±0.01	6.11±0.01	5.80±0.02	5.77±0.04	5.72±0.02	280	1	1.93	1.50 ≤ log a < 2.90	–	
97674	F2III-IV	57.9±1.1	6.38±0.01	6.06±0.01	5.43±0.02	5.34±0.03	5.26±0.02	1000	1	1.76	–	3.60 ≤ log a < 4.65	
98103	A1IV	67.3±1.1	5.29±0.01	5.28±0.01	5.25±0.02	5.31±0.02	5.26±0.02	280	1	2.39	1.50 ≤ log a < 2.90	–	
98421	A4/A5IV	48.5±0.7	5.51±0.01	5.32±0.01	5.04±0.04	5.01±0.02	4.86±0.02	450	1	1.95	1.50 ≤ log a < 2.90	–	
98543	A4III	72.5±1.1	4.87±0.01	4.67±0.01	4.55±0.23	4.44±0.20	4.18±0.02	500	1	2.50	1.50 ≤ log a < 2.90	–	
99655	A3IV-Vn	48.8±0.3	4.42±0.01	4.29±0.01	4.28±0.27	4.17±0.27	4.08±0.38	400	6	2.47	1.50 ≤ log a < 2.90	3.60 ≤ log a < 4.65	
99742	A2V	46.0±0.5	5.03±0.01	4.95±0.01	4.87±0.27	4.80±0.03	4.77±0.02	50	9	2.49	1.50 ≤ log a < 2.90	3.60 ≤ log a < 4.65	
99770	A2V	42.7±0.4	5.12±0.01	4.96±0.01	4.89±0.31	4.69±0.24	4.42±0.02	40	17	2.71	1.50 ≤ log a < 2.90	3.60 ≤ log a < 4.65	
100108	A2V	62.5±1.0	5.63±0.01	5.58±0.01	5.45±0.02	5.47±0.02	5.49±0.02	180	1	2.18	1.50 ≤ log a < 2.90	–	
100526	A2	71.8±1.6	6.93±0.01	6.69±0.01	6.25±0.04	6.21±0.06	6.20±0.02	60	1	1.80	1.50 ≤ log a < 2.90	–	
101093	A7III	41.8±1.1	4.45±0.01	4.23±0.01	3.74±0.25	3.76±0.25	3.72±0.32	630	1	2.20	1.50 ≤ log a < 2.90	–	
101589	A3V	67.5±1.0	4.77±0.01	4.66±0.01	4.82±0.28	4.48±0.03	4.36±0.04	400	1	2.68	1.50 ≤ log a < 2.90	–	
101608	A5II/III	71.1±2.6	6.42±0.01	6.20±0.01	5.79±0.02	5.70±0.04	5.66±0.02	630	1	1.90	–	3.60 ≤ log a < 4.65	
101612	F0V	27.8±0.2	5.10±0.01	4.78±0.01	4.28±0.24	4.02±0.23	4.04±0.24	200	4	1.81	–	3.25 ≤ log a < 4.65	
101800	A2V	57.9±1.1	5.48±0.01	5.42±0.01	5.41±0.02	5.37±0.03	5.30±0.02	30	4	2.47	1.50 ≤ log a < 2.90	–	
102253	A8V	42.8±0.4	5.84±0.01	5.61±0.01	5.18±0.04	5.13±0.05	5.06±0.02	250	1	1.74	1.50 ≤ log a < 2.55	–	
102333	A9IV	24.2±0.1	4.83±0.01	4.53±0.01	3.91±0.28	3.69±0.28	3.82±0.27	630	1	1.65	–	3.25 ≤ log a < 4.65	
102843	A4me...	41.0±0.4	5.29±0.01	5.07±0.01	4.88±0.24	4.61±0.04	4.58±0.03	450	1	1.90	1.50 ≤ log a < 2.90	3.60 ≤ log a < 4.65	
103298	A4V	60.5±1.1	5.69±0.01	5.55±0.01	5.22±0.03	5.17±0.03	5.19±0.02	450	1	2.06	1.50 ≤ log a < 2.90	–	
103460	A2/A3III	54.9±1.4	6.09±0.01	5.89±0.01	5.59±0.02	5.46±0.03	5.49±0.02	180	1	1.87	1.50 ≤ log a < 2.55	–	
104139	A1V	49.7±0.7	4.08±0.01	4.07±0.01	4.37±0.28	4.32±0.22	4.10±0.04	320	1	2.68	1.50 ≤ log a < 2.90	3.60 ≤ log a < 4.65	
104521	A9p	36.3±0.8	5.01±0.01	4.70±0.01	4.28±0.25	4.11±0.19	4.01±0.26	790	1	1.89	1.50 ≤ log a < 2.55	3.25 ≤ log a < 4.65	
105199	A7IV	15.0±0.0	2.73±0.01	2.46±0.01	2.15±0.30	2.13±0.18	2.07±0.24	200	8	2.50	1.50 ≤ log a < 2.20	3.60 ≤ log a < 4.65	
105668	F0V	47.1±0.6	5.82±0.01	5.51±0.01	5.07±0.24	4.96±0.06	4.76±0.02	890	1	1.82	1.50 ≤ log a < 2.55	3.25 ≤ log a < 4.65	
105860	A8m	46.4±1.2	6.35±0.01	6.09±0.01	5.68±0.07	5.49±0.03	5.51±0.03	40	1	1.68	1.50 ≤ log a < 2.90	3.25 ≤ log a < 4.65	
105966	A1V	58.3±1.0	5.44±0.01	5.38±0.01	5.28±0.03	5.37±0.05	5.29±0.02	200	1	2.19	1.50 ≤ log a < 2.90	–	
106654	A7/A8IV	58.4±1.6	5.99±0.01	5.75±0.01	5.32±0.02	5.26±0.02	5.21±0.02	630	1	1.91	1.50 ≤ log a < 2.90	–	
106711	A5V	65.8±1.5	5.27±0.01	5.06±0.01	5.00±0.22	4.61±0.04	4.51±0.02	630	1	2.20	1.50 ≤ log a < 2.90	–	
106786	A7V	54.8±0.7	4.89±0.01	4.70±0.01	4.36±0.25	4.22±0.20	4.25±0.02	500	1	2.39	1.50 ≤ log a < 2.90	3.60 ≤ log a < 4.65	
106856	A9IV-Vn	54.7±0.9	5.97±0.01	5.69±0.01	5.16±0.04	5.10±0.03	5.01±0.02	890	1	1.84	1.50 ≤ log a < 2.90	3.25 ≤ log a < 4.65	
106897	F2V	39.7±0.8	6.13±0.01	5.80±0.01	5.14±0.04	4.99±0.02	4.96±0.03	890	1	1.59	–	3.60 ≤ log a < 4.65	
107302	A7IV/V	53.0±1.2	6.21±0.01	5.98±0.01	5.57±0.03	5.46±0.03	5.41±0.02	450	1	1.77	1.50 ≤ log a < 2.55	–	
107556	kA5hF0mF2III	11.9±0.0	3.21±0.01	2.88±0.01	2.25±0.26	2.06±0.19	2.01±0.22	890	1	1.67	1.50 ≤ log a < 2.20	3.25 ≤ log a < 4.65	
107919	A5	69.8±2.2	6.96±0.01	6.68±0.01	6.20±0.02	6.11±0.04	6.05±0.03	560	1	1.72	–	3.25 ≤ log a < 4.65	
108060	A0Vs	72.3±2.7	5.70±0.01	5.68±0.01	5.61±0.02	5.67±0.02	5.63±0.02	220	1	2.28	1.85 ≤ log a < 2.90	–	
109427	A1Va	28.3±0.7	3.61±0.01	3.52±0.01	3.46±0.27	3.39±0.21	3.38±0.26	450	6	2.17	1.50 ≤ log a < 2.55	3.95 ≤ log a < 4.65	
109521	A5V	56.1±2.3	5.56±0.01	5.40±0.01	5.01±0.04	5.02±0.05	4.96±0.02	500	1	2.04	1.50 ≤ log a < 2.90	3.60 ≤ log a < 4.65	
109667	A3V	63.5±2.1	6.39±0.01	6.21±0.01	5.84±0.02	5.85±0.02	5.74±0.02	280	1	1.86	1.50 ≤ log a < 2.90	–	
109857	F0IV	26.2±0.7	4.51±0.01	4.21±0.01	3.83±0.29	3.67±0.25	3.54±0.31	630	4	1.87	1.50 ≤ log a < 2.20	3.25 ≤ log a < 4.65	
110787	A2m	63.2±0.9	6.03±0.01	5.86±0.01	5.58±0.03	5.57±0.02	5.54±0.03	320	1	2.00	1.50 ≤ log a < 2.90	–	
110935	A4V	43.1±0.7	5.80±0.01	5.59±0.01	5.21±0.04	5.14±0.05	5.05±0.02	250	1	1.76	–	3.25 ≤ log a < 4.65	
111169	A1V	31.5±0.1	3.78±0.01	3.76±0.01	3.83±0.24	3.87±0.21	3.85±0.27	130	1	2.45	1.50 ≤ log a < 2.55	3.60 ≤ log a < 4.65	
111188	A0V	43.8±0.4	4.31±0.01	4.28±0.01	4.34±0.28	4.30±0.19	4.25±0.04	350	11	2.31	1.50 ≤ log a < 2.55	–	

Table 1: The VAST sample

HIP	Spectral type	Distance (pc)	B_T (mag)	V_T (mag)	J (mag)	H (mag)	K_S (mag)	Age ^a (Myrs)	Age Ref.	Mass (M_\odot)	Separation coverage ($\log a$ [au])	
											Adaptive optics	CPM search
111200	A8III	71.6±3.4	6.73±0.01	6.42±0.01	5.77±0.02	5.67±0.03	5.54±0.02	1120	1	1.77	–	3.60 ≤ $\log a$ < 4.65
111674	A8IV	52.6±0.5	4.93±0.01	4.66±0.01	3.75±0.21	3.69±0.19	3.99±0.04	710	1	2.20	1.50 ≤ $\log a$ < 2.90	3.60 ≤ $\log a$ < 4.65
112183	F0	71.8±2.2	7.26±0.01	6.94±0.01	6.28±0.03	6.20±0.02	6.16±0.03	790	1	1.63	–	3.60 ≤ $\log a$ < 4.65
112714	F0IV-V	64.6±2.1	6.89±0.01	6.57±0.01	5.97±0.02	5.87±0.02	5.80±0.02	890	1	1.67	–	3.25 ≤ $\log a$ < 4.65
113048	A3Vm+...	56.9±1.7	6.25±0.01	5.97±0.01	5.17±0.02	5.05±0.02	5.04±9.99	450	1	1.83	1.50 ≤ $\log a$ < 2.90	–
113963	B9III	40.9±0.3	2.46±0.01	2.45±0.01	2.54±0.27	2.74±0.22	2.65±0.31	200	1	3.50	–	3.95 ≤ $\log a$ < 4.65
113996	F2IV+...	64.2±2.5	5.79±0.01	5.47±0.01	4.88±0.02	4.75±0.02	4.67±0.02	890	1	2.00	–	3.60 ≤ $\log a$ < 4.65
114189	A5V	39.4±1.1	6.26±0.01	5.99±0.01	5.38±0.03	5.28±0.02	5.24±0.02	30	2	1.55	1.50 ≤ $\log a$ < 2.55	3.25 ≤ $\log a$ < 4.65
114570	F0V	24.6±0.1	4.87±0.01	4.56±0.01	3.84±0.24	3.76±0.22	3.79±0.29	890	1	1.65	–	3.25 ≤ $\log a$ < 4.65
114822	A3V	71.2±1.6	5.63±0.01	5.56±0.01	5.46±0.02	5.44±0.03	5.40±0.02	350	1	2.25	1.50 ≤ $\log a$ < 2.90	–
115250	A5V	49.6±1.0	4.79±0.01	4.60±0.01	4.33±0.29	4.36±0.22	4.08±0.02	630	1	2.20	1.50 ≤ $\log a$ < 2.55	–
115738	A0p...	47.1±0.6	4.98±0.01	4.92±0.01	5.32±0.27	4.98±0.02	4.90±0.02	60	2	2.37	1.50 ≤ $\log a$ < 2.55	3.60 ≤ $\log a$ < 4.65
115770	A6IV	65.4±0.8	5.80±0.01	5.61±0.01	5.24±0.03	5.18±0.04	5.16±0.02	560	1	2.07	1.50 ≤ $\log a$ < 2.90	3.60 ≤ $\log a$ < 4.65
116611	A1Vn	71.4±1.4	5.48±0.01	5.48±0.01	5.42±0.02	5.45±0.02	5.42±0.02	320	1	2.34	1.50 ≤ $\log a$ < 2.90	–
116758	A7IV	43.6±2.0	5.28±0.01	5.01±0.01	4.89±0.25	4.63±0.22	4.34±0.02	790	1	1.95	1.50 ≤ $\log a$ < 2.90	3.60 ≤ $\log a$ < 4.65
116768	A2m	54.4±2.5	6.23±0.01	5.99±0.01	5.56±0.02	5.49±0.05	5.47±0.02	280	1	1.81	1.50 ≤ $\log a$ < 2.90	3.25 ≤ $\log a$ < 4.65
116928	A7V	32.7±0.2	4.74±0.01	4.51±0.01	4.37±0.30	4.20±0.24	4.06±0.04	400	1	1.94	1.50 ≤ $\log a$ < 2.55	3.60 ≤ $\log a$ < 4.65
117173	A3	68.1±3.0	6.72±0.01	6.56±0.01	6.17±0.02	6.17±0.03	6.12±0.02	30	3	1.76	1.85 ≤ $\log a$ < 2.90	–
117452	A0V	42.1±0.4	4.58±0.01	4.57±0.01	4.80±0.26	4.64±0.08	4.53±0.02	60	2	2.47	1.50 ≤ $\log a$ < 2.55	–
118092	A1IV	66.1±1.4	6.07±0.01	5.96±0.01	5.81±0.02	5.76±0.04	5.70±0.03	140	1	2.04	1.50 ≤ $\log a$ < 2.90	–
118121	A1V	47.4±1.1	5.07±0.01	5.00±0.01	4.91±0.04	4.95±0.03	4.82±0.02	30	2	2.53	1.50 ≤ $\log a$ < 2.90	–

a - Age rounded to nearest isochrone value. Age estimates from: 1 - this work (CMD), 2 - Zuckerman et al. (2011), 3 - Tetzlaff et al. (2010), 4 - Rhee et al. (2007), 5 - Su et al. (2006),

6 - Rieke et al. (2005), 7 - Perryman et al. (1998), 8 - Barrado y Navascués (1998), 9 - Song et al. (2001), 10 - Westin (1985), 11 - Gerbaldi et al. (1999), 12 - Zuckerman & Song (2004),

13- Laureijs et al. (2002), 14 - Stauffer et al. (1995), 15 - Paunzen (1997), 16 - Janson et al. (2011), 17 - Torres et al. (2008).

Table 2: Alternative catalogue identifiers

HIP	Name	Bayer	Flamsteed	HR	HD	ADS	WDS
128					224890		
159					224945		
1473	σ And	25 And	68	1404			
2355		28 And	114	2628	409 AB	J00301+2945	
2381			118	2696			
2472	λ^1 Phe			125	2834	J00314-4848	
2578	β^3 Tuc			136	3003	J00327-6302	
2852				151	3326		
3277	ξ Phe			183	3980	J00418-5630	
3414	π Cas	20 Cas	184	4058			
3521			198	4293			
3965			238	4818			
4436	μ And	37 And	269	5448	788 A	J00568+3830	
4852	σ Scl		293	6178			
4979		26 Cet	301	6288	875 A	J01038+0122	
5186			309	6416			
5300	v Phe			331	6767	J01078-4129	
5310	ψ^2 Psc	79 Psc	328	6695			
5317		41 And	324	6658			
5542	θ Cas	33 Cas	343	6961		J01111+5509	
6514		47 And	395	8374			
6539		44 Cet	401	8511		J01240-0800	
6686	δ Cas	37 Cas	403	8538		J01258+6014	
6960		48 Cet	433	9132	1184 A	J01296-2138	
7345		49 Cet	451	9672			
7447			457	9780			
8122				10638			
8241	q^2 Eri			520	10939		
8588		54 Cet	534	11257			
8847			540	11408			
8903	β Ari	6 Ari	553	11636			
9153	λ Ari	9 Ari	569	11973	1563 A	J01579+2336	
9480	A Cas	48 Cas	575	12111	1598 AB	J02020+7054	
9836	κ Ari	12 Ari	613	12869			
9977		58 And	620	13041			
10054			597	12467			
10064	β Tri	4 Tri	622	13161			
10069			630	13305			
10670	γ Tri	9 Tri	664	14055			
11090			687	14622		J02228+4124	
11102			701	14943			
11138				14619			
11486		12 Tri	717	15257			
11569	ι Cas		707	15089	1860 AB	J02291+6724	
11678		26 Ari	729	15550			
12489		33 Ari	782	16628	2033 A	J02407+2704	
12706	γ Cet	86 Cet	804	16970		J02433+0314	
12828	μ Cet	87 Cet	813	17094		J02449+1007	
12832		38 Ari	812	17093			
13133	RZ Cas			815	17138		
13141	ν Hor			852	17848		
13717				875	18331		
13782		4 Eri	883	18454			
14146	τ^3 Eri	11 Eri	919	18978			
14232			916	18928			
14293	ρ^3 Eri	10 Eri	925	19107			
14551			943	19545			
14862			932	19275			
15197	ζ Eri	13 Eri	984	20320			
15353			1014	20888			
15648	I Per	32 Per	1002	20677			
16285			1075	21882			
16292			1046	21447	2565 A	J03300+5527	
16591			1078	21912			
16599			1073	21819			

Table 2: Alternative catalogue identifiers

HIP	Name	Bayer	Flamsteed	HR	HD	ADS	WDS
17395				1139	23281		
17954				1188	23985	2799	J03503+2535
18217				1192	24141		
18481				1224	24817		
18547				1223	24809		
18907	ν Tau	38 Tau		1251	25490		
19893	γ Dor			1338	27290		
19990	ω Tau	50 Tau		1329	27045		
20087		51 Tau		1331	27176		J04184+2135
20156				1330	27084		
20219	h Tau	57 Tau		1351	27397		J04200+1402
20261		58 Tau		1356	27459		
20507	ξ Eri	42 Eri		1383	27861		
20542		64 Tau		1380	27819		J04241+1727
20635	κ Tau	65 Tau		1387	27934		J04254+2218
20641		67 Tau		1388	27946		J04254+2218
20648		68 Tau		1389	27962	3206 AB	J04255+1756
20711	v Tau	69 Tau		1392	28024		J04263+2249
20713		71 Tau		1394	28052		J04263+1537
20842				1403	28226		J04280+2137
20894	θ^2 Tau	78 Tau		1412	28319		J04287+1552
20901	b Tau	79 Tau		1414	28355		
21029				1427	28527		J04306+1612
21036		83 Tau		1430	28556		J04306+1343
21039		81 Tau		1428	28546		J04306+1542
21238					28693		J04334+4304
21273	ρ Tau	86 Tau		1444	28910		
21402	d Tau	88 Tau		1458	29140	3317 A	J04357+1010
21547	c Eri	51 Eri		1474	29391	3350 A	J04376-0228
21589	c^1 Tau	90 Tau		1473	29388		J04382+1231
21644				1483	29573		J04389-1207
21670				1480	29499		J04391+0752
21673	σ^1 Tau	91 Tau		1478	29479		J04393+1555
21683	σ^2 Tau	92 Tau		1479	29488		J04393+1555
22044				1507	30034		J04444+1109
22192				1525	30422		
22287		4 Cam		1511	30121	3432 A	J04480+5645
22300				1515	30144		
22361				1491	29678		J04488+7556
22565	i Tau	97 Tau		1547	30780		J04514+1850
22845	π^1 Ori	7 Ori		1570	31295		J04549+1009
23179		4 Aur		1592	31647		J04593+3753
23296				1613	32115		
23497	ι Tau	102 Tau		1620	32301		
23554				1645	32667		
23585					32296		
23871		106 Tau		1658	32977		
23875	β Eri	67 Eri		1666	33111		J05078-0505
23983	h Ori	16 Ori		1672	33254		J05093+0950
24340	μ Aur	11 Aur		1689	33641		J05134+3829
25280				1792	35505		
26309				1915	37286		
26382		122 Tau		1905	37147		
26395				1919	37306		
26563	d Ori	49 Ori		1937	37507		
26624				1940	37594		
27249		26 Cam		1969	38091		
27288	ζ Lep	14 Lep		1998	38678		
27321	β Pic			2020	39060		
27947				2094	40292		
28614	μ Ori	61 Ori		2124	40932	4617 AB	J06024+0939
28910	θ Lep	18 Lep		2155	41695		
29711				2234	43319	4865 AB	J06155-0455
29850	l Ori	75 Ori		2247	43525	4890 A	J06171+0957
29852				2265	43940		

Table 2: Alternative catalogue identifiers

HIP	Name	Bayer	Flamsteed	HR	HD	ADS	WDS
29997				2209	42818		
30060			2 Lyn	2238	43378		
30167					44286		
30419		ϵ Mon	8 Mon	2298	44769	5012 A	J06238+0436
30666				2324	45320		
31119				2375	46089		
31167				2386	46304		J06324-0552
32104			26 Gem	2466	48097		
32617				2514	49434		
32938				2558	50445		
33018		θ Gem	34 Gem	2540	50019	5532 A	J06528+3358
33024				2551	50277		
33202		e Gem	38 Gem	2564	50635	5559 AB	J06546+1311
33485			16 Lyn	2585	50973		
34059		H Pup		2672	53811		
34897					54944		
35350		λ Gem	54 Gem	2763	56537	5961 A	J07181+1632
36393			64 Gem	2857	59037		
38235					63847		
38723				3083	64491		
39567			8 Cnc	3163	66664		
40878				3258	69682		
41081				3300	71043		
41152				3277	70313		
41375			2 Hya	3321	71297		J08265-0359
42080		A UMa	2 UMa	3354	72037		
42313		δ Hya	4 Hya	3410	73262		J08377+0542
42425		θ Vol		3460	74405		J08391-7023
42806		γ Cnc	43 Cnc	3449	74198		J08433+2128
42895				3495	75171		
43121		A^2 Cnc	50 Cnc	3481	74873		
43584		σ^1 Cnc	51 Cnc	3519	75698	7057 A	J08526+3228
43932		σ^2 Cnc	59 Cnc	3555	76398		
43970		σ^1 Cnc	62 Cnc	3561	76543		
44001		σ^2 Cnc	63 Cnc	3565	76582		
44127		ι UMa	9 UMa	3569	76644		J08592+4803
44342			67 Cnc	3589	77190		J09018+2754
44574				3606	77660		
44901		f UMa	15 UMa	3619	78209		
45001		ϵ Pyx		3644	78922		J09099-3022
45493		e UMa	18 UMa	3662	79439		
45510					79765		
45688			38 Lyn	3690	80081		J09188+3648
47204				3840	83520		J09372-5340
47300			42 Lyn	3829	83287		
47479				3863	84121		J09407-5759
47701		f Leo	15 Leo	3861	84107		
47777					83599		
48319		v UMa	29 UMa	3888	84999	7534 A	J09510+5902
48341			6 Sex	3899	85364		
48763					86266	7591 AB	J09568-2633
49593			21 LMi	3974	87696		
50372		λ UMa	33 UMa	4033	89021		
51056			30 LMi	4090	90277		
51194				4115	90874		
51200				4096	90470		J10275+4136
51384				4062	89571		
51658				4132	91312	7826 A	J10332+4026
51907				4155	91858		
51974				4160	91992		
52457			41 LMi	4192	92825		
52513				4197	92941		
53824		c Leo	59 Leo	4294	95382	8019 A	J11007+0606
53954		b Leo	60 Leo	4300	95608		
54027				4303	95771		

Table 2: Alternative catalogue identifiers

HIP	Name	Bayer	Flamsteed	HR	HD	ADS	WDS
54063					95804		
54214				4315	96220	J11056-1105	
54477			10 Crt	4334	96819		
54688				4341	97244		
54746				4350	97495	J11125-4905	
54872	δ Leo	68 Leo		4357	97603	J11141+2031	
54879	θ Leo	70 Leo		4359	97633		
55033				4366	97937		
55084	ϕ Leo	74 Leo		4368	98058	J11167-0339	
55266			55 UMa	4380	98353	J11191+3811	
55488					98747		
55705		γ Crt	15 Crt	4405	99211	8153 A	J11249-1741
56034			57 UMa	4422	99787		J11291+3920
56083				4424	99859		
56253				4429	99945		
56920					101397		
57013				4502	101615		
57328	ξ Vir	2 Vir		4515	102124		
57562		A ¹ Vir	4 Vir	4528	102510		J11479+0815
57606				4531	102590	8311 AB	J11486+1417
57646				4535	102660		
57779				4543	102910	8320 A	J11509+1217
58001	Phecdra	γ UMa	64 UMa	4554	103287		
58684			67 UMa	4594	104513		J12021+4303
58758		θ^1 Cru		4599	104671		J12030-6319
59394			3 Crv	4635	105850		
59608			12 Vir	4650	106251		
59774	Megrez	δ UMa	69 UMa	4660	106591		J12154+5702
59819			6 Com	4663	106661		
59923				4673	106887	8501 A	J12175+2856
60018				4680	107055		
60595				4722	108107		
61498				4796	109573		J12360-3952
61558		f Vir	25 Vir	4799	109704		
61622		τ Cen		4802	109787		
61688				4809	109931		
61692			9 CVn	4811	109980		
61932		γ Cen		4819	110304		J12415-4858
61937			27 Vir	4824	110377		J12416+1026
61960		ρ Vir	30 Vir	4828	110411		
62788				4881	111786		
62933			41 Vir	4900	112097		
62983				4901	112131		J12543-1139
63320					112734		
63491					112934		
64246			17 CVn	4971	114447	8805 A	J13101+3830
64692			19 CVn	5004	115271		J13155+4051
64979				5025	115810	8861 D	J13196+3507
65109		ι Cen		5028	115892		
65241			64 Vir	5040	116235		
65477	Alcor	g UMa	80 UMa	5062	116842		J13239+5456
65728				5085	117376	8919 C	J13288+5956
66065				5097	117716		
66200		ω Vir	78 Vir	5105	118022		
66223				5108	118156	8956 A	J13344+3847
66234			24 CVn	5112	118232		
66249		ζ Vir	79 Vir	5107	118098		
66458			25 CVn	5127	118623	8974 AB	J13375+3618
66634			82 UMa	5142	119024		
66798				5162	119476		
67194				5179	120047		
67483				5204	120600		
67782				5229	121164		
69483		κ^2 Boo	17 Boo	5329	124675	9173 A	J14135+5147
69592				5333	124713		

Table 2: Alternative catalogue identifiers

HIP	Name	Bayer	Flamsteed	HR	HD	ADS	WDS
69713		ι Boo	21 Boo	5350	125161	9198 A	J14162+5122
69732		λ Boo	19 Boo	5351	125162		
69951					125558		
69974		λ Vir	100 Vir	5359	125337		
69995				5357	125283		
70022				5368	125489		
70035				5349	125158		
70400				5392	126248		
70931				5413	126983		J14303-4931
71075		γ Boo	27 Boo	5435	127762	9300 A	J14321+3818
71618			33 Boo	5468	129002		
71759				5473	129153		
71908		α Cir		5463	128898		J14425-6459
72066					130044		
72220			109 Vir	5511	130109		
72622		α^2 Lib	9 Lib	5531	130841		J14509-1603
74000				5633	134064	9505 AB	J15073+1827
74488					135027		
74689			4 Ser	5679	135559		
74824		β Cir		5670	135379		
75342			8 Ser	5721	137006		
75695		β CrB	3 CrB	5747	137909		J15278+2906
75736				5491	129723		
75761			10 Ser	5746	137898		
76106				5762	138413		
76291				5791	138936		
76852		ι Ser	21 Ser	5842	140159	9744 AB	J15416+1940
76878		τ^7 Ser	22 Ser	5845	140232		
76952		γ CrB	8 CrB	5849	140436	9757 AB	J15427+2618
76996		ρ Oct		5729	137333		J15433-8428
77060		η Lib	44 Lib	5848	140417		
77233		β Ser	28 Ser	5867	141003	9778 A	J15462+1525
77464			30 Ser	5875	141378		
77622		ϵ Ser	37 Ser	5892	141795		
77660		b Ser	36 Ser	5895	141851		J15513-0305
77952		β TrA		5897	141891		J15551-6326
78045				5905	142139		
78078				5930	142703		
78180				5960	143466		
78286				5964	143584		
78554		π Ser	44 Ser	5972	143894		
79781				6067	146514		
79797				6037	145689		
79881		d Sco		6070	146624		
80170		γ Her	20 Her	6095	147547	10022 A	J16219+1909
80480				6173	149681		
80628		v Oph	3 Oph	6129	148367		J16278-0822
80883		λ Oph	10 Oph	6149	148857	10087 AB	J16309+0159
80953				6162	149303		J16318+4536
80975		ω Oph	9 Oph	6153	148898		
82321			52 Her	6254	152107	10227 ABC	J16492+4559
82402		k Her	47 Her	6250	151956		
83187				6297	153053		J17001-5436
83317				6379	155154		
83494				6351	154431		
83613			60 Her	6355	154494	10334 A	J17054+1244
84012		η Oph	35 Oph	6378	155125	10374 AB	J17104-1544
84150				6381	155259		
84183				6421	156295		
84379		δ Her	65 Her	6410	156164	10424 A	J17150+2450
84606		e Her	69 Her	6436	156729		
84880		ν Ser	53 Ser	6446	156928	10481 A	J17208-1251
85157			73 Her	6480	157728		
85340		b Oph	44 Oph	6486	157792		
85537				6507	158352		

Table 2: Alternative catalogue identifiers

HIP	Name	Bayer	Flamsteed	HR	HD	ADS	WDS
85699			24 UMi	6811	166926		
85819		ν^1 Dra	24 Dra	6554	159541	10628 B	J17322+5511
85822		δ UMi	23 UMi	6789	166205		
85829		ν^2 Dra	25 Dra	6555	159560	10628 A	J17322+5511
85922				6534	159170		
86178				6570	160054		
86263		ξ Ser	55 Ser	6561	159876		J17376-1524
86305		π Ara		6549	159492		
86565		o Ser	56 Ser	6581	160613		
87108		γ Oph	62 Oph	6629	161868		
87212			30 Dra	6656	162579		J17491+5047
87813				6681	163336	10891 A	J17563-1549
87836				6680	163318		
88528				6754	165373		
88565				6767	165645	11054 A	J18050+4157
88726				6749	165189		J18068-4325
88771			72 Oph	6771	165777	11076 AB	J18073+0934
88866		π Pav		6745	165040		
89925			108 Her	6876	168913		
90156		b Dra	39 Dra	6923	170073	11336 AB	J18239+5848
90806				6944	170680	11411 A	J18314-1824
90991				6962	171130		
91196				7013	172569		
91919		ϵ^1 Lyr	4 Lyr	7051	173582	11635 AB	J18443+3940
91926		ϵ^2 Lyr	5 Lyr	7054	173607	11635 CD	J18443+3940
91971		ζ^1 Lyr	6 Lyr	7056	173648	11639 A	J18448+3736
91973		ζ^2 Lyr	7 Lyr	7057	173648	11639 D	J18448+3736
92024				7012	172555		J18454-6452
92161			111 Her	7069	173880		J18470+1811
92269				7096	174481		
92405		ν Lyr	9 Lyr	7102	174602	11737 A	J18499+3233
93408			16 Lyr	7215	177196	11964 A	J19014+4656
93506		ζ Sgr	38 Sgr	7194	176687	11950 AB	J19026-2953
93580				7214	177178		
93747		ζ Aql	17 Aql	7235	177724	12026 AB	J19054+1352
93843				7253	178233		
94083			59 Dra	7312	180777		
95077				7327	181240		
95081		π Dra	58 Dra	7371	182564		
95168		ρ^1 Sgr	44 Sgr	7340	181577		
95793		c Aql	35 Aql	7400	183324		
95853		ι Cyg	10 Cyg	7420	184006		
96313					184761		
97229		v Aql	49 Aql	7519	186689		
97319				7533	186998		
97421		ν Tel		7510	186543		
97423				7532	186984		
97674				7524	186786		
98103		ϕ Aql	61 Aql	7610	188728		
98421		θ^2 Sgr		7624	189118		J19599-3442
98543			15 Vul	7653	189849		
99655			33 Cyg	7740	192696		
99742		ρ Aql	67 Aql	7724	192425		
99770		b^3 Cyg	29 Cyg	7736	192640		J20145+3648
100108			36 Cyg	7769	193369		
100526					194444		
101093		θ Cep	2 Cep	7850	195725		
101589		ζ Del	4 Del	7871	196180		
101608				7865	196078		
101612		ϕ^1 Pav		7848	195627		
101800		ι Del	5 Del	7883	196544		
102253			4 Cep	7945	197950		
102333		η Ind		7920	197157		
102843			56 Cyg	7984	198639		J20501+4404
103298			16 Del	8012	199254	14429 A	J20556+1234

Table 2: Alternative catalogue identifiers

HIP	Name	Bayer	Flamsteed	HR	HD	ADS	WDS
103460				8018	199443		
104139		θ Cap	23 Cap	8075	200761		
104521		γ Equ	5 Equ	8097	201601	14702 AB	J21103+1008
105199	Alderamin	α Cep	5 Cep	8162	203280	14858 A	J21186+6235
105668			18 Aqr	8187	203705		J21242-1253
105860				8210	204188		
105966			35 Vul	8217	204414		
106654			8 PsA	8253	205471		J21362-2610
106711			74 Cyg	8266	205835		
106786		ξ Aqr	23 Aqr	8264	205767		J21378-0751
106856			4 Peg	8270	205924	15157 A	J21385+0546
106897				8276	206043		
107302			45 Cap	8302	206677		
107556		δ Cap	49 Cap	8322	207098	15314 A	J21470-1608
107919					207861		
108060					8358	208108	
109427		θ Peg	26 Peg	8450	210418		
109521				8463	210715	15708 A	J22112+5049
109667					8464	210739	
109857		ϵ Cep	23 Cep	8494	211336		J22150+5703
110787			28 Cep	8578	213403		
110935				8547	212728		
111169		α Lac	7 Lac	8585	213558	16021 A	J22313+5017
111188		β PsA	17 PsA	8576	213398		J22315-3221
111200			58 Aqr	8583	213464		
111674			9 Lac	8613	214454		
112183					215322		
112714				8681	216048		
113048				8708	216608	16345 AB	J22537+4445
113963	Markab	α Peg	54 Peg	8781	218045		
113996		h Aqr	83 Aqr	8782	218060	16497 AB	J23052-0742
114189				8799	218396		
114570			7 And	8830	219080		
114822				8840	219402		
115250		τ Peg	62 Peg	8880	220061		
115738		κ Psc	8 Psc	8911	220825		J23269+0115
115770				8918	220974		
116611			75 Peg	8963	222133		J23379+1824
116758		ω^1 Aqr	102 Aqr	8968	222345		
116768				8970	222377		
116928		λ Psc	18 Psc	8984	222603		
117173					222962		
117452		δ Scl		9016	223352	17021 AB	J23489-2808
118092				9060	224361		
118121		η Tuc		9062	224392		